Optogenetic Tachypacing-induced Heart Failure in Larval Zebrafish

by

Katherine Purvis

Submitted in partial fulfilment of the requirements

for the degree of Master of Science

at

Dalhousie University

Halifax, Nova Scotia

June 2023

Table of Contents

List of Tables

List of Figures

Abstract

Chronic tachypacing is commonly used in mammals to model heart failure (HF). Alternative methods of chronic tachypacing involving the use of light-activated ion channels (‘optogenetics’) have been explored in cultured heart tissue. However, this model lacks the complexity of native myocardium. Recent efforts have explored zebrafish as a model for human cardiac dysfunction based on their electrophysiological similarities. Larval zebrafish offer a particularly attractive tool as they are translucent, allowing for *in vivo* measurement of cardiac activity. A study by Kossack et al. (2017) investigated the use of larval zebrafish as a model for HF using chronic sympathetic stimulation with isoproterenol. Differences in the genetic response were found in comparison to mammalian models, which suggested different mechanisms of isoproterenol-induced cardiac dysfunction. This study aims to establish a model of chronic tachypacing-induced HF in larval zebrafish using optogenetics to potentially overcome these limitations. The effects of chronic optogenetic tachypacing of larval zebrafish hearts between 2 to 6 and 3 to 7 days post fertilization (dpf) with two opsins (channelrhodopsin-2, ChR2, and anion channelrhodopsin-1, ACR1) were compared. Furthermore, we investigated the effects of continuous and interval chronic tachypacing. To determine the effects of chronic optical tachypacing, we assessed changes in cardiac morphology, function, and gene expression. Cardiac morphology and function were measured from *in vivo* brightfield microscopic recordings, and morphology was further assessed using fluorescent microscopy. Changes in gene expression were quantified using qRT-PCR. It has been shown that chronic continuous tachypacing results in cardiac development defects, while interval pacing with ChR2-expressing larvae results in morphological changes reminiscent of HR. Furthermore, interval pacing led to an increase in mRNA levels of several markers for heart failure, including levels of ANP, BNP, and TGF-ß1, as well as the marker for hypertrophy, Myh6.

Acknowledgements

I would firstly like to thank my family for their constant support throughout my academic journey. In particular, I would like to thank my sister Emma. Whether it be picking me up from the lab late at night, or coming home to a home cooked meal, your support throughout this journey has been exceptional and very appreciated. To my partner Nevin, thank you for being so caring and supportive throughout my education.

I would also like to thank colleagues who have supported me throughout the project, particularly those who aided in teaching me the techniques and advising me on the protocols for the qRT-PCR experiments, including Gabriela Gomes, Saby Mathavarajah, and Mat Nightingale. Additionally, I would like to thank the members of my committee, Dr. Ketul Chaudhary, Dr. Thomas Pulinilkunnil. and Paul Linsdell for the appreciated guidance and mentorship.

Lastly, I would like to thank the Quinn lab for such a wonderful experience. To Matt, Jon, Jessi, Ahmed, Zach, and Michael, it has been such a pleasure working with all of you and I have made such impactful memories from my time here. Thank you all for being so helpful, caring, and supportive, and also for the jokes and the occasional drinks. Most significantly, it has been an honour to work as a student for Dr. Alex Quinn. Your contagious passion for your research and unwavering support for your students is remarkable. You have been an excellent mentor and have really shaped me as a student. I cannot thank you enough for the constant guidance, words of wisdom, and encouragement throughout this.

Chapter 1: Introduction

1.1. Heart Failure

Heart failure (HF) is a global pandemic affecting more than 64 million people worldwide, with only 30% of Canadian patients surviving one-year post-hospitalization (Lippi & Sanchis-Gomar, 2020; Virani et al., 2017). Heart failure is a progressive condition that is at the end-stage of various cardiovascular conditions, and typically resulting from damage to the myocardium, which impairs cardiac pump function and reduces the heart's ability to meet the body's metabolic needs (Dassanayaka & Jones, 2015). Neurohormonal compensatory mechanisms are activated in response to HF, including the adrenergic nervous system and the renin-angiotensin-aldosterone system (RAAS), which temporarily improves cardiac output (Dzau et al., 1981; Eisenhofer et al., 1996). However, when compensatory mechanisms are sustained, molecular, cellular, genetic, neurohormonal, metabolic and inflammatory changes lead to pathological structural remodelling of the heart, in which cardiac function is lost (Ahmad et al., 2005; Bertero & Maack, 2018; Cohn et al., 2000).

With the aging Canadian population and the increase in risk factors for cardiovascular diseases (Curtis et al., 2018; North & Sinclair, 2012), healthcare costs related to HF in Canada are expected to exceed 2.8 billion per year by 2030 (Tran et al., 2016). Therefore, there is an increasing demand to understand the underlying mechanisms of HF and to improve treatment efficacy. However, mechanisms driving HF are challenging to distinguish in the human condition due to the ambiguity of when HF begins and from the confounding effects of the associated therapeutics (Vanoli et al., 2004). Experimental models of chronic HF can be utilized to allow us to understand the

complex nature of HF and perform interrogations that cannot be easily isolated clinically.

1.2. Experimental Models of Heart Failure

Experimental models of HF should strive to simulate the human condition, to enhance clinical translatability. Due to the various etiologies and comorbidies present in human HF, choosing the appropriate experimental model can be challenging (Poon & Brand, 2013). Well-established models of HF include hemodynamic overload, myocardial infarction, ischemia-reperfusion injury, drug-induced, DOCA-salt hypertension, genetic mutation-based, and pacing-induced tachycardia. While these models have contributed imperative information to our understanding of HF, each has its limitations.

1.2.1. Hemodynamic Overload

Hemodynamic overload models of HF include pressure overload and/or volume overload. Typically, the effects on cardiac morphology depend on whether the model induces pressure or volume overload. In pressure overload models, concentric hypertrophy is a common consequence, while volume overload models often produce eccentric hypertrophy (Pitoulis & Terracciano, 2020). One of the most common methods to induce pressure overload is with transverse aortic constriction (TAC), in which a band is placed around the transverse aorta, constricting blood flow and increasing left ventricular pressure **(**Milani-Nejad & Janssen, 2014). A common method to induce volume overload is by creating an arteriovenous fistula. In this method, the infrarenal aorta is punctured into the vena cava using a needle. The needle is removed and the aortic puncture site is sealed (Anderson et al., 2006)**.** As an effect of the fistula, blood

flow is shunted to right-sided circulation resulting in a rise in preload (Stern & Klemmer, 2011).

Models of hemodynamic overload have been implemented in mice (Rai et al., 2018), rats (Rungatscher et al., 2014), rabbits (Apitz et al., 2012), dogs (Kerbaul et al., 2004), sheep (Hon et al., 2001), pigs (Schmitto et al., 2009), chicks (Schroder et al., 2002), and primates (K. T. Weber et al., 1987). Hemodynamic overload models can be used to study congestive HF (Scheuermann-Freestone et al., 2001), as well as to enhance our understanding of how HF can be derived from human conditions like aortic stenosis (deAlmeida et al., 2010), aortocaval fistulas (Guzman et al., 2002), and aortic or mitral regurgitation (Magid et al., 1994; Watanabe et al., 2018).

Models of hemodynamic overload are beneficial as they closely resemble several cardiac incidents which progress to human HF. Additionally, the models are often highly tuneable, by increasing or decreasing modifiers of hemodynamic pressure or volume (Moens et al., 2009). Nevertheless, there are several limitations associated with models of hemodynamic overload. For example, the TAC model of pressure overload has been criticized for being highly variable, requiring larger sample sizes (Mohammed et al., 2012). Furthermore, the increase in hemodynamic overload inflicted in these models is often stable, which does not simulate the progressive overload that exists clinically. Lastly, most models of hemodynamic overload require proficient surgical techniques, which can be technically challenging and add stressors to the model animal.

1.2.2. Myocardial Infarction

Myocardial infarction (MI), commonly known as a heart attack, results from a coronary occlusion which disrupts blood flow to the myocardium and leads to ischemic

myocardial necrosis. Myocardial necrosis disturbs the structure and function of the myocardium and can cause sudden death (Thygesen et al., 2012). Myocardial infarction survivors are at substantial risk of developing HF due to the compromised function of the myocardium (Lewis et al., 2003). Several models exist to represent the progression of HF post-MI, including coronary artery ligation (Hood et al., 1967), microembolization (Smiseth & Mjøs, 1982), ameroid constrictors (Firoozan et al., 1999), coiling (Li et al., 2000), and cryonecrosis (Li et al., 1999). Ultimately, each model simulates an MI using surgical techniques to disrupt coronary circulation, similar to the human condition, Animal models of MI consist of canine (Eaton & Bulkley, 1981), ovine (Moainie et al., 2002), rabbit (Fujita et al., 2004), porcine (Li et al., 2000), rat (Srikanth et al., 2009), mouse (Wang et al., 2006), hamster (Zhang et al., 2021), and guinea pig (Gaide et al., 1985).

Myocardial infarctions are the most common cause of HF and, therefore, are beneficial models as they represent the progression of the majority of clinical cases (Das, 2000; Schmitto et al., 2009). For instance, the ability of angiotensin-converting enzyme (ACE) inhibitors to improve life expectancy for diagnoses of advanced congestive HF was first demonstrated by Pfeffer et al. (1985) in a rat model of coronary artery ligation. This finding was later confirmed in humans and ACE inhibitors have now become a standard clinical treatment for HF (Savarese et al., 2023; Sutton et al., 1997).

However, coronary artery ligation models of MI-induced HF have been criticized for lacking reproducibility, which is partly attributed to large variation in surgical procedures (Degabriele et al., 2004; Shin et al., 2021). Additionally, most MI-induced HF models are limited to invasive surgical interventions that do not reflect the pathophysiological

mechanisms of clinical MI, as it is often triggered by atherosclerosis (Shin et al., 2021). While catheter-based occlusions offer a non-invasive method to inflict MI, substantial variation has been discovered among studies, attributed to differences in occlusion site and duration (Garcia-Dorado et al., 1987).

1.2.3. Ischemia-Reperfusion Injury

Reperfusion is necessary to restore oxygen to the ischemic myocardium and prevent further myocardial necrosis. However, reperfusion can lead to its respective injuries, accounting for roughly 50% of the resulting myocardial infarct size in animal models (Fröhlich et al., 2013; Jennings et al., 1960). It has been shown that reperfusion leads to the generation of reactive oxygen species (ROS), intracellular Ca^{2+} overload, and mitochondrial dysfunction, which can lead to cardiomyocyte death (Frank et al., 2012; Granger & Kvietys, 2015; Halestrap, 2009). As a result, current efforts seek to further our understanding of ischemia-reperfusion (I/R) injury to improve the therapeutic potential of reperfusion and mitigate further cardiac damage following its use (Aldor et al., 2000; Flaherty et al., 1994). Additionally, I/R injury models have been utilized to study the progression of HF by inflicting cardiac damage (Chouchani et al., 2014; Smiley et al., 2014).

Ischemia-reperfusion injury models have been used in animal models like mice (Nossuli et al., 2000; Smiley et al., 2014), pigs (Garcia-Dorado et al., 1987), rats (Ciuffreda et al., 2014), canines (Velasco et al., 1991), and rabbits (Gao et al., 2013). Myocardial infarction models are commonly compared to I/R injury models as they follow similar technical procedures, differing in that I/R models remove the occlusion to allow for reperfusion. The I/R injury model of HF may possess superior clinical

translation compared to MI-induced HF due to the fact 70-85% of patients receive reperfusion therapy for MI (Cohen et al., 2010; Gharacholou et al., 2010). However, the I/R injury model is criticized for its greater variability, which is often attributed to changes in the ischaemic stimulus (Ishikawa et al., 2014; Michael et al., 1999). Furthermore, since I/R re-oxygenates the myocardium, there are smaller infarcts produced, making studying the mechanisms behind the progression of cardiac remodelling and HF following myocardial injury more challenging (De Villiers & Riley, 2020).

1.2.4. Drug-induced

Pharmaceuticals can be administered to pathologically affect cardiac function and induce HF. For example, monocrotaline has been previously used to induce pulmonary hypertension leading to a pressure overload model of HF (Guild et al., 2016; Hołda et al., 2020). Furthermore, isoproterenol has long been used to trigger cardiac dysfunction (Bourdier & Robelet, 2019; Grimm et al., 1998; Rona et al., 1959). Isoproterenol disrupts cardiac function through the activation β-adrenergic (β-AR) receptors. Chronic β-AR leads to increased HR, desensitization of β-AR receptors, and generation of ROS, which can lead to a loss of cardiac contractility and the development of HF (Belmonte & Blaxall, 2011; Murray et al., 2000; Shin et al., 2021; Shizukuda et al., 1998). Alternatively, clinical cases of drug-induced HF can be modelled using commonly prescribed pharmaceuticals, which exert cardiotoxic side effects, like amrinone, anthracycline, and cyclophosphamide (Alousi et al., 1985; Manthorpe & Svensson, 1996; Volkova & Russell, 2011).

Drug-induced HF models have been used in animal models like mice (Rau et al., 2015), rats (Grimm et al., 1998), pigs (Kim et al., 2014), sheep (Chekanov, 1999), goats

(Tessier et al., 2003), canines (Bristow et al., 1980), and rabbits (Muders et al., 1999). A benefit of drug-induced models of HF is that they are technically simple to implement and are highly reproducible within species (Muders & Elsner, 2000). Additionally, as mentioned previously, this model makes an excellent model for clinical cases of drug-induced HF by mimicking the etiology. However, there are limitations of drug-induced HF as well. One limitation is that pharmaceuticals often have widespread effects, leading to undesired secondary and nonspecific toxic consequences (Riehle & Bauersachs, 2019). Secondly, drug-induced models of HF can be limited in their relevant etiology of HF. In the example of isoproterenol models of induced HF, while chronic adrenergic activation is a prominent aspect of the development of clinical HF, it is only one aspect of how most HF progresses (Riehle & Bauersachs, 2019). Furthermore, pharmaceuticals can have extended wash-out times between treatments and lengthy metabolism periods, leading to challenges in achieving temporal precision with drug-induced models.

1.2.5. DOCA-Salt Hypertension

Deoxycorticosterone acetate (DOCA)-salt treatment is another widely used method to induce HF. In this model, DOCA is administered, leading to greater sodium and water reabsorption from the kidneys. As a result, there is an increase in blood volume and blood pressure leading to systemic hypertension (Zicha et al., 1989). This model often combines a high salt diet and a uninephrectomy to reduce kidney mass and increase hypertension pressure (Collister et al., 2018).

DOCA-salt hypertension models have been used to model HF with preserved ejection fraction (HFpEF), as this model effectively leads to hypertrophy, fibrosis, and

conduction irregularities in the absence of changes in ejection fraction (Brilla & Weber, 1992; Loch et al., 2006; Schwarzl et al., 2015). DOCA-salt treatment models of HF have been used in various animals, such as dog (Hamed & Lokhandwala, 1981), pig (Schwarzl et al., 2015), rabbit (Ayitey-Smith & Kalsner, 1977), mouse (Cao et al., 2019) and rat (Ammarguellat et al., 2001).

A major benefit to the DOCA-salt model is that salt sensitivity is a crucial predisposition to the development of clinical hypertension. Thus, the DOCA-salt model allows for a reliable investigation of the role of sodium in the mechanisms of hypertension-induced HF (Basting & Lazartigues, 2017). However, while similar cardiac remodelling occurs in patients with hypertension-induced HF, these patients are typically not consuming salt-retaining compounds (Iyer et al., 2010). Consuming DOCA-salt has been linked to nonspecific side effects, like chronic kidney disease and cerebral microvascular inflammation (Hartner et al., 2003; Rodrigues & Granger, 2012).

1.2.6. Genetic Mutation-based

Genetic manipulation allows for the study of the genetic abnormalities underlying hereditary cardiovascular diseases and HF. While identifying genetic abnormalities cannot always translate to a therapeutic target, it can expand diagnostic capabilities and facilitate interventions at a preventative stage (Ackerman et al., 2011). Furthermore, genetic manipulations have progressed the knowledge of the molecular mechanisms behind cardiac function and dysfunction by manipulating the expression of signalling molecules and structural proteins (Olson & Schneider, 2003; Yutzey & Robbins, 2007). For instance, in one study by Arber et al. (1997), mice were genetically manipulated to be deficient in the muscle LIM protein (*MLP)* gene. As result of the deficiency, the

researchers demonstrated the disruption of the cardiomyocyte cytoarchitecture, which appeared similar to that of a dilated cardiomyopathy.

Models of genetic mutation are commonly performed in small animal models. For instance, viral vectors can be used in smaller animal models, like mice (Matsumori & Kawai, 1984) and rats (Katz et al., 2022), whereas larger animals require unfeasible amounts of viral vectors (Milani-Nejad & Janssen, 2014). Additionally, the efficiency of transgene introduction in large animals is traditionally much poorer than in rodents, leading to poorer results, more animals required, and greater ethical and financial concerns. Furthermore, smaller animals typically have short gestation periods allowing for faster development of transgenic lines (Hau & Schapiro, 2010). However, recent advancements in gene modification technology target regions of the genome with greater precision, like through site-specific nucleases, therefore allowing for genetic mutations in large animals to become more feasible (West & Gill, 2016).

A limitation of models of genetic manipulation-based HF is that models can express the mutated gene at non-physiological levels, which leads to possible consequences that would be unreflective of the genetic anomaly in a clinical setting (Habets et al., 2003). Furthermore, genetic manipulation can lead to unwanted off-target consequences that can stimulate pathogenic editing, the production of toxic substances, or cancerous cells (Cao et al., 2021; de Graeff et al., 2019). Additionally, the challenges in implementing genetic manipulations in larger animal models makes it difficult to study the mechanisms of more physiologically representative models of human HF, thus, impacting the clinical translation of these models (Hornyik et al., 2022). Lastly, in transgenic and gene knock-out models, genetic modifications are implemented during

embryonic development, which poses challenges for modelling the progression of HF experienced in human adulthood (Fan et al., 2005). However, current genetic technological advances have permitted temporally controlled genetic manipulations, advancing the potential for models of genetic modifications in adults (Parlakian et al., 2005).

1.2.7. Tachypacing

Whipple et al. (1962) first developed the tachypacing-induced model of HF in canine models and it continues to be used in numerous animal models to date (Finckh et al., 1991; Gao et al., 2018; Mazumder et al., 2004; Spinale et al., 1990). Across species, tachypacing-induced models of HF have demonstrated numerous characteristics indicative of human HF, like declined contractility, increased neurohormonal signalling, β-AR desensitization, and various cardiac cellular and molecular remodelling (Briston et al., 2011; Riegger & Liebau, 1982; Shannon et al., 1991; Spinale et al., 1998; Zellner et al., 1991). In particular, chronic tachypacing has demonstrated its ability to repeatedly cause dilated cardiomyopathy (DCM), the third most common cause of HF, characterized by chamber dilation and wall thinning (Maron et al., 2006).

While the exact mechanisms of tachypacing-induced HF are not well understood, several studies have provided evidence that chronic tachypacing leads to hemodynamics changes (Tomita et al., 1991), a depletion of energy stores (Coleman et al., 1971), oxidative stress (Yamamoto et al., 2006), and ischemia (Spinale, Tanaka, et al., 1992). A summary of the proposed mechanisms of tachycardiomyopathy was obtained from Raymond-Paquin et al. (2018) (Fig. 1).

Hemodynamic alterations are believed to commence as early as 24 hours after tachypacing (Ellis & Josephson, 2013). Rapid pacing leads to an increase in filling pressures, and systolic and diastolic dysfunction (Howard et al., 1991; Tomita et al., 1991). For instance, tachypacing leads to less time in diastole, which reduces ventricular filling and stroke volume, thus, decreasing cardiac output (Strafford, 2006).

Additionally, sustaining rapid beating rates increases the metabolic requirements. However, due to the hemodynamic dysfunction, these demands are more challenging to meet. As a result, there is a discrepancy between metabolic supply and demand (Cardin et al., 2008; Raymond-Paquin et al., 2018). Studies of tachypacing-induced HF have revealed a decline in myocardial energy stores, an increase in enzymes of metabolic oxidation, and mitochondrial dysfunction and damage (Coleman et al., 1971; Langenbacher et al., 2020; O'Brien et al., 1990; Spinale et al., 1990).

Furthermore, myocardial ischemia has been another proposed mechanism behind the progression of tachypacing induced HF, which has been supported with evidence of coronary capillary vasculature remodelling and a decline in myocardial blood flow (Spinale et al., 1992). However, this mechanism requires more conclusive support as it is unknown whether the vasculature remodelling leads to ischemia or is driven by the increased metabolic demand (Ellis & Josephson, 2013).

Lastly, in response to the hemodynamic impairments and an increase in metabolic demands, there is an increase in neurohormonal signalling, including adrenergic activation, RAAS, endothelin, and the natriuretic peptides. Endothelin, adrenergic and RAAS activation improve cardiac output through peripheral arterial vasoconstriction, enhanced contractility, and an increase in salt and water retention (Hartupee & Mann,

2017; Marín-García et al., 2002; Redfield et al., 1993). The increase atrial and ventricular wall stretch leads to the activation natriuretic peptides to regulate blood pressure through vasodilation and diuresis (Song et al., 2015). However, when neurohormonal activation is sustained in chronic tachycardia, it can lead to pathological effects. For instance, chronic adrenergic stimulation from tachycardia has produced β-AR receptor desensitization, and an uncoupling of the β-AR from the intracellular components of the β-AR system which reduces adrenergic signalling and contractile reserve (Burchell et al., 1992; Spinale et al., 1994; Tanaka et al., 1993).

Tachypacing-induced models of HF have been implemented in the dog (Gao et al., 2018), sheep (Byrne et al., 2002), pig (Citerni et al., 2020), rabbit (Shimano et al., 2008), rat (Finckh et al., 1991) and mouse (Hulsmans et al., 2018). A major advantage of the chronic tachypacing model is that it generates a highly reproducible and predictable degrees of left ventricular dilation, contractile dysfunction, and neurohormonal changes (Damiano et al., 1987; Moe et al., 1988; Redfield et al., 1993). The predictability and reliability of the tachypacing-induced model allows it to be a suitable candidate for studies of translational medicine and the development of potential therapeutics (Lionetti et al., 2005; Trochu et al., 2003). A disadvantage of this model is that it is limited to modelling DCM, as the observed myocardial structure resulting from chronic tachypacing is different than how HF progresses from other etiologies, like ischemic injury or volume overload (Dixon & Spinale, 2009). Lastly, chronic tachypacing is typically achieved through the implementation of an electronic pacemaker, which involves a surgical procedure that can be strenuous for the animal (Quill et al., 2010).

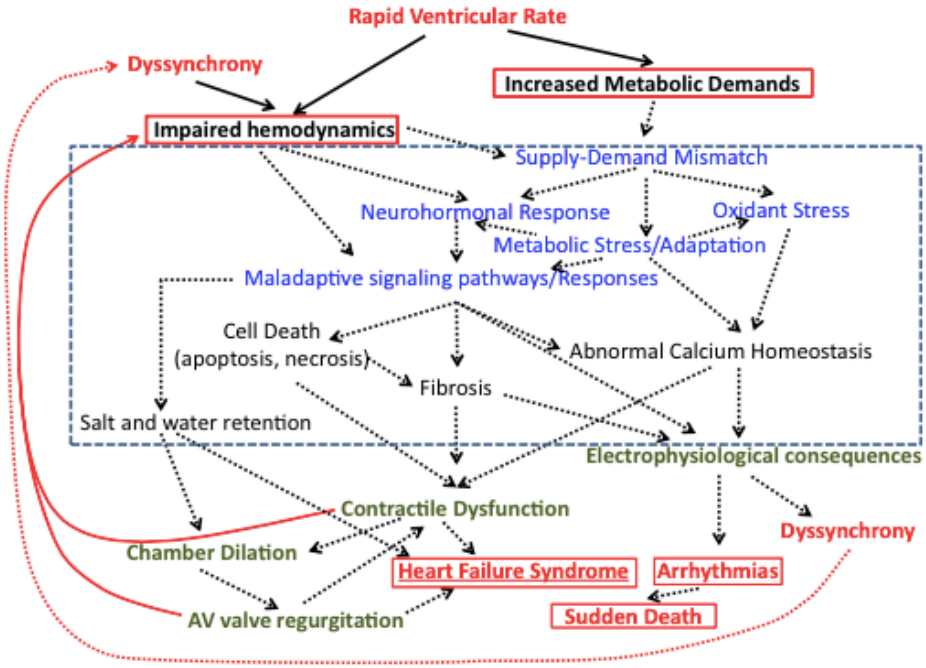

Fig. 1. A summary of the proposed mechanisms of tachycardiomyopathy. The figure was obtained from Raymond-Paquin et al. (2018). It is believed that that chronic tachypacing leads to hemodynamics change and an increase in metabolic demands. As a result, there is an energetic supply and demand mismatch and chronic neurohormonal signalling, both of which contribute to the pathological remodelling and heart failure syndrome.

1.3. Zebrafish as a Model Organism for Cardiac Research

Within the last few decades, zebrafish have become an increasingly popular model species for cardiovascular research and studies of HF (Bakkers, 2011). The relevancy of the zebrafish model is attributed to its physiological similarities to the human heart, technical simplicity, and capabilities for genetic mutation-based studies (Giardoglou & Beis, 2019). However, there are drawbacks to the use of zebrafish, including their ectothermic regulation of body temperature, duplicated genome, and differences in cardiac morphology, ion channel orthologues, and calcium handling.

1.3.1. Advantages

A major attraction of zebrafish models is their simplicity for genetic manipulations. The zebrafish genome is entirely sequenced and it is reported that 69% of its protein-coding genes are orthologs to the human genome (Howe et al., 2013; Sassen & Köster, 2015). Furthermore, zebrafish embryos are fertilized externally, which is ideal for the creation of transgenic or knock-out lines (Culp et al., 1991).

An additional benefit to the use of zebrafish is the simple handling and housing. Zebrafish are small animals that can be stored in large volumes in small spaces. For instance, as many as 30 adults can be housed in a tank, similar to the size of typical cage for a single mouse (Gut et al., 2017). Furthermore, a single breeding of zebrafish can produce hundreds of offspring per mating, providing the potential for large sample sizes, which is particularly beneficial when establishing transgenic lines (Castranova et al., 2011).

Another main advantage to the use of zebrafish in cardiac research is the similarities between zebrafish and human cardiac electrophysiology. Remarkably, the zebrafish

ventricular cardiomyocyte action potential has a similar morphology to humans with both species demonstrating a long plateau phase (Ravens, 2018). The action potential acquires its distinctive morphology through the underlying activity of ion channels that permit depolarizing and repolarizing currents. The human ventricular cardiomyocyte action potential can be divided into five characteristic phases, and the zebrafish demonstrates each phase with the exclusion of phase one. Phase one is produced by the cessation of the inward sodium current and the activation of the transient outward current (I_{to}); in zebrafish I_{to} is believed to not be present (Nemtsas et al., 2010)

Interestingly, zebrafish can regenerate damaged cardiomyocytes and have been used to study the mechanisms behind cardiac regeneration (Schnabel et al., 2011). Understanding the cellular and molecular processes behind cardiac regeneration is of interest, as it could aid in developing regenerative therapeutics to prevent the progression of HF following cardiac damage or MI. However, this unique feature may also pose as a limitation for the use of zebrafish, as their regenerative capacity could impede the progression of HF in experimental models.

1.3.2. Limitations

A principal limitation of using zebrafish for cardiac research is its anatomy. The zebrafish has a two-chambered heart consisting of one atrium and one ventricle, which contrasts the four-chambered heart of humans (Farrell & Pieperhoff, 2011). Furthermore, zebrafish are ectothermic (Haesemeyer, 2020). As a result, heart rate, and cardiac action potential duration and ion channel function depend on external temperature (Denvir et al., 2008; Haverinen et al., 2021; Nemtsas et al., 2010). The

ectothermic physiology of zebrafish is unrepresentative of the human endothermic condition and requires temperature-controlled experiments to reduce variability.

Furthermore, the zebrafish belongs to the teleosei infraclass, in which the ancestor of the teleosei experienced a whole-genome duplication (Amores et al., 1998, 2011). Whole-genome duplication can lead to subfunctionalization, in which genetic copies divide ancestral gene function by assuming subfunctions. Furthermore, whole-genome duplication can produce neofunctionalization, where one genetic copy preserves its ancestral purpose while the other obtains a different function (Force et al., 1999). As a result of the asymmetrical evolution that occurs after whole genome duplication, the duplicated genome of the zebrafish complicates genetic comparisons to humans, whereby non-orthologue genes may control certain genetic functions, or gene orthologues may have only resumed partial ancestral gene function. For instance, differences in the composition of cardiac ion currents between zebrafish and humans can be partly attributed to various currents within the zebrafish produced by non-orthologous, like those originating from paralogous genes (Vornanen & Hassinen, 2015).

Lastly, there are notable differences in cardiac Ca^{2+} handling between zebrafish and humans (van Opbergen et al., 2018). Zebrafish cardiomyocytes do not possess transverse tubules, a critical element of the mammalian heart's excitation-contraction coupling, which disperses electrical activity throughout the cardiomyocyte and facilitates close interactions between the ryanodine receptors (RyR) of the sarcoplasmic reticulum to the sarcolemma (Brette et al., 2008). Furthermore, the RyRs of the zebrafish sarcoplasmic reticulum has minimal sensitivity to calcium-induced calcium release

(Bovo et al., 2013). Consequently, the zebrafish relies on the calcium channels within the sarcolemma for the production of the majority of calcium transients (Bovo et al., 2013). Similar to mammalian cardiomyocytes, calcium efflux is predominately regulated through the use of the sodium-calcium exchanger at the sarcolemma (van Opbergen et al., 2018).

1.3.3. HF Models

Due to the advantages of the zebrafish cardiac model, numerous models of HF have been implemented within this species. Their genetic manipulability has permitted several genetic mutation-based HF models, including cardiac hypertrophy, dysfunction, remodelling, and dilated cardiomyopathies (Y. Chen et al., 2013; Fang et al., 2020; Gu et al., 2017). Furthermore, various models of drug-induced HF have been implemented within the zebrafish. In a recent study by Kossack et al., (2017), HF was induced in both adult and embryonic zebrafish through the chronic administration of isoproterenol. However, the findings of this study specified that the adult zebrafish better modelled the human condition for isoproterenol-induced HF. Given the many benefits of the use of larval zebrafish for cardiac modelling, the study indicated a need to investigate alternative methods to chronically induce HF in the larvae.

For a model of HF in zebrafish, irregular cardiac structure**,** morphology, and cardiac function must be demonstrated (Narumanchi et al., 2021). Functional assessments observe cardiac changes in heart rate and rhythm, stroke volume, diastolic and systolic function, ejection fraction, and fractional shortening (Fink et al., 2009; Milan et al., 2003; Paavola et al., 2013; Sun et al., 2017). HF in zebrafish can lead to changes in cardiac structure and morphology, like hypertrophy, chamber dilation and wall thinning, and

changes in myofibril organization (Shi et al., 2020; Shimizu et al., 2017; Tsoupri & Capetanaki, 2013; Xu et al., 2002). Another strong indication of HF in zebrafish is changes in expression of biochemical markers of HF. The most recognized biomarkers of HF include atrial natriuretic peptide (ANP) and brain natriuretic peptide (BNP), which are expected to increase during HF within zebrafish (Becker et al., 2012; Shi et al., 2017). Additional support for the establishment of HF in zebrafish includes the demonstration of pericardial edema, tachypnea, inability to exercise, and an increased mortality (Narumanchi et al., 2021; Wang et al., 2011).

1.3.4. The Use of Larval Zebrafish

Larval zebrafish provide an additional advantage of an optically transparent appearance. Therefore, the larvae permit non-invasive *in vivo* studies of physiological functions like cardiac activity (Bakkers, 2011). Furthermore, their transparent appearance, small size, and large breeding clutches make larval zebrafish highly beneficial for high-throughput phenotypic assays in pharmaceutical testing (Patton et al., 2021). High-throughput phenotype-based screens have traditionally been restricted to cell culture models. While cell culture-based drug screening has provided important innovations, the model lacks the physiological aspects of studies in the whole organism. The larval zebrafish offers the unique opportunity for *in vivo* high-throughput pharmaceutical testing, where for example, rapid and automated imaging and analysis could be performed, for potentially more clinically relevant results (Lubin et al., 2021).

A limitation of the use of larval zebrafish for studies of HF is that the model species is undergoing cardiac development. Consequently, results could become confounded with developmental disturbances that are inconsistent with the mechanisms of HF

development in the adult heart. However, while HF is predominately a condition observed in adults, the condition can also exist in developing hearts. Pediatric HF can be caused by a plethora of disorders, for instance, shunting abnormalities, congenital heart defects, cardiac malformations, and arrhythmias (Davey et al., 2012). The most prevalent tachyarrythmia in infants is a supraventricular tachycardia, which can even develop prenatally (Kothari & Skinner, 2006). When supraventricular tachycardias are sustained, a dilated cardiomyopathy can result as well as symptoms of congestive heart failure (Paul et al., 2000). Larval zebrafish can then provide an opportunity for models of pediatric HF, where in the example of a supraventricular tachycardia, larvae can undergo rapid atrial pacing.

1.3.5. Larval Zebrafish Cardiac Development

Larval zebrafish have their initial heartbeat at roughly 1 dpf (Battista et al., 2019). During this stage of development, the heart exists as a singular tube, with an absence of valves and no clear distinction between the atrium and the ventricle (Stainier, 2001). At 1 dpf, a primitive sinoatrial node is present, and cardiac conduction travels in a linear pattern within the heart tube, flowing from the atrium to ventricle (Tu & Chi, 2012). The distinction of the chambers begins around 1.5 dpf, when the chamber ballooning commences, and the atrium and ventricle expand (Dietrich et al., 2014). Additionally, cardiac contraction transitions from peristaltic waves to sequential chamber contractions (Lindsey et al., 2014).

At 2 dpf, initial cardiac looping begins, where the heart forms an S-shape with the ventricle to the right of the atrium (Chen et al., 1997). At this stage, the chambers have morphologically assembled, and the atrioventricular conduction delay has been reported

(Sedmera et al., 2003). Furthermore, endocardial cushions form, which are the predecessors to the septal walls and the valves (Battista et al., 2019; Haack & Abdelilah-Seyfried, 2016).

By 3 dpf, trabeculation begins to develop within the ventricle, which results in the development of cardiac conduction throughout this chamber (Chi et al., 2008). Zebrafish lack specialized Purkinje fibers, and as a result, rely on trabeculation to disperse the electrical activity throughout the ventricle (Sedmera et al., 2003). Additionally at 3 dpf, primitive atrioventricular valve leaflets have formed which prevents retrograde blood flow (Scherz et al., 2008). Furthermore, at 3 dpf, the sinoatrial node matures and becomes confined to the dorsal right region of the atrium (Martin & Waxman, 2021).

After 4 dpf, the valves have a similar appearance to the adult valves, containing both a superior and an inferior valve leaflet, however, the development of the valves is reportedly completed by roughly 16 dpf (Martin & Bartman, 2009; Scherz et al., 2008). By 5 dpf, there is the final cardiac rotation, whereby the atrium migrates deeper into the thoracic cavity and shifts posterior to the ventricle, meanwhile the ventricle repositions from a right-side to medial location (Singleman & Holtzman, 2012). After which, the chambers are in their final orientation in the pericardial cavity. The cardiac chambers continue to develop into adulthood, which is reached at roughly 90 dpf (Poon & Brand, 2013). As the chambers mature, the coronary arteries develop within the subepicardium to vascularize the myocardium (Harrison et al., 2015).

1.4. Optogenetics

Optogenetics refers to the expression of light-sensitive proteins. Optogenetic tools consist of sensors and actuators. Optogenetic sensors are genetically encoded

fluorescent sensors that can monitor changes in membrane potential and ion movement (Tantama et al., 2012). For instance, genetically encoded calcium indicators (GECI) utilize calmodulin as a calcium-sensing element to fluorescence when associated with intracellular calcium (Miyawaki et al., 1997). Fluorescent signals can then be detected to indicate changes in calcium transients.

Optogenetic actuators use light-sensitive ion channels (opsins) to alter membrane potential and cellular activity (Guru et al., 2015). Channelrhodopsin-2 (ChR2) is an opsin excited by blue light and is derived from the microalgae *Chlamydomonas reinhardtii*. Channelrhodopsin-2 is a non-specific cation channel with a reversal potential of 0 mV, and therefore, at resting membrane potential, it can depolarize cardiomyocytes (Keshmiri Neghab et al., 2021; Nagel et al., 2003). Anion channelrhodopsin-1 (ACR1) is an opsin that can also depolarize cardiomyocytes at resting membrane potential; however, it does so through the selection of different ions. Specifically, ACR1 is selective for the chloride, which has a reversal potential of -40 to -30 mV (Clemo et al., 1999; Kopton et al., 2018). Anion channelrhodopsin-1 also differs from ChR2 in that it is derived from the algae *Guillardia theta* and is excited by green light (Govorunova et al., 2015; Liu et al., 2023).

1.4.1. Cardiac Optogenetics

Initially, optogenetic actuators were implemented in neurons to stimulate an action potential and manipulate neuronal activity (Boyden et al., 2005). However, within the last decade, optogenetic actuators have been used in cardiomyocytes, providing a tool with high spatial and temporal precision to control cardiac activity (Arrenberg et al., 2010; Entcheva & Kay, 2021). Optogenetic actuators can be used to modulate cardiac

action potential morphology, induce bradycardia or tachycardia, and simulate atrioventricular blocks and cardiac arrest (Ambrosi et al., 2014; Arrenberg et al., 2010; Park et al., 2014).

1.4.2. Cardiac Optogenetics in Zebrafish

Due to their genetic accessibility and electrophysiological relevance, zebrafish have been used as a model species for studies of cardiac function using optogenetics (Arrenberg et al., 2010; Kopton et al., 2018). The transparent nature of larval zebrafish provides an additional benefit for studies of cardiac optogenetics in which stimulation can be accomplished *in vivo* (Baillie et al., 2021; van Opbergen et al., 2018).

A study by Arrenberg et al. (2010) first demonstrated the potential for optogenetic actuators in larval zebrafish. This study investigated the use of halorhodopsin (NpHR) and ChR2. Using NpHR, the researchers tracked the development of the pacemaker region within developing larval zebrafish. Additionally, the study demonstrated the capabilities to manipulate heart rate and rhythm using ChR2.

Furthermore, a recent study by Kopton et al. (2018) demonstrated the potential for the use of GtACR1 by comparing and contrasting its effects in isolated rabbit cardiomyocytes, and adult zebrafish hearts. In this study, the researchers demonstrated that sustained illumination of GtACR1 could depolarize or repolarize the heart, depending on the phase of the action potential (*i.e.*, systole or diastole), and in extreme cases, sustained illumination inhibit electrical activity. Furthermore, the researchers demonstrated that pulsed light of supra-threshold intensity could be used to optically pace the heart.

1.4.3. Optogenetic-based Tachypacing-induced HF

In recent work by Lemme et al. (2019) and Lemoine (2020), optogenetic tachypacing was administered chronically to human induced pluripotent stem cell-derived cardiomyocytes (hiPSC-CMs) to demonstrate its capabilities as a tachypacing-induced model of HF. In the first study by Lemme et al. (2019), ventricular-like hiPSC-CMs expressing ChR2 were optogenetically tachypaced for three weeks. As a result, faster contraction kinetics were induced and vulnerability to tachycardia was increased. In the second study by Lemoine (2020), atrial-like hiPSC-CMs expressing ChR2 were similarly tachypaced for three weeks, leading to electrical alterations consistent with that of atrial fibrillation and arrhythmic spontaneous beating patterns.

While the two studies discussed above pioneered models of optogenetic tachypacing-induced HF, there are physiological limitations of a hiPSC-CM model. Without the whole organism, the use of hiPSC-CM lacks relevant mechanisms important for the progression of HF, such as hemodynamic and autonomic factors. Therefore, the previous studies highlight the need to characterize optogenetic tachypacing-induced HF in whole animal studies.

1.5. Goal and Hypothesis

The goal of my work was to establish an *in vivo* model of chronic optogenetic tachypacing-induced HF in larval zebrafish. To evaluate the effects of optogenetic tachypacing, I used two opsins, ChR2 and ACR1. Comparing the effects of these two opsins allowed me to gain insight regarding effects related to the passage of their respective ions. I hypothesized that chronic optical tachypacing will lead to cardiac remodeling on the structure, function, and gene expression of the heart would depend

on the mode of optogenetic stimulation, including: (i) the developmental period of stimulus application; (ii) the opsin used; and (iii) continuous *versus* interval pacing.

Chapter 2: Methods

2.1. Ethics Statement

The use of zebrafish within this study followed the approved ethical guidelines granted by the Dalhousie University Animal Care Committee and followed the recommendations of the Canadian Council on Animal Care for the housing and handling of zebrafish.

2.2. Zebrafish Husbandry

Zebrafish embryos from 0-7 days post-fertilization (dpf) were used for this study. The embryos were housed in a temperature-controlled incubator at 28 °C for the duration of the experiment. The embryos were placed in E3 embryo medium (0.17 mM KCl, 5 mM NaCl, 0.4 mM $CaCl_2$, and 0.16 mM $MgSO_4$, pH 7.2, 10-5% Methylene Blue) and the medium was changed daily.

2.3. Transgenic Zebrafish Lines

Humanized ChR2 (hChR2) was expressed in cardiomyocytes of *casper* zebrafish using the tol2 transposase system by Sara Rafferty (Rafferty & Quinn, 2018). The plasmid was created using hChR2 combined with an eYFP (enhanced yellow fluorescent protein) reporter (pME-hChR2(H134R)-eYFP), provided by Dr. Karl Deisseroth (Stanford University, Boston, Massachuetts, USA), a cardiac myosin light chain-2 promotor (p5E-cmlc2) obtained from Dr. Ian Scott (University of Toronto, Ontario, Canada). The myosin light chain promotor allowed for the expression of the opsin in the cardiomyocytes of the heart. A p3E-polyA and pDestTol2 acquired from Dr. Jason Berman (Dalhousie University). The plasmid was injected into zebrafish embryos at the one-cell stage. At 2-3 dpf, injected embryos were screened for eYFP

fluorescence in cardiomyocytes and assessed for a response to light stimulation. Responsive embryos were raised to adulthood and out-crossed for two generations before use.

To generate GtACR1-expressing transgenic zebrafish, a multisite Gateway system for Tol2 transposon transgenesis was utilised by Sara Rafferty (Rafferty & Quinn, 2018). The 5′ entry plasmid p5E-cmlc2, 3′ entry plasmid p3E-polyA, destination plasmid pDestTol2pA2, and donor plasmid pME-TA were provided by from Dr. Jason Berman (Dalhousie University). The middle entry plasmid was generated by confirming the sequence of L13_CMV_GtACR1-eGFP using primers CMV_Forward: 5′-CGCAAATGGGCGGTAGGCGTG-3′ and EGFP-C-REV: 5′-GTTCAGGGGGAGGTGTG-3′. Polymerase chain reaction (PCR) using primers for GtACR1: 5′-GCCACCATGAGCAGCATTAC-3′ and EGFP-stop_rev: 5′-TTTACTTGTACAGCTCGTCCAT-3′ was performed, and the GtACR1-eGFP PCR product was purified using a G QIAEX II Gel Extraction Kit (Qiagen, Hilden, Germany). The purified product was combined with a polyA (pA) tail and was ligated to pME-TA to generate the resulting middle entry plasmid pME-GtACR1-eGFP-pA. The expression plasmid was produced by ligating p5E-cmlc2, p3E-polyA and pME-GtACR1-eGFP-pA with pDestTol2pA2. Confirmation of the resulting expression plasmid was confirmed by restriction digest analysis and sequencing. The plasmid was purified with a PCR Purification Kit (Qiaquick, Qiagen, Venlo, Netherlands) and was then injected into the zebrafish embryos at the one-cell stage. Injected embryos were screened for enhanced green fluorescent protein (eGFP) fluorescence and response to light stimulation. Responsive embryos were raised and out-crossed for two generations prior to use.

2.4. Zebrafish Screening

Prior to the use of embryos for experimentation, 2 dpf zebrafish embryos were screened for the expression of the ChR2-eYP and ACR1-eGFP using a Stereo Discovery V20 microscope (Zeiss, Oberkochen, Germany) to assess the presence of their fluorescent reporter eYFP or eGFP, respectively. Embryos with similar fluorescence and normal cardiac morphology were selected for the experiment.

2.5. Optogenetic Stimulation

2.5.1. Control of Light Stimulus

A high voltage light emitting diode (LED) controller was created by Ahmed Ramadan (a fellow graduate student in the lab), to control the optogenetic light stimulus delivery. In brief, the controller consists of two Nano series microcontrollers (Arduino, Turin, Italy), an LMC 555CN complementary metal oxide semiconductor camera (CMOS) timer (Texas Instruments, Dallas, Texas, USA), TIP-122 transistor (STMicroelectronics, Geneva, Switzerland), and an output liquid crystal display (LCD) screen (Elegoo, Shenzhen, China). The LED controller was programmed using Arduino software. The LED controller was connected to the LEDs used for this study. Two wavelengths of LEDs were selected according to the excitation wavelengths of ChR2 (457 nm, LZ4-00B208 LED Engin, San Jose, California, USA) and ACR1 (525 nm, LZ4-00G108, LED Engin).

2.5.2. Assessment of Pacing Capturing of Larval Zebrafish

The zebrafish larvae were exposed to pulsed light with a 5 ms pulse duration at a range of frequencies from 2.5-8 Hz to determine the ability to pace the hearts. The ability to pace was assessed in both ChR2- and ACR1-expressing larvae at 2-7 dpf. The

larvae were anesthetized prior to recordings using 3% Tris-buffered tricaine solution (0.45 mM, pH 7.4; Tris: BP152, Fisher Scientific, Waltham, MA; tricaine: MS-222, Sigma-Aldrich, St. Louis, MO). Cardiac recordings were performed *in vivo* by placing samples in a 3.5 cm diameter petri-dish with 3% methyl cellulose, which was used to keep larvae in a stable position where the heart could be observed. The petri-dish was then placed in a temperature-controlled chamber (Medical Systems Corporation, Greenvale, New York, USA), which allowed experiments to be conducted at 28 °C. Recordings were captured by a CMOS camera (DMK 23UP-1300, The Imaging Source, Charlotte, NC) coupled to an Olympus SZ61 stereomicroscope (Olympus, Shinjuku-ku, Tokyo, Japan) using IC Capture software (The Imaging Source). The LED at the excitation wavelength of the opsin was placed beneath the sample and focused on the diameter of the petri-dish. The LED was set to pulse at the given frequency, and the camera recorded the cardiac activity of the larvae. The recordings were slowed to be visually inspected to determine if larval zebrafish hearts were captured. Successful capturing was determined by consistent cardiac contraction following each light stimulation.

2.5.3. Protocol for Chronic Optogenetic Tachypacing

Larval zebrafish were placed into 6-well plates at densities of 15 larvae per well and were housed in an incubator at 28 °C. LEDs were placed beneath each of the well plates. The LEDs were focused on the circumference of the wells and a plexiglass stage was constructed to hold the 6-well plate at this distance (with the help of Ahmed Ramadan). The optimal frequency of light stimulus was determined to be 4.7 Hz, which was delivered for five days. To manipulate the developmental period of application,

experiments began at either 2 dpf or 3 dpf. Opsin-specific effects were assessed by comparing the effects of chronic tachypacing in ChR2 and ACR1-expressing larvae. To assess changes in on/off cycle timing, we compared the effects of continuous and interval pacing, in which trains of light stimuli were applied for 15 seconds, followed by 15 seconds without light, in accordance with the methods of chronic ChR2 stimulation performed by Lemme et al. (2019). A graphical summary of the protocol for chronic optical pacing, and assessment of cardiac function, morphology, and mRNA expression is demonstrated in Fig. 2 and 3.

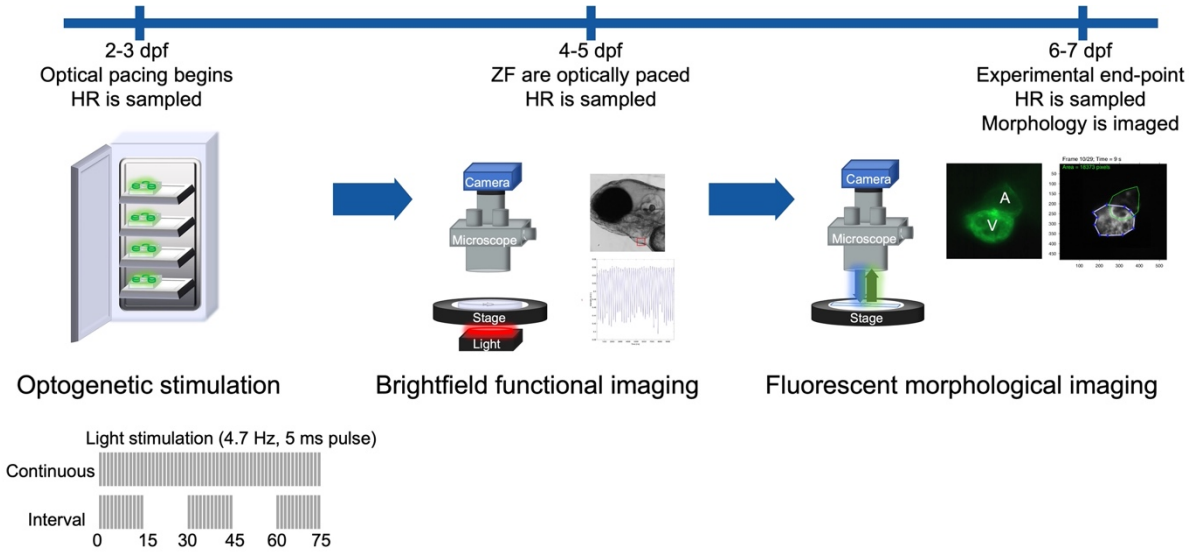

Fig. 2. Graphical summary of the pacing protocol for chronic optical stimulation, and assessment of cardiac function and morphology. At 2 or 3 dpf, larval zebrafish were placed into a temperature-controlled incubator to allow for the chronic administration of the optical stimulus. Larvae were paced for 5 days, using either continuous or interval pacing. At each day, larvae were sampled for changes in resting heart rate using brightfield microscopy. At the experimental endpoint of either 6 or 7 dpf, the resting heart rate was recorded, and samples were euthanized and fixed for fluorescent microscopy to observe changes in cardiac morphology.

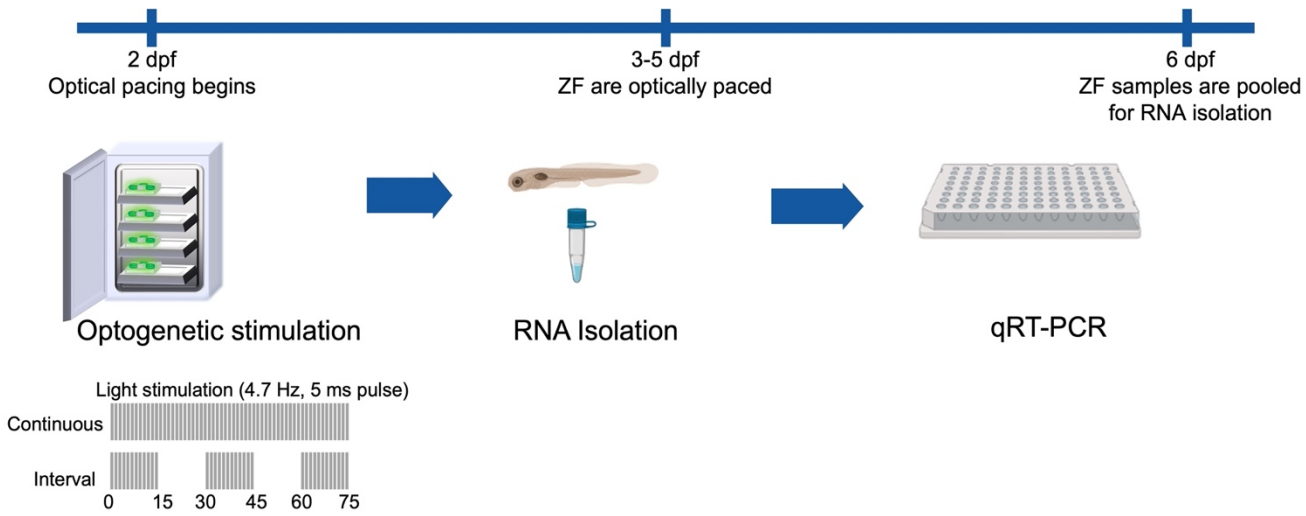

Fig. 3. Graphical summary of the pacing protocol for chronic optical stimulation and assessment for changes in mRNA expression. At 2 dpf, larval zebrafish were placed into a temperature-controlled incubator to allow for the chronic administration of the optical stimulus. Larvae were paced for 5 days, using either continuous or interval pacing. At 6 dpf, RNA was isolated from a pool of 40 larvae. The RNA was then converted into cDNA for the use of qRT-PCR.

2.6. Bright-field Microscopy of Cardiac Function

Recordings of resting heart rate were obtained each day over the 5-day experiment. Three control groups were used to assess the effects on resting heart rate. The first control was opsin-expressing larvae not exposed to the light stimulus, the second was a Myl7:eGFP (*casper*) expressing larval zebrafish exposed to light, and lastly a Myl7:eGFP (*casper*) expressing larvae not exposed to light. To obtain recordings of resting heart rate, a Labophot-2 fluorescence microscope (Nikon, Tokyo, Japan) was used with a 2.5X, 0.08 NA objective (Zeiss) to focus on the heart. A 640/20 excitation filter (ET640/20m, Chroma Technology; Bellows Falls, Vermont, United States) was placed over the top of the light source to utilize red-shifted light and avoid activating the opsins.

Heart rate measurements were obtained using a CMOS camera (DMK 23UP-1300, The Imaging Source) and IC Capture software (The Imaging Source). Cardiac recordings were performed *in vivo* by placing sedated larval zebrafish in a 3.5 cm diameter petri-dish with 10 μL of E3 medium. The petri-dish was placed in a temperature-controlled chamber (Medical Systems Corporation) at 28 °C. The recordings were then analyzed using custom MATLAB (Math Works, Natick, USA) routines that allow for the determination of heart rate based on the change of intensity within a region of interest placed over the heart.

2.7. Fluorescent Microscopy of Cardiac Morphology

Following measurement of heart rate, the larvae were euthanized in tricaine (0.2 g/L). The tricaine was removed from the samples, which were then fixed overnight at 4°C in 4% paraformaldehyde (PFA). Embryos were washed 3 x 10 minutes in PBS and

3 X 5 minutes in 100% methanol and stored at -20°C. Fixed samples were imaged using a fluorescent microscope (Eclipse 80i, Nikon). The fluorescent microscope was focused on the heart with a 40X, 0.75 NA objective (Plan Fluor, Nikon). A super high-pressure mercury lamp (HB-10101AF, Nikon) was used to produce fluorescent light, which was filtered to the excitation wavelength of YFP and GFP using 480/40 nm excitation (HQ480/40x, Chroma Technology), 506 nm dichroic (FF506-Di03-25x36, Semrock, Rhochester, New York, USA), and 535/50 nm emission (HQ535/50m, Chroma Technology) filters. A CMOS camera (DFK 33UP-1300, The Imaging Source) and IC Capture software (The Imaging Source) were used to obtain images of the heart. The recordings were then analyzed using a custom MATLAB (Math Works) program that allowed for tracing of the atrium and ventricle to measure pixel area, which was converted to μm^2 by using a stage micrometer to determine the scale (μm/pixel) at the magnification of our recordings.

2.8. qRT-PCR

2.8.1. RNA Isolation

RNA was extracted from 40 pooled embryos using the RNeasy Plus Mini Kit (Qiagen) according to the manufacturer's instructions. Following RNA isolation, samples were assessed for purity and concentration using an Epoch spectrophotometer (BioTek, Winooski, Vermont, USA). Purity was evaluated by determining the $Abs_{260/280}$ ratio, and samples with ratios between 1.9-2.0 were selected for the study. Samples were examined for integrity using a Qubit 4 Fluorometer (Invitrogen, Waltham, Massachusetts, USA). Integrity was assessed by following the manufacturer's instructions for the Qubit Broad Assay and Qubit IQ Assay Kit (Invitrogen). Samples with IQ values between 8.0-10 were used to produce cDNA.

2.8.2. cDNA Synthesis

To obtain complementary DNA (cDNA), 2 μg of RNA sample was used with an Omniscript RT Kit (Qiagen) by following the manufacturer's instructions. A non-reverse transcriptase (NRT) control was produced by generating an additional sample in which the Omniscript Reverse Transcriptase was replaced with nuclease-free water.

2.8.3. Optimal Concentration of cDNA

Before collecting results from the quantitative reverse transcription PCR (qRT-PCR) assay, several parameters were optimized, such as cDNA concentration, stability of reference genes, and primer amplification efficiency. To optimize the concentration of cDNA used per reaction, we assessed the cycle threshold (Ct) values obtained from a 5-point serial dilution between 1-10 ng of cDNA.

2.8.4. Primer Amplification Efficiency

A 4-5-point 10-fold serial dilution curve of cDNA was used to assess the amplification efficiency of each primer pair. The Ct values were plotted as a standard curve against the respective concentration for each primer. The linear regression was determined from the standard curve. A coefficient of determination (R^2) value was determined from the linear regression, and primers with $R^2 > 0.98$ were used in this study. After obtaining the slope from the linear regression, the amplification efficiency (E) was calculated using the formula:

$$E = ((-1 + 10^{-\frac{1}{slope\ of\ the\ standard\ curve}}) \text{ x } 100))$$

Primers with efficiency values of 90-110% were selected for the study. A complete list of primers used for candidate reference genes and genes of interest can be found in Tables 1 and 2, respectively.

Table 1. List of primers used for candidate reference genes.

Gene symbol	Forward sequence	Reverse sequence
Efa1	TT CTC AGG CTG ACT GTG C	CCG CTA GCA TTA CCC TCC
Rpl13a	TCT GGA GGA CTG TAA GAG GTA TGC	AGA GC ACA ATC TTG AGA GCA
b-actin	CGA GCT GTC TTC CCA TCC A	TCA CCA ACG TAG CTG TCT TTC TG

Table 2. List of primers used for genes of interest and the protein the genes encode for.

Gene symbol	Forward sequence	Reverse sequence	Protein	Role of protein
ANP	ACA GAG ACC GAG AGG AAG	AGG GTG CTG GAA GAC CCT AT	Atrial natriuretic peptide	Responds to atrial wall stretch
BNP	CAT GGG TGT TTT AAA GTT TCT CC	CTT CAA TAT TTG CCG CCT TTA C	Brain natriuretic peptide	Responds to ventricular wall stretch
ACTA2	CCC ATC GAG CAC GGA ATC AT	AGT CCA GCA CAA TGC CTG TT	Alpha smooth muscle actin 2	Fibrosis
Myh7	TGG TGA GGG AGG AAA GAG CAT	CGC AGA ATC TTA CCC TCC TCG	Myosin heavy chain 7	Hypertrophy
Myh6	CAC CAG ACA CTG GAT G	GCT CCA AGT CCA TTC TGA C	Myosin heavy chain 6	Hypertrophy
TGF-ß1	TCA TTT CTT CGC TCA GTT CAA CAG TGC	AGC GGA TTG AGG CTA TTC GGG GT	Transforming growth factor beta 1	HF/inflammation

2.8.5. Reference Gene Stability

Cycle threshold (Ct) values obtained from 15 samples across all experimental conditions were used to determine the stability of our reference genes. The values obtained were imported to RefFinder (Xie et al., 2012), to obtain the stability analysis from the algorithms NormFinder (Andersen et al., 2004) and BestKeeper (Pfaffl et al., 2004), and the comparative delta-Ct method (Silver et al., 2006), as well as RefFinder's comprehensive ranking. A script provided for GeNorm (Perkins et al., 2012; Vandesompele et al., 2002) was then used within RStudio (RStudio Team, 2021) to assess the M value for stability, in which reference genes were determined to be stable if $M < 0.5$. The pairwise variation value with a cut-off value of less than 0.15 was used to determine the optimal number of reference genes.

2.8.6. qRT-PCR Assay

Quantitative RT-PCR was performed in a CFX-96 Real Time PCR Detection System (Bio-Rad, California, USA) with embryos from the opsin-expressing and exposed to light, Myl7:eGFP and exposed to light, and Myl7:eGFP and not exposed to light groups. Reactions were carried out in 10 μL volumes with PowerTrack SYBR Green qPCR Master Mix (ThermoFisher, Waltham, Massachusetts, USA), following the manufacturer's instructions. The standard thermocycling comprised enzyme activation at 95.0 °C for 2 minutes for one cycle, denaturing at 95.0 °C for 15 seconds, and annealing at 60°C for 60 seconds for 40 cycles. Each assay was performed with technical triplicates and with three biological repeats from independent experiments. The fold changes in expression of the genes of interest were determined using the $\Delta\Delta C_t$ method (Livak & Schmittgen, 2001).

2.9. Data Analysis

Statistical analysis was performed in Prism 9 (GraphPad). For each assessment, a one-way ANOVA was completed. If there was significant variation across the groups, a Dunnett's multiple comparison test was performed, in which each group was compared to the opsin exposed to light group. Significance was indicated by $p<0.05$.

Chapter 3: Results

3.1. Optimization of Optogenetic Stimulation

The maximal optical pacing of opsin-expressing larvae was assessed from 2-7 dpf in six fish at each day (Fig. 4, 5). The lowest average maximal optical pacing rate in ChR2 fish was found at 6 dpf with a frequency of 4.9 $\pm$ 0.2 Hz (Fig. 4B). In ACR1-expressing larvae, the lowest average maximal optical pacing rate was found at 2 dpf with a frequency of 4.2 $\pm$ 0.4 Hz (Fig. 5B). However, to produce a dilated cardiomyopathy, the heart rate imposed should be supernormal. For instance, it has been reported in the canine model that to achieve a dilated cardiomyopathy, pacing should be at least three times higher than resting heart rate (Powers & Recchia, 2018). In our model, resting heart rate at times exceeded 240 bpm (4 Hz) (Fig. 7). Therefore, to obtain a high percentage of captured larvae and also produce supernormal tachycardia to cause dysfunction, samples were chronically paced at 4.7 Hz.

To observe possible desensitization, a preliminary experiment was performed to assess for effects of continuous pacing for one hour. Two samples from each ChR2 and ACR1 were assessed from 2-7 dpf at 4.5 Hz. While most samples were successfully captured for the duration of the recording, a few samples appeared to develop inconsistent capture, which began after over 20 minutes of pacing. As a result, we investigated chronic interval pacing to reduce possible desensitization of the channels. An interval of 15 seconds on and 15 seconds off was chosen based on the results of Lemme et al. (2019) and Lemoine et al. (2020), in which ChR2-expressing engineered heart tissue was successfully chronically paced at this interval.

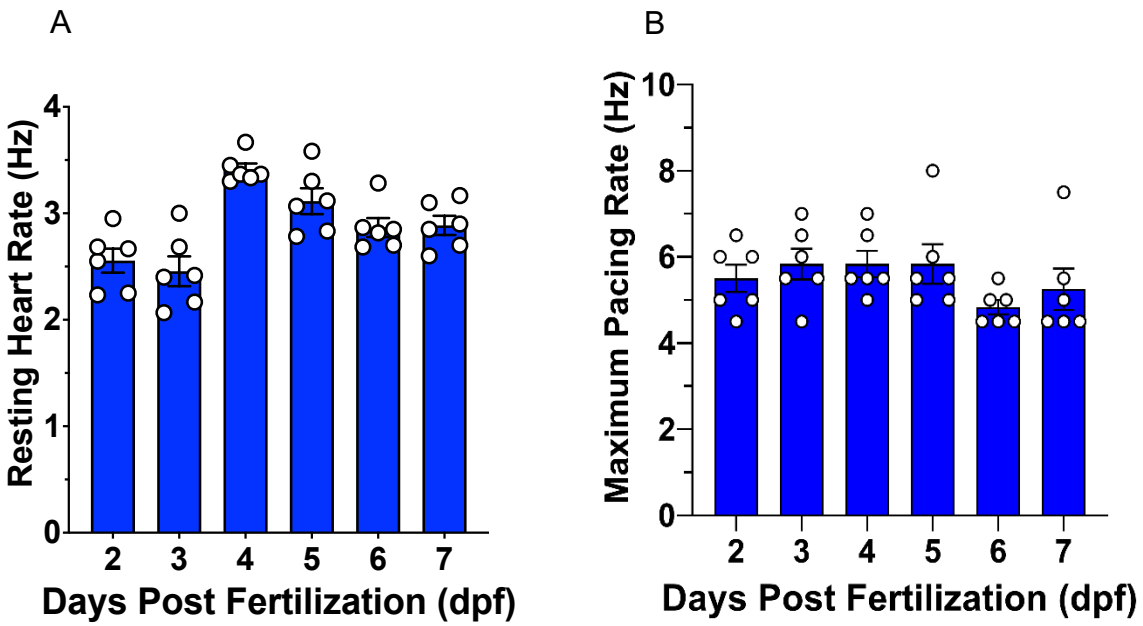

Fig. 4. (A) The average resting heart rate of ChR2-expressing larval zebrafish from 2-7 days post-fertilization (dpf) prior to the assessment of optical capturing. Error bars represent $\pm$ the standard error from the mean. Clutch size was variable for each dpf. Sample size = 6 for each dpf. (B) Average maximal pacing rate of ChR2-expressing larvae from 2-7 days post-fertilization (dpf). Larvae were exposed to a 10-second continuous stimulus. Successful capturing was determined by consistent cardiac contraction of both chambers following pulsed light stimulation. Capturing was assessed over a range of frequencies from 3.5-8.0 Hz. The lowest average maximal optical pacing rate was found at 6 dpf with a frequency of 4.9 $\pm$ 0.2 Hz.

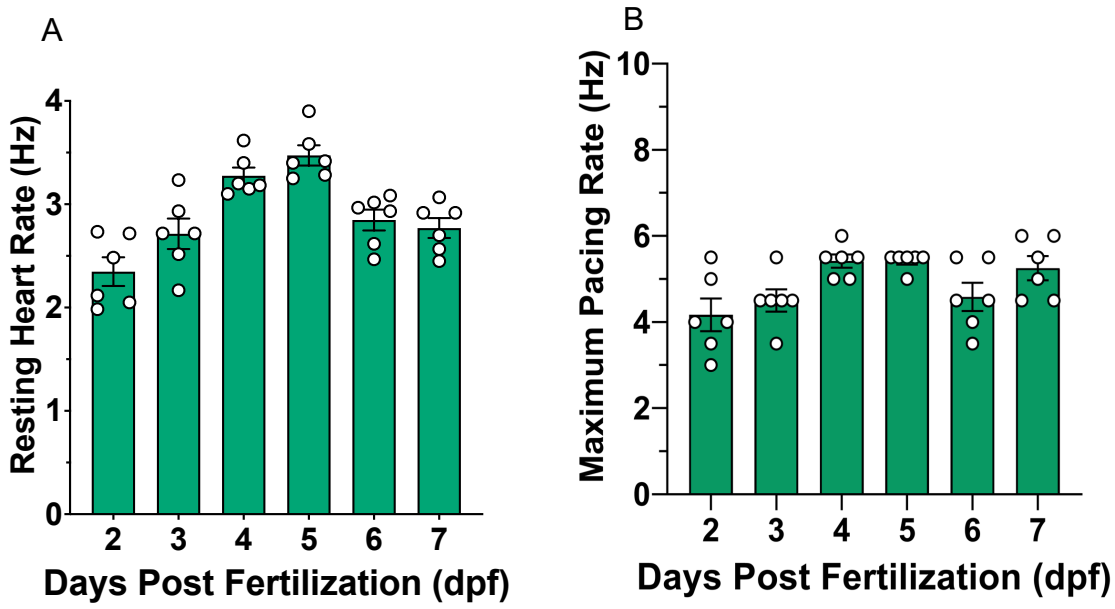

Fig. 5. (A) The average resting heart rate of ACR1-expressing larval zebrafish 2-7 days post-fertilization (dpf) prior to the assessment of optical capturing. Error bars represent $\pm$ the standard error from the mean. Clutch size was variable for each dpf. Sample size = 6 for each dpf. (B) Average maximal pacing rate of ACR1-expressing larvae from 2-7 days post-fertilization (dpf). Larvae were exposed to a continuous 10-second stimulus. Successful capturing was determined by consistent cardiac contraction of both chambers following pulsed light stimulation. Capturing was assessed over a range of frequencies from 3.5-8.0 Hz. The lowest average maximal optical pacing rate was found at 2 dpf with a frequency of 4.2 $\pm$ 0.4 Hz.

3.2. QRT-PCR

3.2.1. Primer Efficiency

To determine the efficiency of primers used in this study a 4-5-point 10-fold serial dilution curve of cDNA was used to assess each primer pair amplification efficiency. Primers with an efficiency value between 90-110 % were used in the study (Table 3). A coefficient of determination (R^2) value was determined from the linear regression, and primers with $R^2 > 0.98$ were used.

Table 3. The efficiency values and coefficient of determination (R^2) of the primers used.

Primer	Average Efficiency (%)	R^2-value
Efa1	103	1.00
Rpl13a	110	0.99
b-actin	95	1.00
ANP	98	0.99
BNP	107	0.99
ACTA2	98	0.99
Myh7	104	0.99
Myh6	108	1.00
TGF-β1	101	1.00

3.2.2. Reference Gene Stability

The gene selection software RefFinder was used to perform the algorithms of the Delta CT method, BestKeeper, and NormFinder, as well as to perform its own comprehensive ranking (Fig. 6A, B, C). Analysis using the Delta CT method, Normfinder, and RefFinder indicated that Rpl13a was the most stably expressed candidate. According to BestKeeper algorithm, suitable reference genes are those with standard deviations < 1, indicating Rpl13a and Efa1 would be suitable (Fig. 6D).

The geNorm algorithm was then implemented in RStudio (RStudio Team, 2021) to determine stability values (M) and pairwise variation of the candidate reference genes (Fig. 6E, Table 4). All candidate reference genes had a stable expression as their M values were determined to be below 0.5. A pairwise variation with a cut-off of 0.15 determined the suitable minimum number of reference genes to be two. As a result, Rpl13a and Efa1 were chosen as the reference genes for this study.

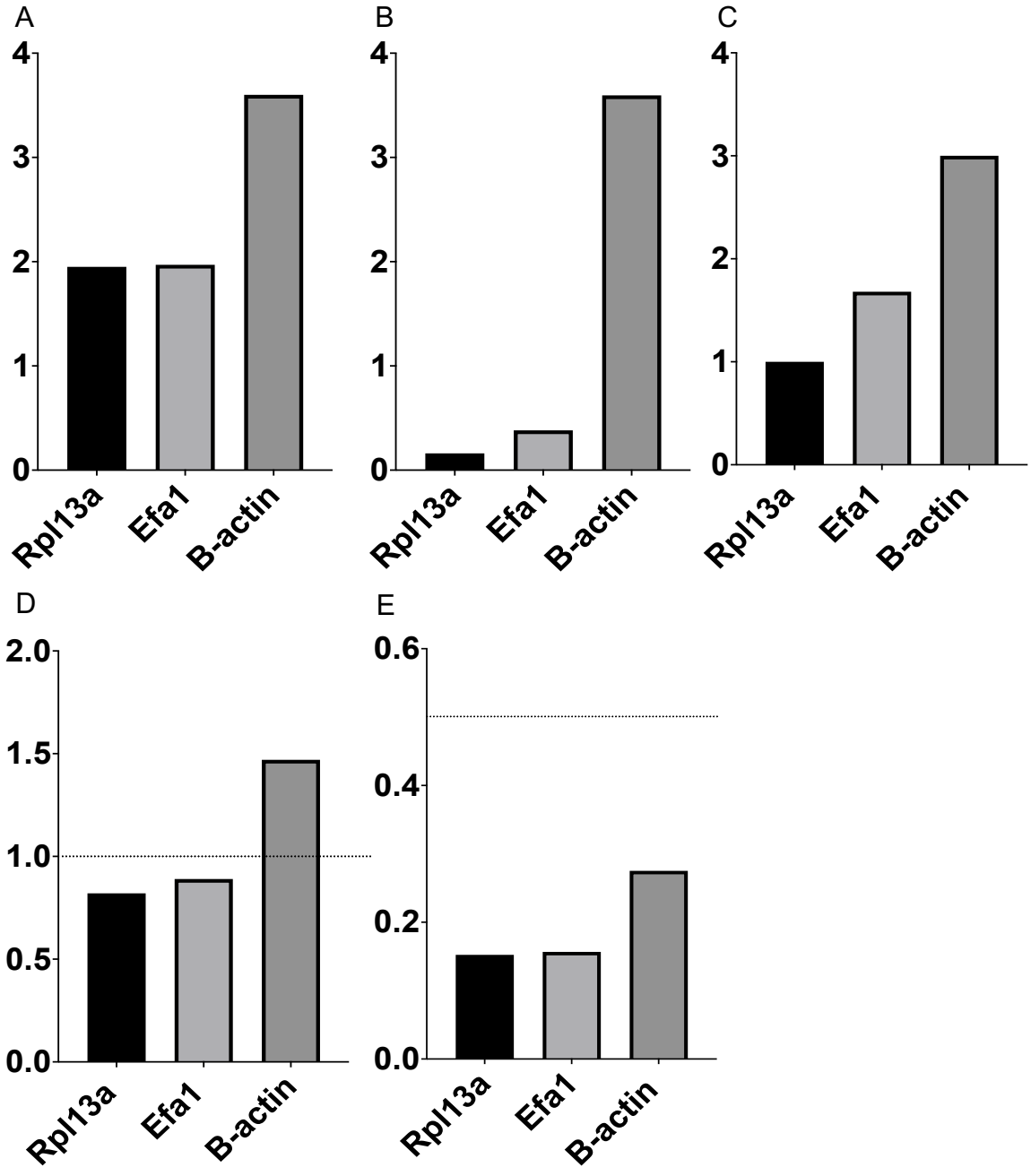

Fig. 6. The expression stability of the three candidate reference genes across 15 samples of pooled larval zebrafish at 6 days post fertilization (dpf) calculated by different algorithms using the RefFinder software. Reference genes are presented in increasing order of stability by (A) Delta CT method, (B) NormFinder, and (C) RefFinder geometric mean of ranking values. BestFinder (D) algorithm with a cut-off value of 1.0 determined Rpl13a and EFa1 to be suitable reference genes. GeNorm algorithm (E) was used to determine the stability value (M) of candidate reference genes. A cut-off value of 0.5 was used to determine stable reference genes, which found all candidate reference genes to be stable.

Table 4. GeNorm algorithm stability values (M) and pairwise variation of candidate reference genes. A cut-off value of 0.5 was used for M values. The pairwise variation was used with a cut-off value of 0.15.

Reference Gene	*Rpl13a*	*Efa1*	*B-actin*
Stability values M:	0.152	0.157	0.275
Pairwise variation (2/3)	0.09		

3.3. Continuous Pacing at 4.7 Hz Starting at 2 DPF

3.3.1. Changes in Resting Heart Rate and Morphology in ChR2-expressing Larvae

When ChR2-expressing larval zebrafish were exposed to continuous optical pacing, resting heart rate was lower than the controls after two days (Fig. 7). Furthermore, when resting heart rate in the treatment group was compared to pre-stimulation (2 dpf), no change was observed at each day during continuous pacing. When resting heart rate was compared to prior to stimulation in the control groups, heart rate varied from 4-6 dpf as the heart developed.

Fluorescent microscopy images of cardiac morphology revealed a tubular heart defect consistently found within the ChR2-expressing larvae at 6 dpf exposed to the light stimulus (Fig. 8). When chamber area was measured from fluorescent images, a decline in ventricular area was found in the ChR2-expressing larvae exposed to light (Fig. 9).

Additionally, a pericardial edema was found to be associated with the ChR2-expressing larvae exposed to light stimulation (Fig. 10A, B, C). A mild pericardial edema was commonly found in treated larvae without the tubular defect, whereas those with the tubular defect presented a severe pericardial edema. The percentage of ChR2-expressing larvae exposed to the light stimulus that demonstrated neither an edema or tubular defect, only an edema, or both an edema and tubular defect was then assessed (Fig. 10D). Prior to stimulation (2 dpf), all samples were found to be without a pericardial edema or a tubular defect. However, after one day of treatment (3 dpf), all samples possessed a pericardial edema. As the treatment progressed, a greater proportion of samples possessed both a pericardial edema and a tubular defect. Furthermore, atrial,

and ventricular area was measured from 2-6 dpf in fluorescent images to observe the progression of the tubular defect (Fig. 11). At 2 dpf, in both chambers the area was the same between the treatment group and the control. However, after exposure to the light stimulation, the ventricular area ceased to increase in the treatment group.

Resting heart rate was then analyzed based upon which phenotype the treated larvae presented, non-tubular or tubular defect (Fig. 12). The decline in resting heart rate appeared to be more pronounced in the ChR2-expressing zebrafish larvae with the tubular heart defect. When heart rate was compared to chamber size, a weak association was found between the two variables (Fig. 13).

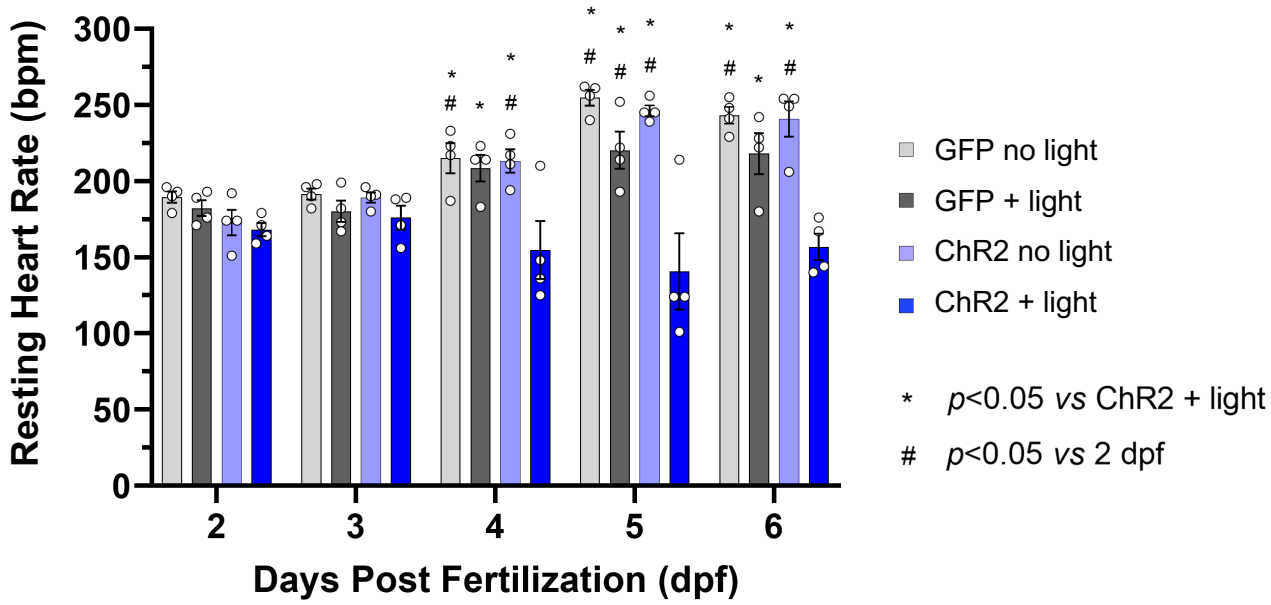

Fig. 7. The average resting heart rate in beats per minute (bpm) of ChR2-expressing larval zebrafish exposed to optical continuous pacing from 2-6 days post-fertilization (dpf). Error bars represent ± the standard error from the mean. Clutch size = 2, sample size = 4 for each dpf. The "*" represents statistical significance of the control groups when compared to the treatment group (ChR2 + light) within each dpf. The "#" represents statistical significance of the groups at each dpf when compared to prior to stimulation (2 dpf). Resting heart rate was lower in Myl7:hChR2-eYFP-expressing stimulated larvae by 4 dpf when compared to the control groups, which were larval zebrafish expressing Myl7:eGFP not exposed to light, Myl7:eGFP exposed to light, and Myl7:hChR2-eYFP not exposed to light. When compared to prior to stimulation (2 dpf), the ChR2-expressing stimulated larvae's resting heart rate did not change.

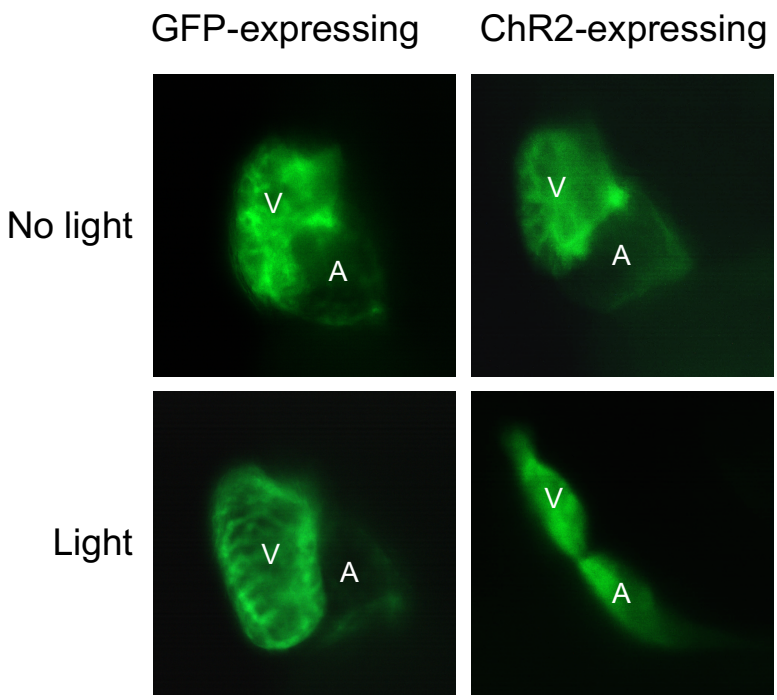

Fig. 8. Fluorescent microscopy images of cardiac morphology in GFP-expressing and ChR2-expressing larvae at 6 days post-fertilization (dpf) exposed to the light continuous stimulus. Fluorescent images captured both the ventricle (V) and atrium (A). A tubular heart defect was found in ChR2-expressing larvae exposed to the light stimulus.

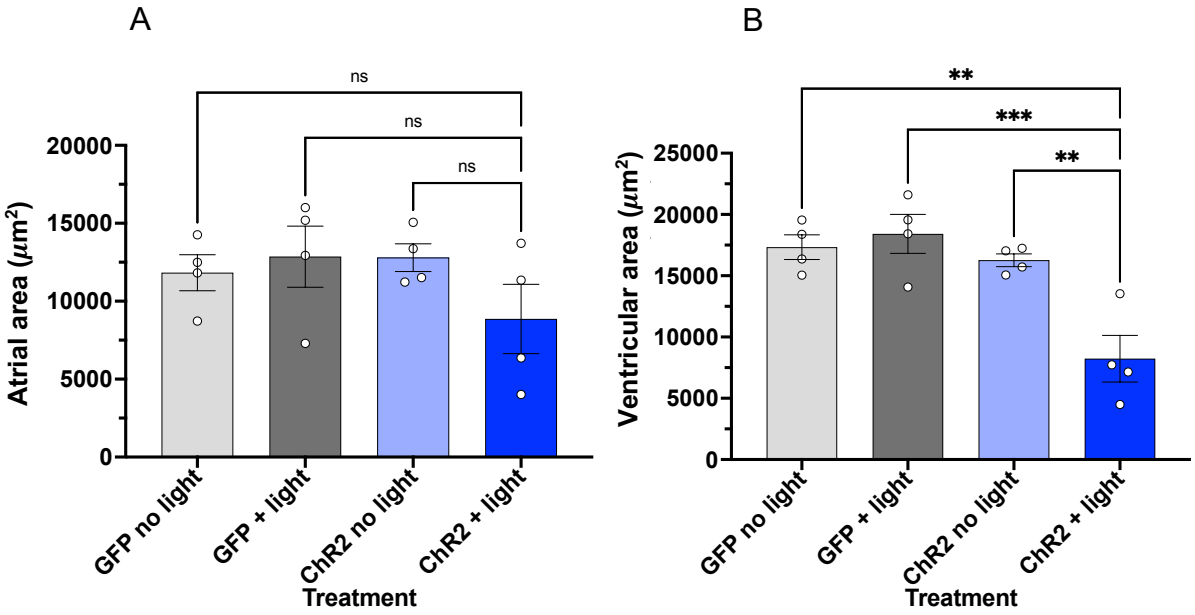

Fig. 9. The average atrial (A) and ventricular (B) area in μm^2 was measured for ChR2-expressing larvae at 6 dpf from fluorescent microscopy images of cardiac morphology. Error bars represent $\pm$ the standard error from the mean. Clutch size = 2, sample size = 4. A decline in ventricular area was determined in ChR2-expressing larvae exposed to the light stimulus.

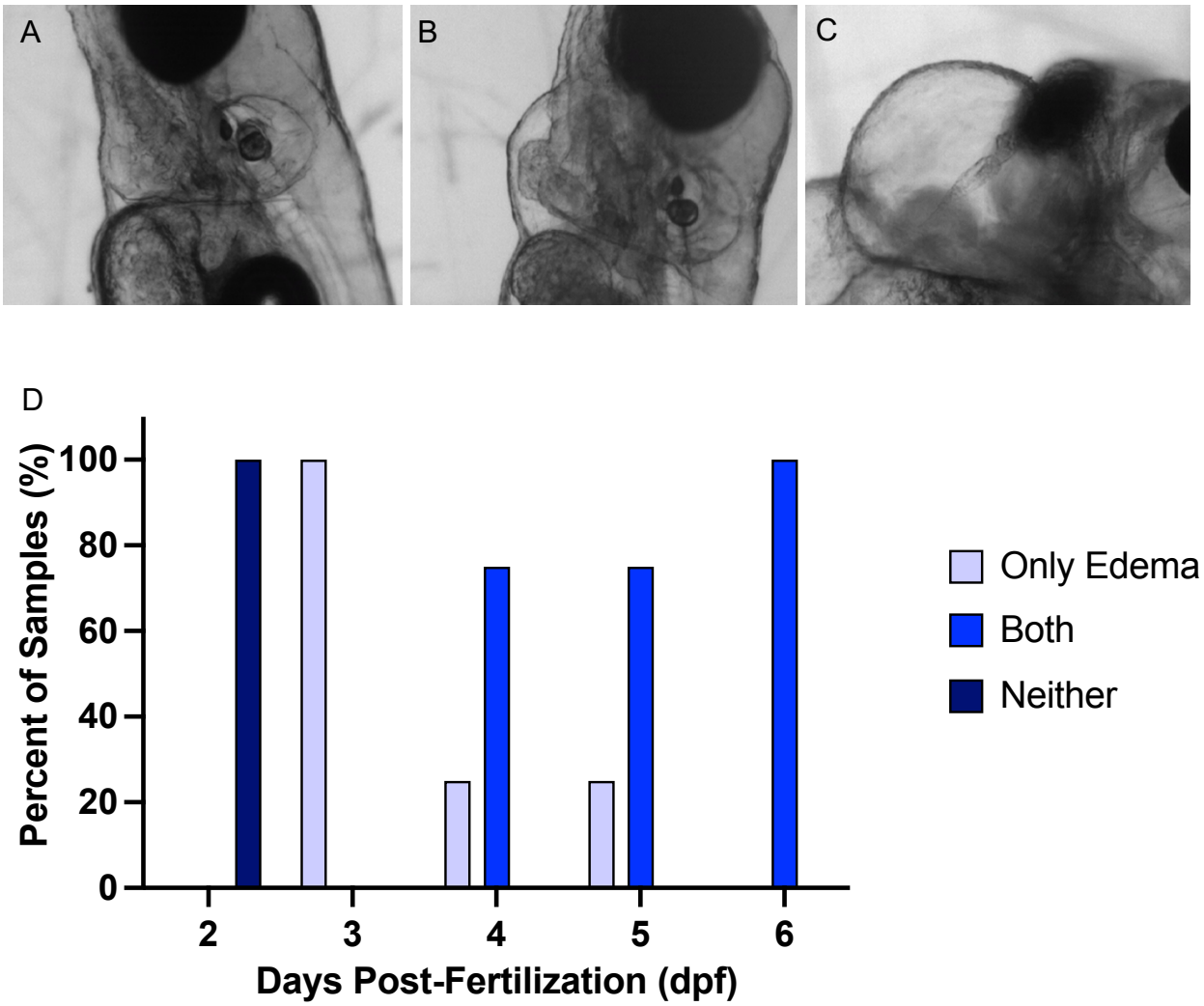

Fig. 10. (A, B, C) Representative images of control (A), and ChR2-expressing larval zebrafish with a non-tubular (B) or tubular (C) phenotype. In treated larvae, a pericardial edema presented, in which it was mild in the non-tubular groups and severe in those with the tubular defect. Images were acquired at 5 days post-fertilization (dpf) under a brightfield microscope. (D) Percentage of ChR2-expressing larvae exposed to the light stimulus that demonstrated neither an edema or tubular defect, only an edema, or both an edema and tubular defect. Clutch size = 2, sample size = 4. All samples possessing a tubular defect were found to have a pericardial edema, and therefore, they were considered as both. Prior to stimulation (2 dpf), all samples were found to be without a pericardial edema or a tubular defect. However, after one day of treatment (3 dpf), all samples possessed a pericardial edema. As the treatment progressed, a greater proportion of samples possessed both a pericardial edema and a tubular defect.

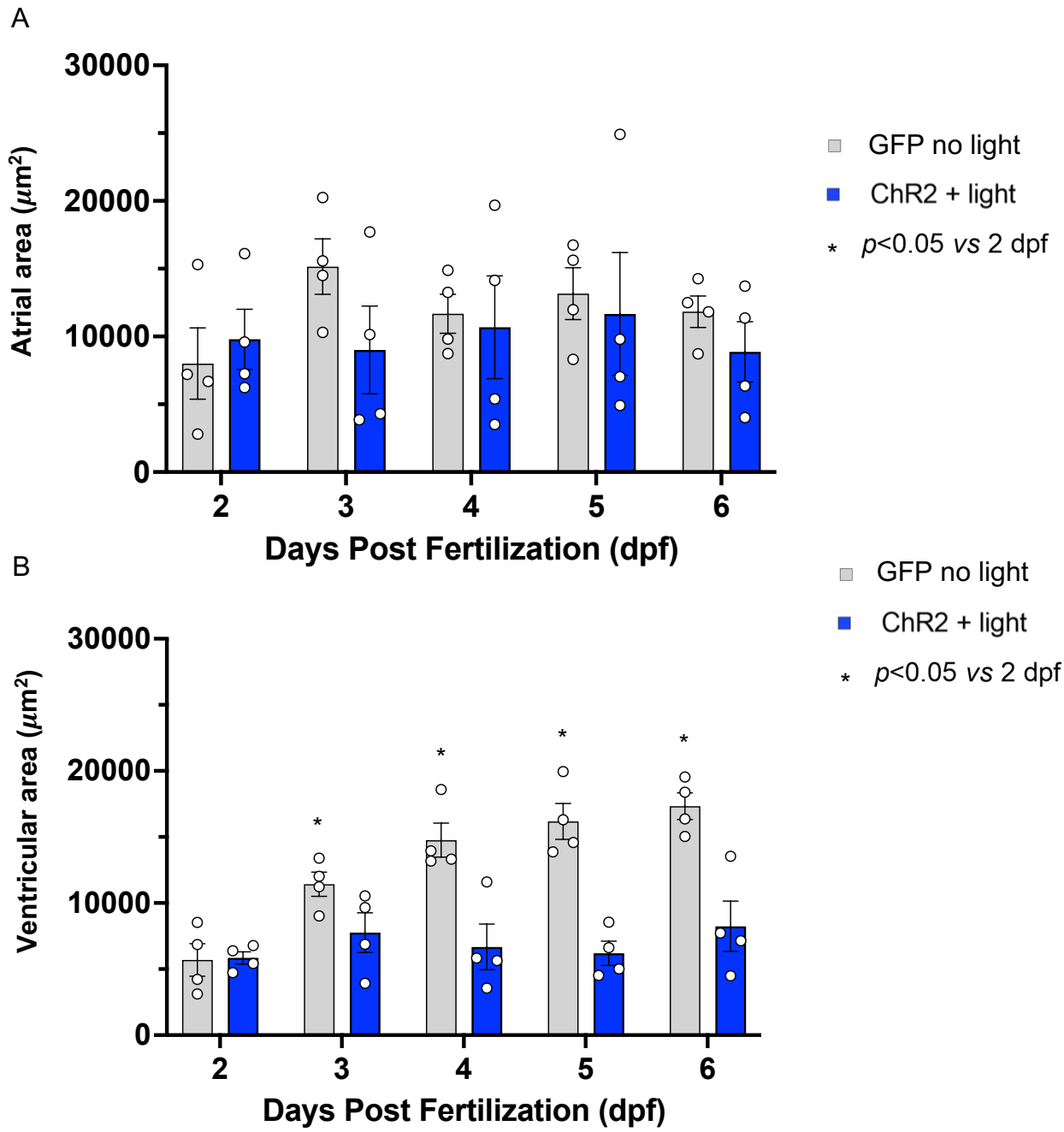

Fig. 11. The average atrial (A) and ventricular (B) area (μm^2) measured for ChR2-expressing larvae from 2-6 days post-fertilization (dpf) using fluorescent microscopy images of cardiac morphology. Error bars represent $\pm$ the standard error from the mean. Clutch size = 2, sample size = 4. When compared to prior to stimulation (2 dpf), a lack of growth in ventricular area was observed in ChR2-expressing larvae exposed to the light stimulus.

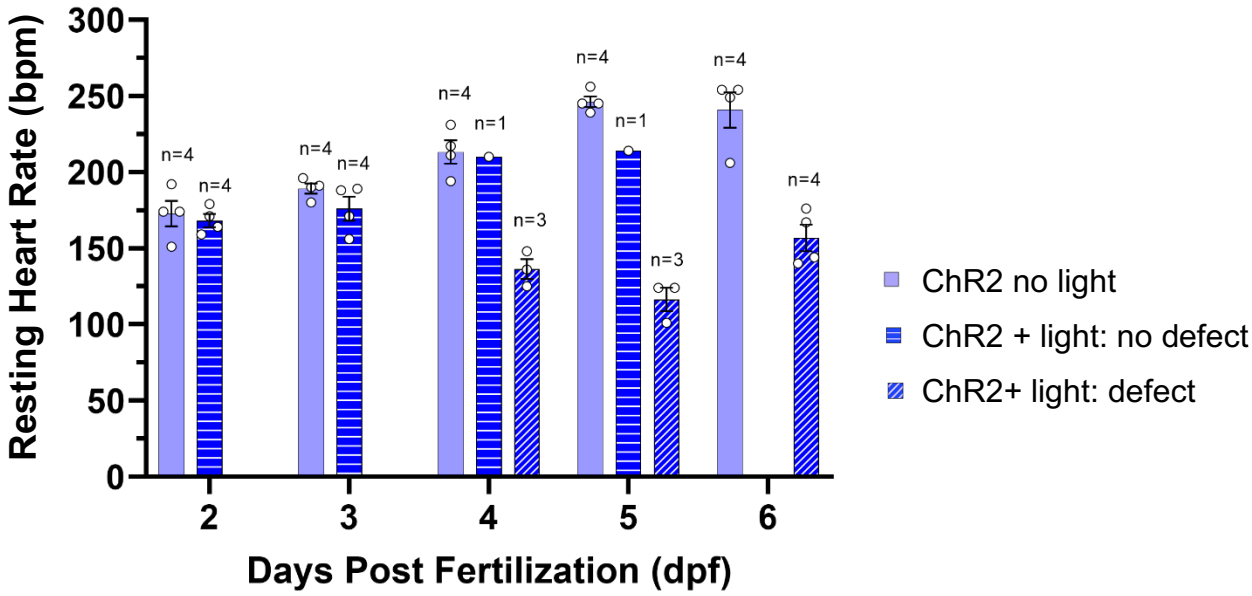

Fig. 12. The average resting heart rate was further interpretated as to whether the ChR2-expressing larval zebrafish larvae had a tubular heart defect, no tubular defect, or was not exposed to light. Error bars represent ± the standard error from the mean. The decline in resting heart rate appeared to be more pronounced in the ChR2-expressing zebrafish larvae with the tubular heart defect by 4 dpf.

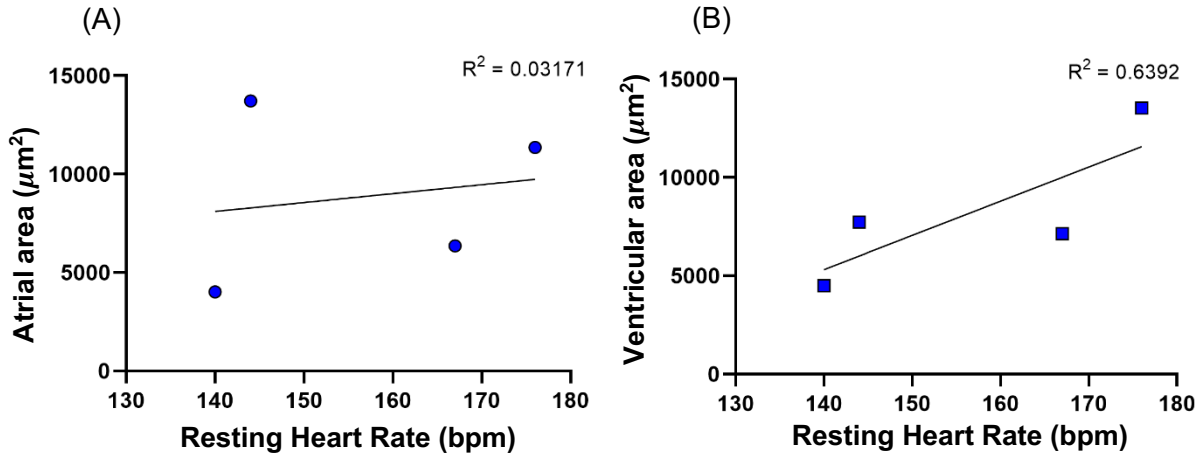

Fig. 13. The average resting heart rate in beats per minute (bpm) was compared to chamber area in light exposed ChR2-expressing larvae at 6 days post fertilization (dpf). Clutch size = 2, sample size = 4. The data was fitted with a simple linear regression to determine the relationship between the two variables. (A) A coefficient of determination (R^2) value of 0.03171 was determined for atrial area compared to heart rate indicating a lack of association between the two variables. (B) A coefficient of determination (R^2) value of 0.6392 was determined for ventricular area compared to heart rate indicating a weak association between the two variables.

3.3.1.1. mRNA Expression in Continuous Pacing in ChR2-expressing Larvae

Quantitative RT-PCR was used to determine relative gene expression of several genes of interests for larvae at 6 dpf (Fig. 14). Brain natriuretic peptide was found to be significantly increased in ChR2-expressing larvae exposed to the continuous light stimulus.

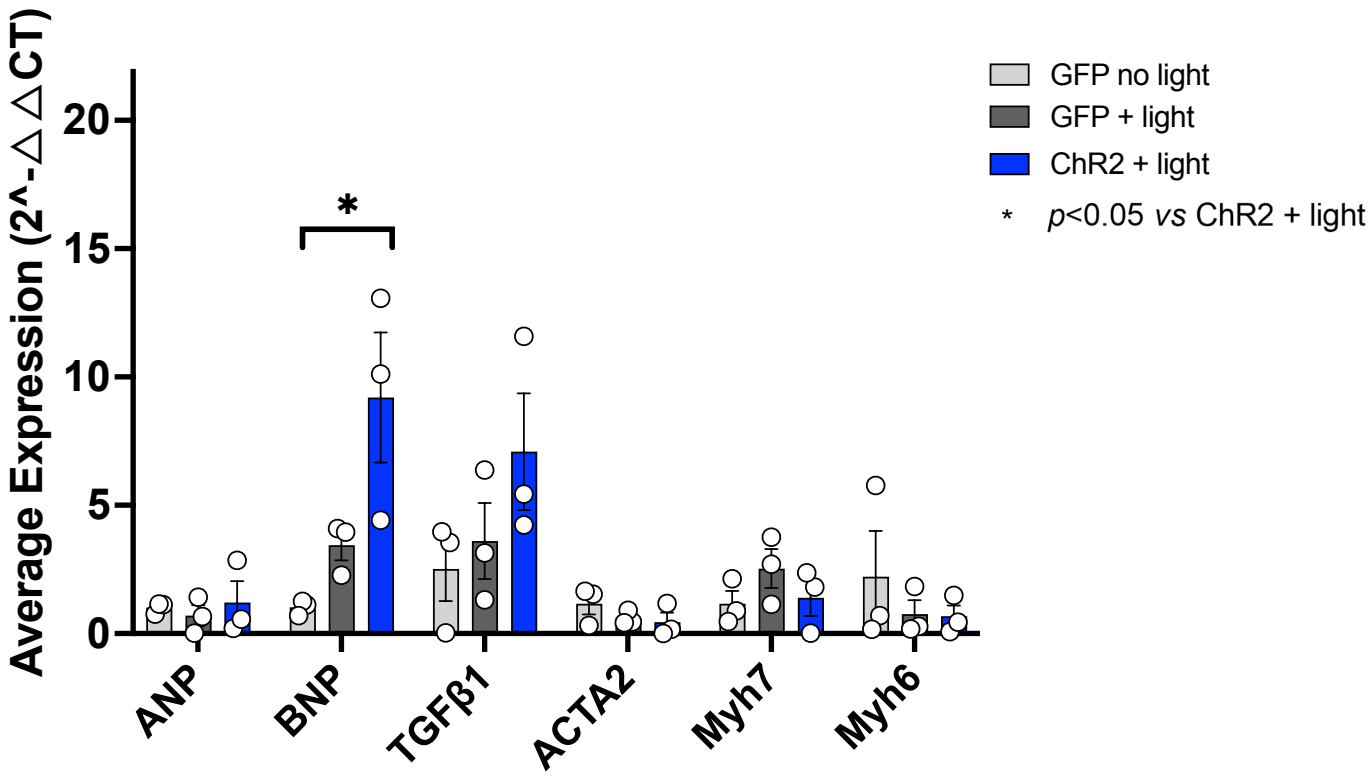

Fig. 14. qRT-PCR relative gene expression of genes of interest determined for ChR2-expressing larvae at 6 days post fertilization (dpf) exposed to continuous light stimulation. The results were normalized to two reference genes, Efa1 and Rpl13a. The results represent the average from three samples obtained from independent experiments. Error bars represent ± the standard error from the mean. Brain natriuretic peptide was found to be significantly increased in ChR2-expressing larvae exposed to the continuous light stimulus.

3.3.2. Changes in Resting Heart Rate and Morphology in ACR1-expressing Larvae

When ACR1-expressing larvae were exposed to continuous optical pacing, the resting heart rate was decreased by the experimental end-point when compared to the controls (Fig. 15). Fluorescent microscopy images of cardiac morphology revealed a tubular heart defect and a ventricular dilation in the ACR1-expressing larvae exposed to the light stimulus at 6 dpf (Fig. 16). When atrial and ventricular area was measured from fluorescent images, a decrease was found in the ACR1-expressing larvae exposed to light with a tubular defect, when compared to the control group (Fig. 17). In the non-tubular defect group, chamber area was seemingly elevated but lacked statistical power to determine changes. Furthermore, a mild pericardial edema was commonly found in treated larvae without the tubular defect, whereas those with the tubular defect presented a severe pericardial edema (Fig. 18A, B, C). When the percentage of ACR1-expressing larvae exposed to the light stimulus that demonstrated neither an edema or tubular defect, only an edema, or both an edema and tubular defect was compared at each dpf, it was found that prior to stimulation, all samples were without a pericardial edema or a tubular defect (Fig. 18D). However, after one day of treatment (3 dpf), all samples possessed either a pericardial edema or both edema and a tubular defect. As the treatment progressed, a greater proportion of samples possessed both a pericardial edema and a tubular defect. Furthermore, atrial and ventricular area was measured from 2-6 dpf in fluorescent images to observe the progression of the tubular defect (Fig. 19). At 2 dpf, the area of both chambers was the same between the treatment group and the control. However, after exposure to the light stimulation, the ventricular area declined as the tubular defect progressed.

When resting heart rate was analyzed based upon which phenotype the treated larvae presented, non-tubular or tubular defect, the decline in resting heart rate appeared to be more pronounced in the ACR1-expressing zebrafish larvae with the tubular heart defect (Fig. 20). A comparison between heart rate and chamber size revealed a strong association for both the atrium and ventricle (Fig. 21).

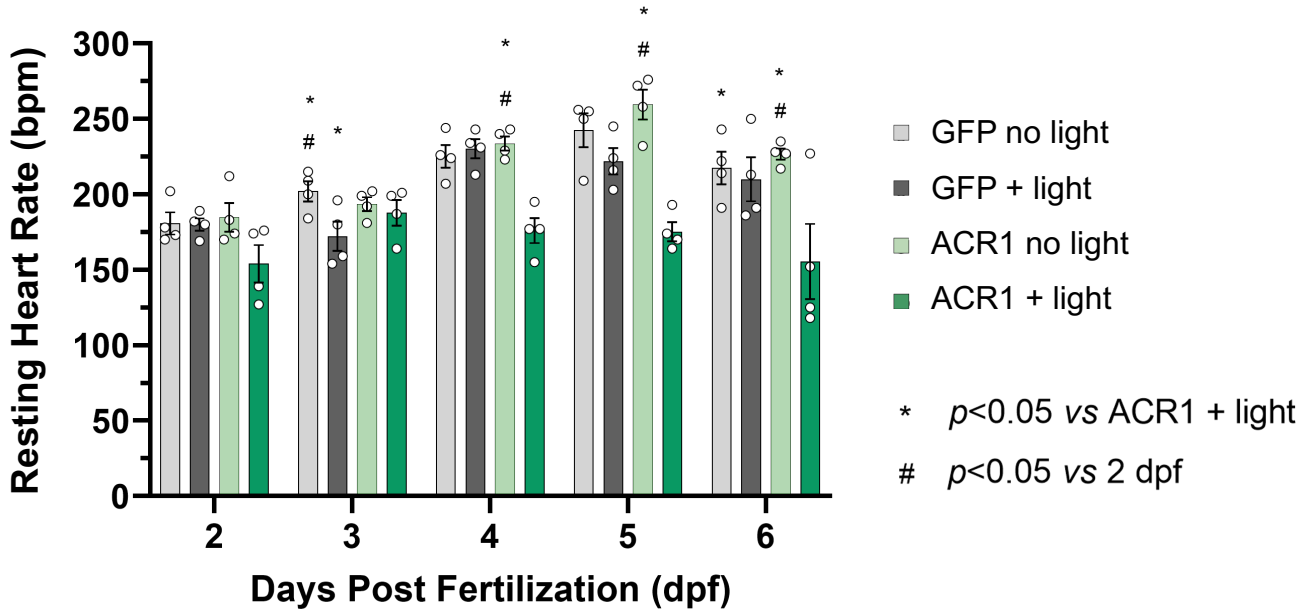

Fig. 15. The average resting heart rate in beats per minute (bpm) in ACR1-expressing larval zebrafish exposed to optical continuous pacing from 2-6 days post-fertilization (dpf). Error bars represent ± the standard error of the mean. Clutch size = 2, sample size = 4. The "*" represents statistical significance of the control groups when compared to the treatment group (ACR1 + light) within each dpf. The "#" represents statistical significance of the groups at each dpf when compared to prior to stimulation (2 dpf). Resting heart rate was lower in Myl7:GtACR1-eGFP-expressing stimulated larvae by 6 dpf when compared to the control groups which were larval zebrafish expressing Myl7:eGFP not exposed to light, Myl7:eGFP exposed to light, and Myl7:GtACR1-eGFP not exposed to light.

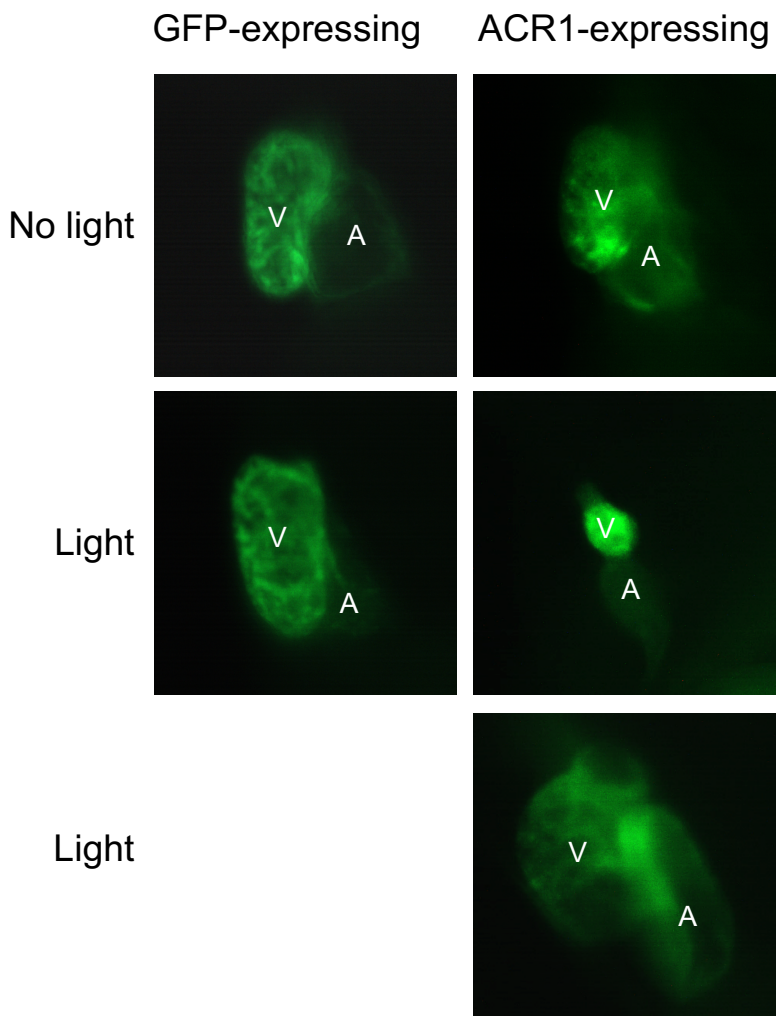

Fig. 16. Fluorescent microscopy images of cardiac morphology in GFP-expressing and ACR1-expressing larvae at 6 days post-fertilization (dpf) exposed to the light stimulus. Fluorescent images captured both the ventricle (V) and atrium (A). A tubular heart defect as well as a ventricular dilation was found in ACR1-expressing larvae exposed to the light stimulus.

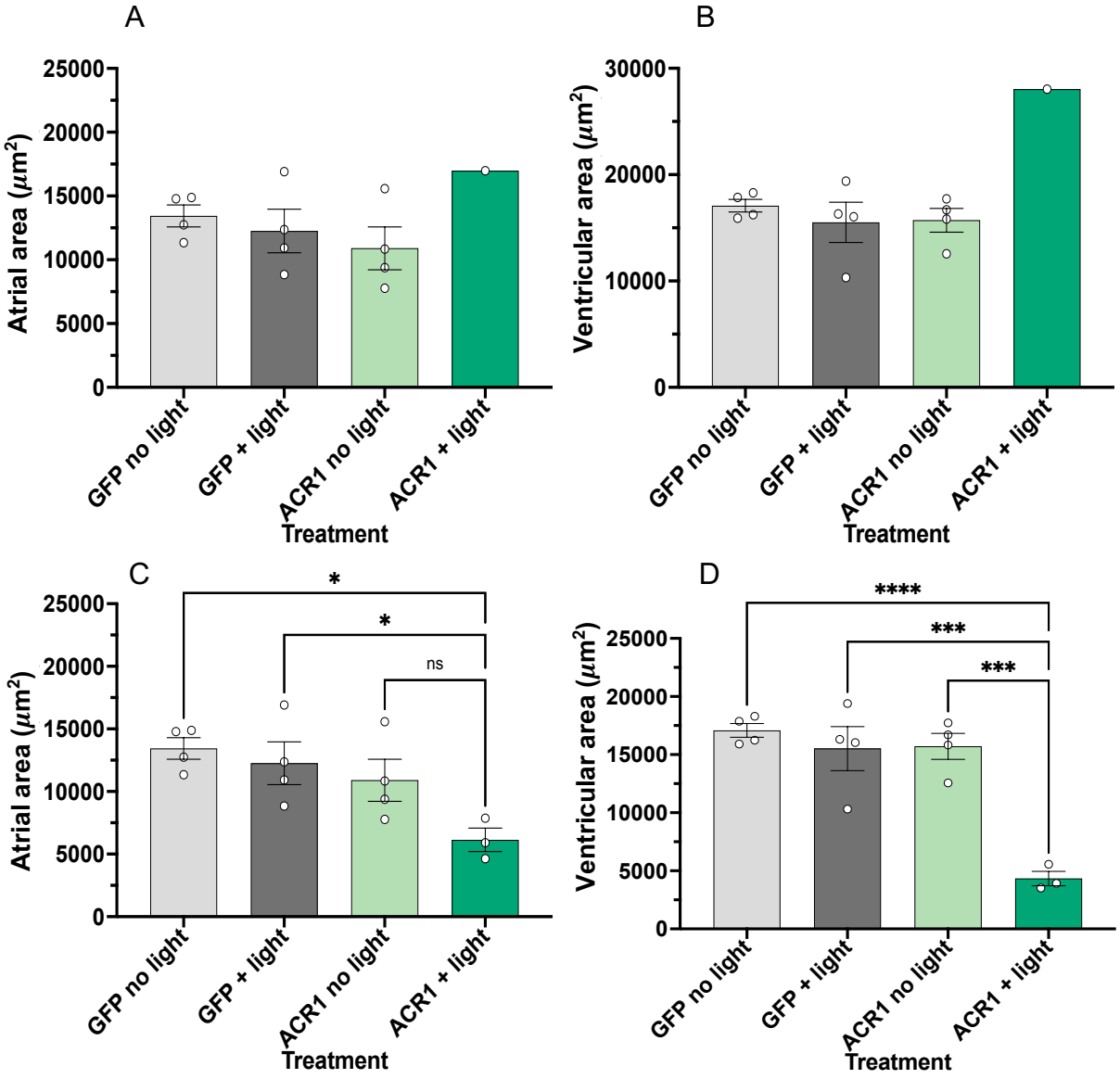

Fig. 17. The average atrial (A,C) and ventricular (B,D) area in μm^2 was determined for larvae at 6 dpf from fluorescent microscopy images of cardiac morphology. Error bars represent $\pm$ the standard error from the mean. Clutch size = 2, sample size = 4. Area measurements were compared to whether the ACR1-expressing larvae exposed to light presented a chamber dilation (A,B), or tubular defect (C,D). In the tubular defect phenotype, a decline in atrial (C) and ventricular (D) area was observed.

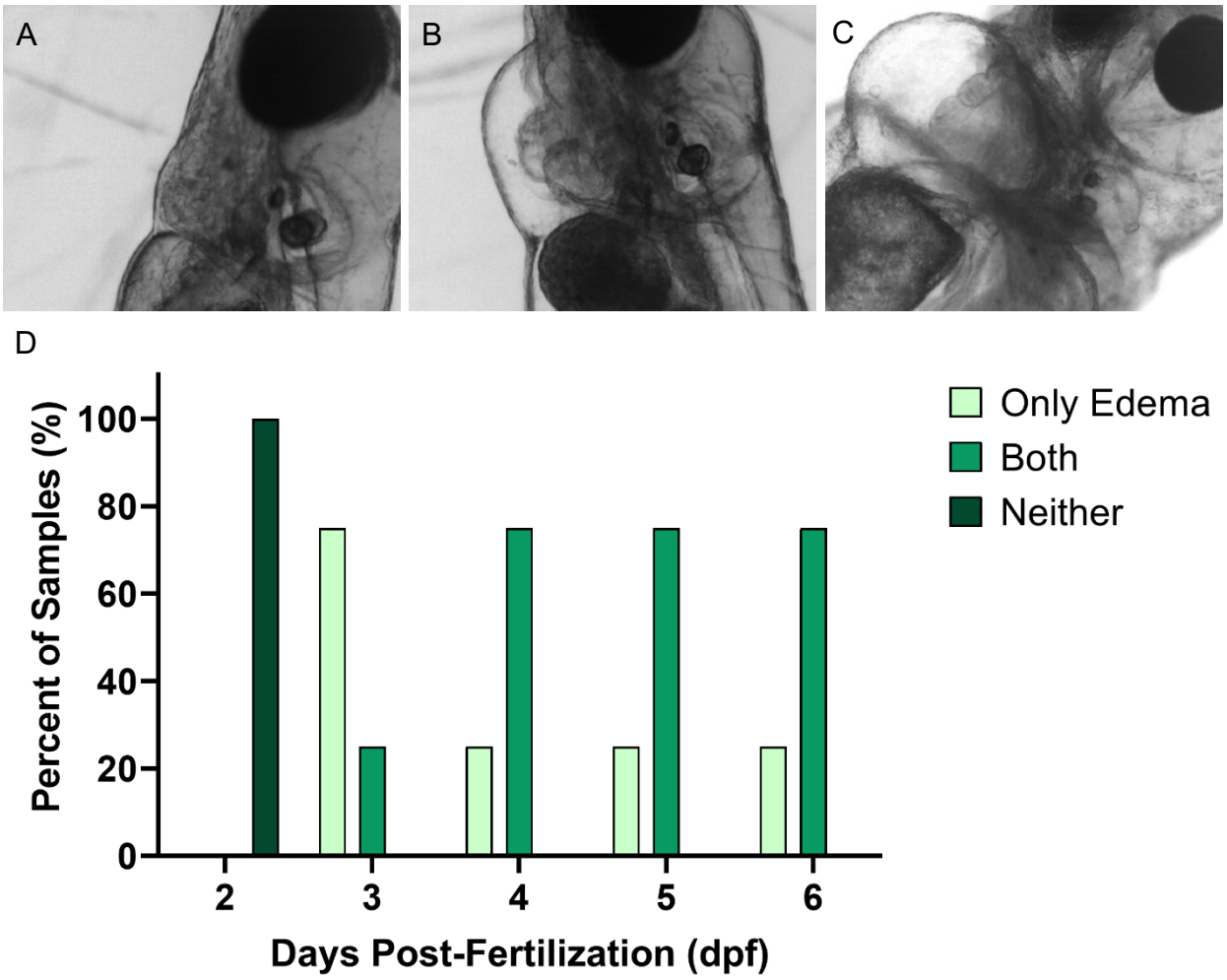

Fig. 18. (A, B, C) Representative images of control (A), and ACR1-expressing larval zebrafish with a non-tubular (B) or tubular (C) phenotype. In treated larvae, a pericardial edema presented, in which it was mild in the non-tubular groups and severe in those with the tubular defect. Images were acquired at 5 days post-fertilization (dpf) under a brightfield microscope. (D) Percentage of ACR1-expressing larvae exposed to the light stimulus that demonstrated neither an edema or tubular defect, only an edema, or both an edema and tubular defect. Clutch size = 2, sample size = 4. Prior to stimulation, all samples were found to be without a pericardial edema or a tubular defect. However, after one day of treatment (3 dpf), all samples possessed either a pericardial edema or both edema and a tubular defect. As the treatment progressed, a greater proportion of samples possessed both a pericardial edema and a tubular defect.

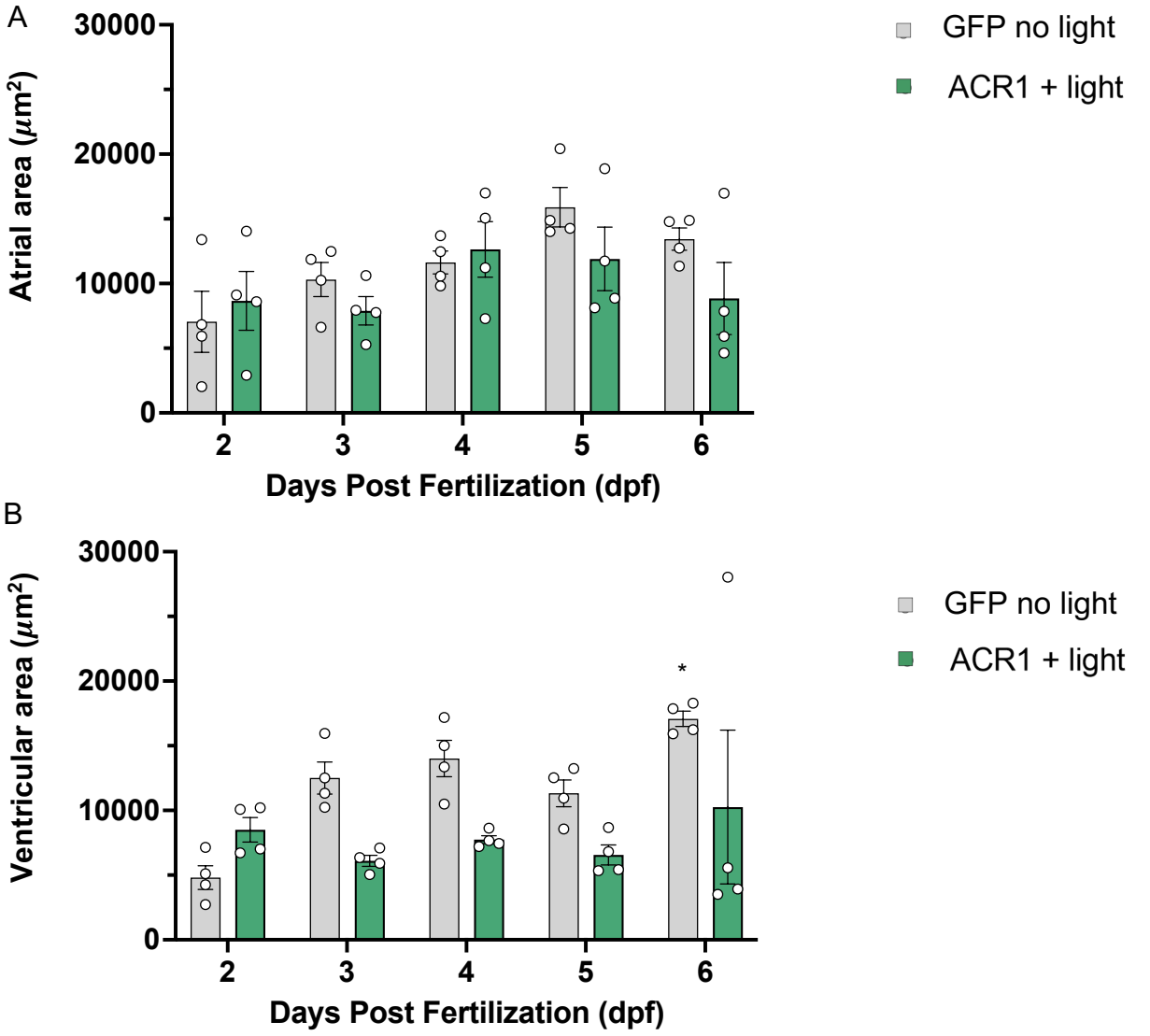

Fig. 19. The average atrial (A) and ventricular (B) area in μm^2 was measured for ACR1-expressing larvae from 2-6 days post-fertilization (dpf) using fluorescent microscopy images of cardiac morphology. Error bars represent $\pm$ the standard error from the mean. Clutch size = 2, sample size = 4. A decline in ventricular area was determined in ACR1-expressing larvae exposed to the light stimulus.

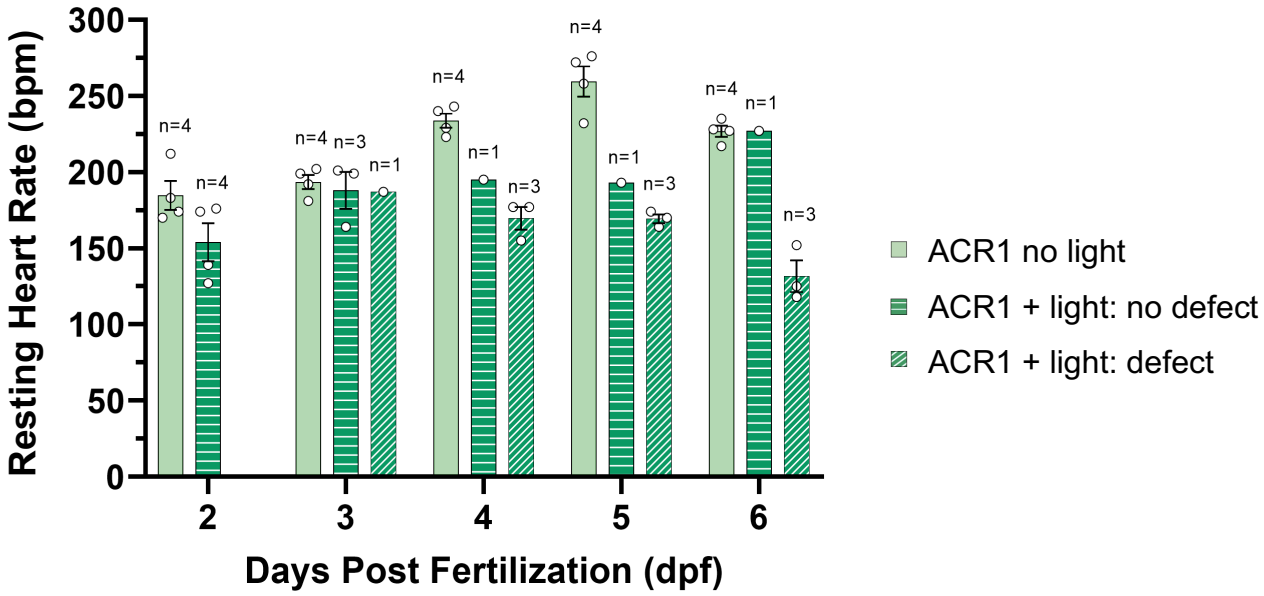

Fig. 20. The average resting heart rate was further interpretated as to whether the ACR1-expressing zebrafish larvae had a tubular heart defect, no tubular defect, or was not exposed to light. Error bars represent ± the standard error from the mean. The decline in resting heart rate appeared to be more pronounced in the ACR1-expressing zebrafish larvae with the tubular heart defect by 6 dpf.

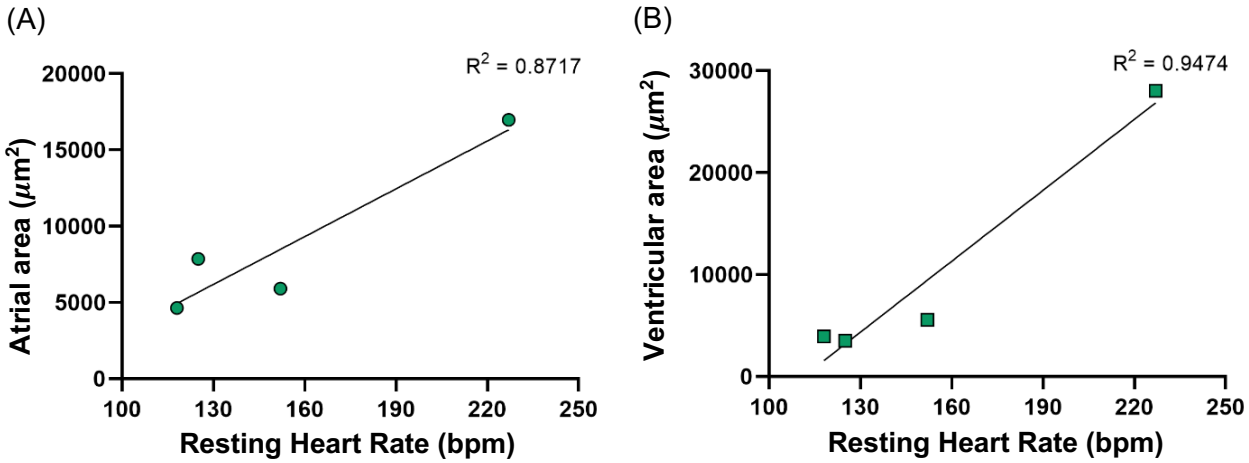

Fig. 21. The average resting heart rate in beats per minute (bpm) was compared to chamber area in light exposed ACR1-expressing larvae at 6 days post fertilization (dpf). Clutch size = 2, sample size = 4. The data was fitted with a simple linear regression to determine the relationship between the two variables. A coefficient of determination (R^2) value of 0.8717 was determined for atrial area (A) and 0.9474 for ventricular area (B) when compared to heart rate indicating a strong association between these variables.

3.3.2.1. mRNA Expression in Continuous Pacing in ACR1-expressing Larvae

Quantitative RT-PCR was used to determine relative gene expression of several genes of interest for larvae at 6 dpf (Fig. 22). Brain natriuretic peptide and TGF-β1 were found to be significantly increased in ACR1-expressing larvae exposed to the continuous light stimulus.

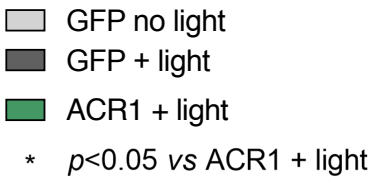

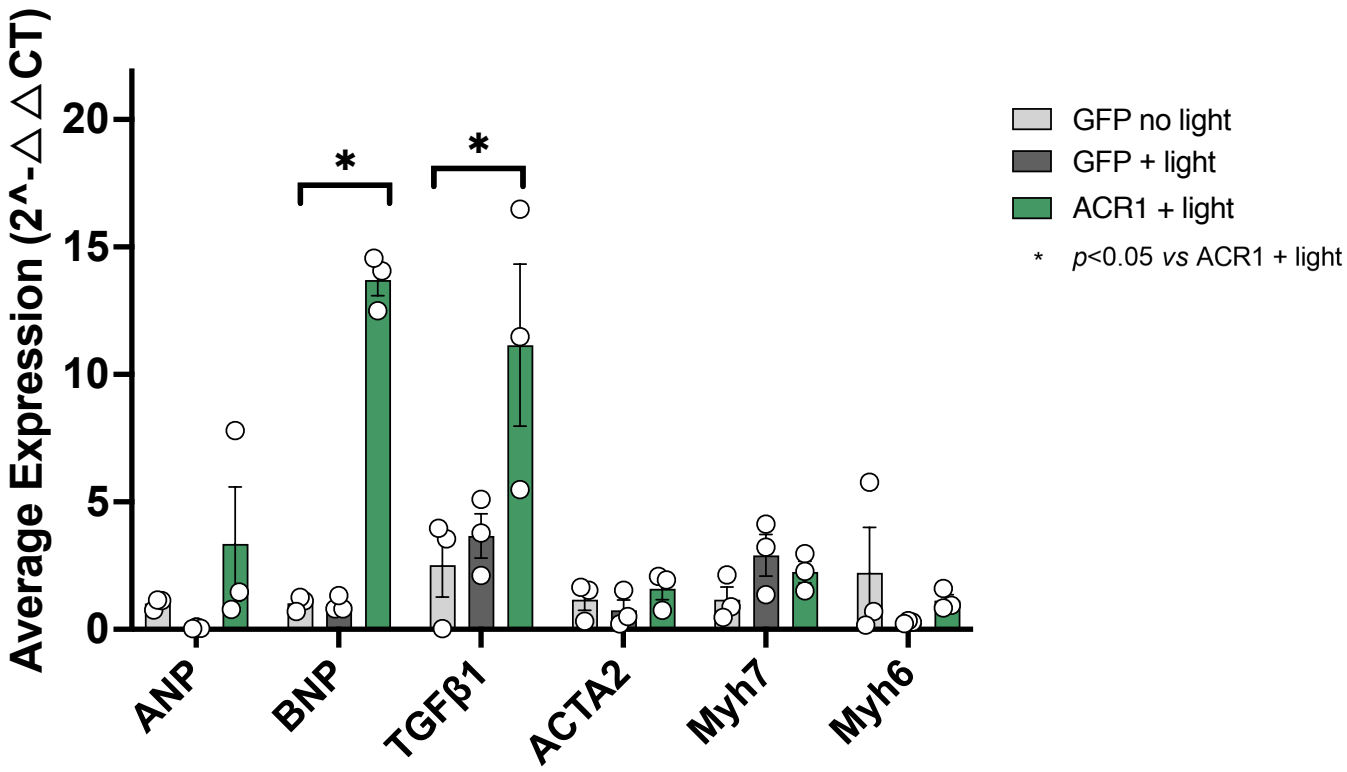

Fig. 22. qRT-PCR relative gene expression of genes of interest determined for ACR1-expressing larvae at 6 days post fertilization (dpf) exposed to continuous light stimulation. The results were normalized to two reference genes, Efa1 and Rpl13a. The results represent the average from three samples obtained from independent experiments. Error bars represent ± the standard error from the mean. Brain natriuretic peptide and TGF-β1 were found to be significantly increased in ACR1-expressing larvae exposed to the continuous light stimulus.

3.4. Continuous Pacing at 4.7 Hz Starting at 3 DPF

3.4.1. Changes in Resting Heart Rate and Morphology in ChR2-expressing Larvae

To allow for further cardiac development to potentially prevent the formation of the tubular defect, we began the chronic continuous pacing a day later in development (3 dpf). Chronic continuous tachypacing beginning at 3 dpf resulted in decreased resting heart rate in the treatment group after two days of pacing when compared to the control groups (Fig. 23). Fluorescent microscopy images of cardiac morphology revealed a tubular heart defect and an atrial dilation found within the ChR2-expressing larvae exposed to the light stimulus at 7 dpf (Fig. 24). When atrial and ventricular area was measured from fluorescent images, a decline in atrial and ventricular area was observed in the ChR2-expressing larvae exposed to light with a tubular defect, however, the study lacked the statistical power to determine significance (Fig. 25). In the non-tubular defect group, atrial area appeared to increased in the treatment group. Furthermore, a mild pericardial edema was commonly found in the treated larvae without the tubular defect, whereas those with the tubular defect presented a severe pericardial edema (Fig. 26A, B, C). The percentage of ChR2-expressing larvae exposed to the light stimulus that demonstrated neither an edema or tubular defect, only an edema, or both an edema and tubular defect was then determined from the bright field recordings (Fig. 26D). Prior to stimulation, all samples were found to be without a pericardial edema or a tubular defect. After one day of treatment, all samples possessed either a pericardial edema or both edema and a tubular defect, except for one sample at 7 dpf, which possessed neither.

When resting heart rate was then analyzed based upon which phenotype the treated larvae presented, non-tubular or tubular defect, the decline in resting heart rate appeared to be more pronounced in the ChR2-expressing zebrafish larvae with the tubular heart defect (Fig. 27). A comparison between heart rate and chamber size revealed a strong association for both the atrium and ventricle (Fig. 28).

Furthermore, due to the similar results found from continuous pacing beginning at either 3 dpf or 2 dpf, changes in mRNA expression were not investigated for this pacing protocol.

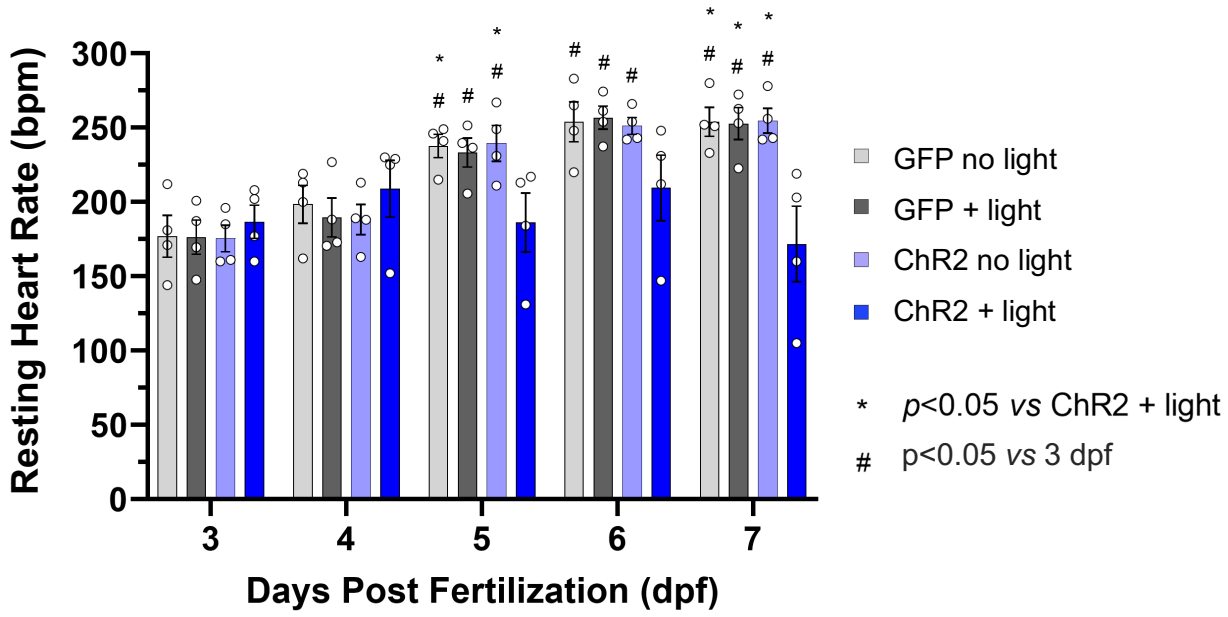

Fig. 23. The average resting heart rate in beats per minute (bpm) of ChR2-expressing zebrafish larvae exposed to optical continuous pacing from 3-7 days post-fertilization (dpf). Error bars represent ± the standard error from the mean. Clutch size = 2, sample size = 4 for each dpf. The "*" represents statistical significance of the control groups when compared to the treatment group (ChR2 + light) within each dpf. The "#" represents statistical significance of the groups at each dpf when compared to prior to stimulation (3 dpf). Resting heart rate was lower in Myl7:hChR2-eYFP-expressing stimulated larvae by 5 dpf when compared to the control groups, which were larval zebrafish expressing Myl7:eGFP not exposed to light, Myl7:eGFP exposed to light, and Myl7:hChR2-eYFP not exposed to light. When compared to prior stimulation (3 dpf), the ChR2-expressing stimulated larva's resting heart rate did not change.

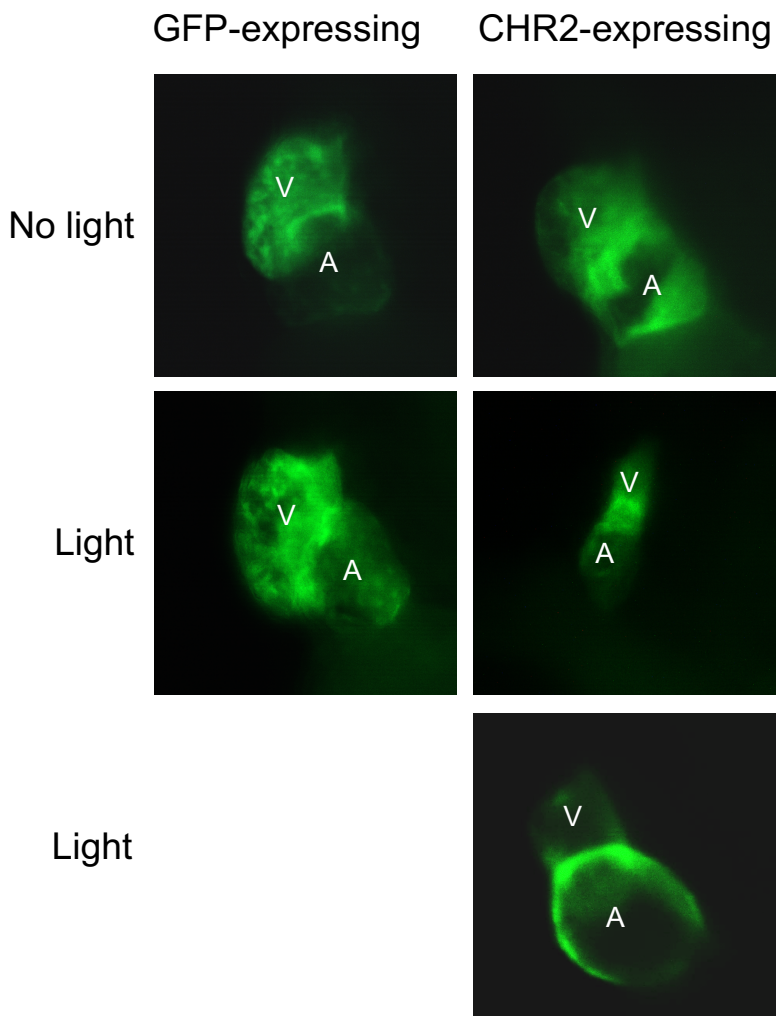

Fig. 24. Fluorescent microscopy images of cardiac morphology in GFP-expressing and ChR2-expressing larvae at 7 post-fertilization (dpf) exposed to the continuous light stimulus. Fluorescent images captured both the ventricle (V) and atrium (A). A tubular heart defect as well as an atrial dilation was found in ChR2-expressing larvae exposed to the light stimulus.

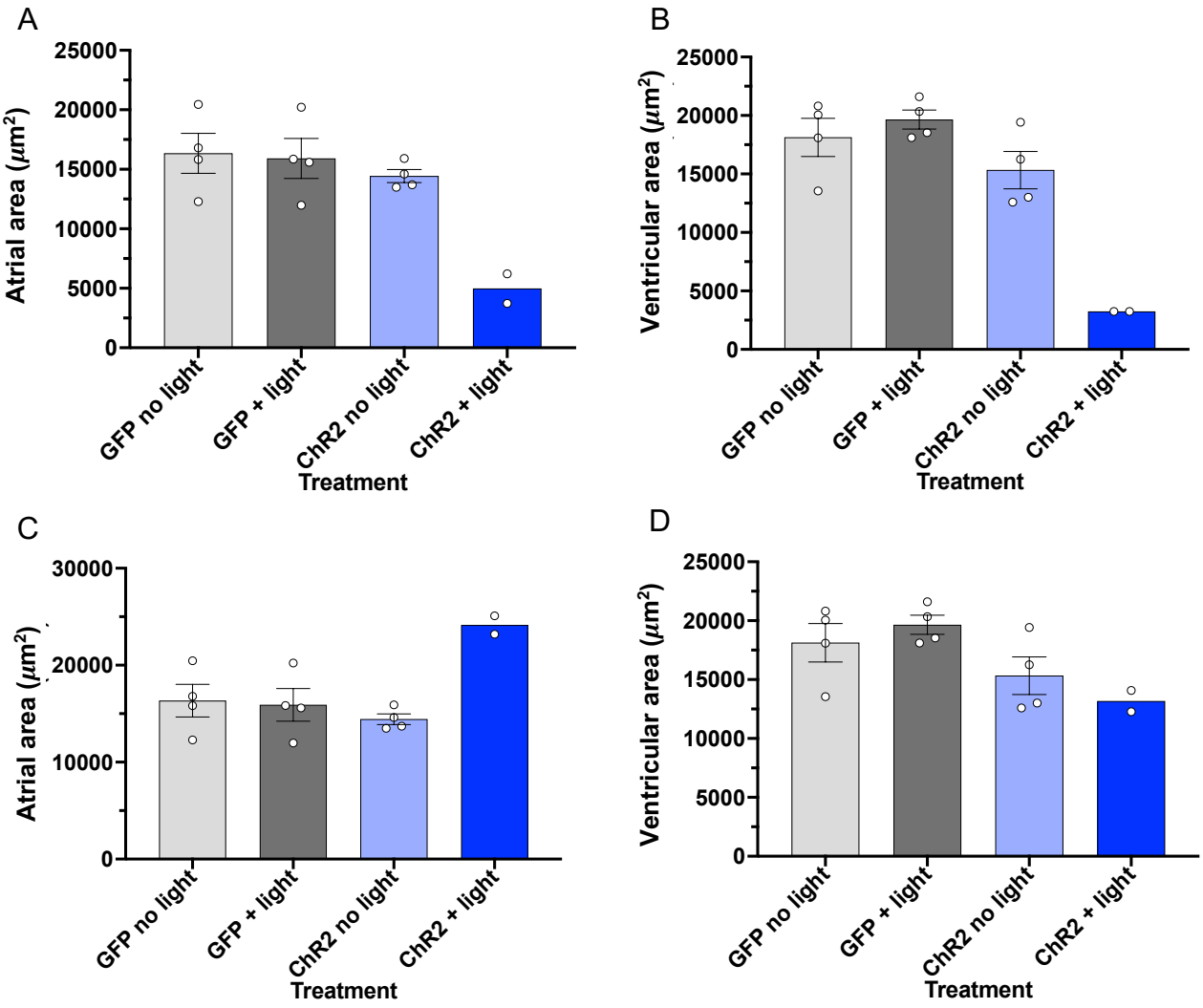

Fig. 25. The average atrial (A,C) and ventricular (B,D) area in μm^2 was determined for ChR2-expressing larvae at 7 post-fertilization (dpf) from fluorescent microscopy images of cardiac morphology. Error bars represent $\pm$ the standard error from the mean. Clutch size = 2, sample size = 4. Area measurements were compared to whether the ChR2-expressing larvae exposed to light presented the dilation (A,B), or the tubular defect (C,D). An increase in atrial (A) area was found in the dilation phenotype. A decline in atrial (C) and ventricular (D) area was observed in the tubular phenotype, however the study lacked the statistical power.

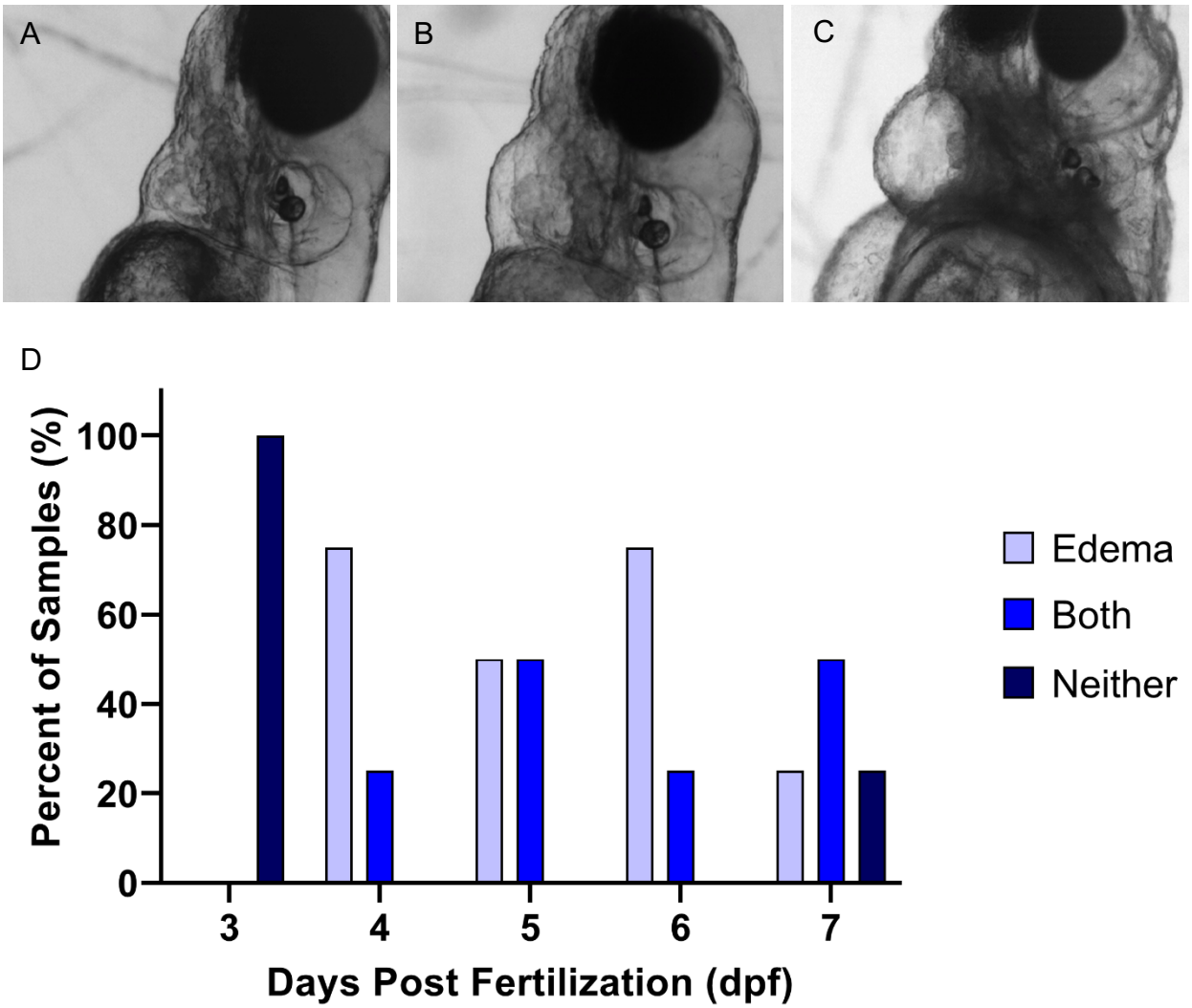

Fig. 26. (A, B, C) Representative images of control (A), and ChR2-expressing larval zebrafish with a non-tubular (B) or tubular (C) phenotype. In treated larvae, a pericardial edema presented, in which it was mild in the non-tubular groups and severe in those with the tubular defect. Images were acquired at 6 days post-fertilization (dpf) under a brightfield microscope. (D) Percentage of ChR2-expressing larvae exposed to the light stimulus that demonstrated neither an edema or tubular defect, only an edema, or both an edema and tubular defect. Clutch size = 2, sample size = 4. Prior to stimulation, all samples were found to be without a pericardial edema or a tubular defect. After one day of treatment (4 dpf), all samples possessed either a pericardial edema or both edema and a tubular defect. However, at 7 dpf, one of the treated samples did not possess either an edema or both an edema and tubular defect.

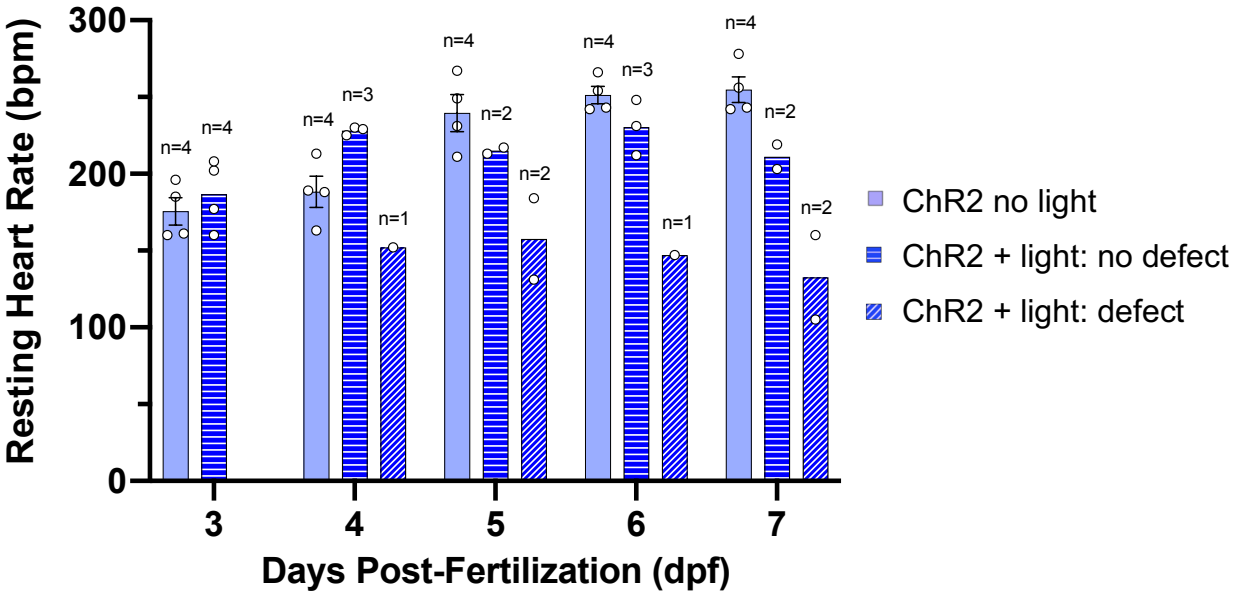

Fig. 27. The average resting heart rate was further interpretated as to whether the ChR2-expressing zebrafish larvae had a tubular heart defect, no tubular defect, or was not exposed to light. Error bars represent ± the standard error from the mean. The decline in resting heart rate appeared to be more pronounced in the ChR2-expressing zebrafish larvae with the tubular heart defect by 4 dpf.

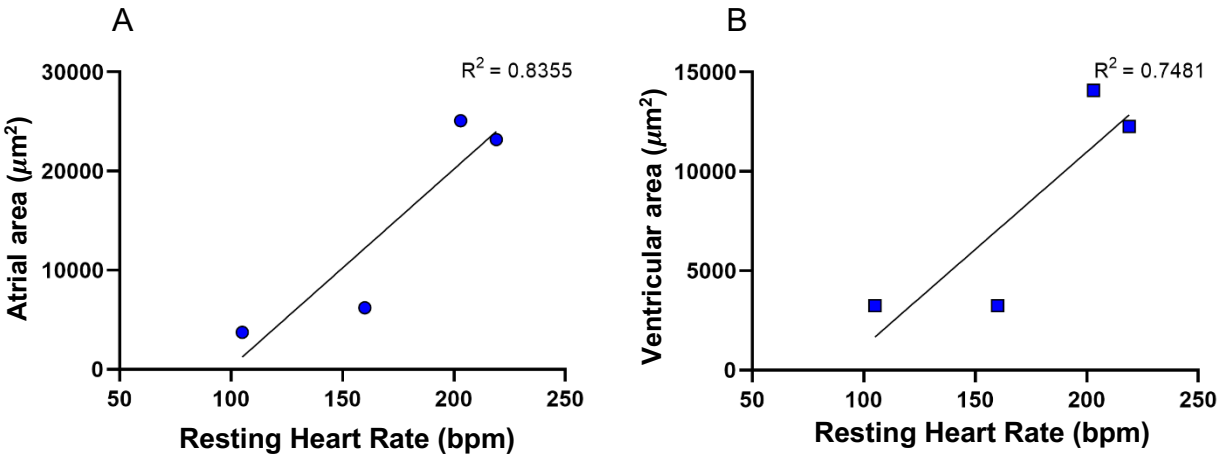

Fig. 28. The average resting heart rate in beats per minute (bpm) was compared to chamber area (μm^2) in continuous light exposed ChR2-expressing larvae at 7 days post fertilization (dpf). Clutch size = 2, sample size = 4. The data was fitted with a simple linear regression to determine the relationship between the two variables. A coefficient of determination (R^2) value of 0.8355 was determined for atrial area (A) and 0.7481 for ventricular area (B) when compared to heart rate indicating a strong association between these variables.

3.4.2. Changes in Resting Heart Rate and Morphology in ACR1-expressing Larvae

Chronic continuous tachypacing beginning at 3 dpf resulted in no change in resting heart rate in the ACR1-expressing larvae when compared to prior to the expose to the stimulus (3 dpf) (Fig. 29). Fluorescent microscopy images of cardiac morphology revealed a tubular heart defect and an atrial dilation found within the ACR1-expressing larvae exposed to the light stimulus at 7 dpf (Fig. 30). When the chamber area was measured from fluorescent images, a decreased atrial and ventricular area was observed in the ACR1-expressing larvae exposed to light with a tubular defect when compared to the control group, however, there was a lack in sample size to perform statistics (Fig. 31). Furthermore, a mild pericardial edema was commonly found in treated larvae without the tubular defect, whereas those with the tubular defect presented a severe pericardial edema (Fig. 32A, B, C). The percentage of ACR1-expressing larvae exposed to the light stimulus that demonstrated neither an edema or tubular defect, only an edema, or both an edema and tubular defect was then determined (Fig. 32D). Prior to stimulation, all samples were found to be without a pericardial edema or a tubular defect. After one day of stimulation, all ACR1-expressing larvae exposed to the light stimulus possessed a pericardial edema. As chronic stimulation progressed, a greater proportion of ACR1-expressing samples possessed both a tubular defect and a pericardial edema. However, at 7 dpf, one of the treated samples did not possess either an edema or a tubular defect.

When resting heart rate was analyzed based upon which phenotype the treated larvae presented, non-tubular or tubular defect, the decline in resting heart rate appeared to be more pronounced in the ACR1-expressing zebrafish larvae with the

tubular heart defect by 6 dpf (Fig. 33). A comparison between heart rate and chamber size revealed a strong association with atrial area and a weak association with ventricular area (Fig. 34).

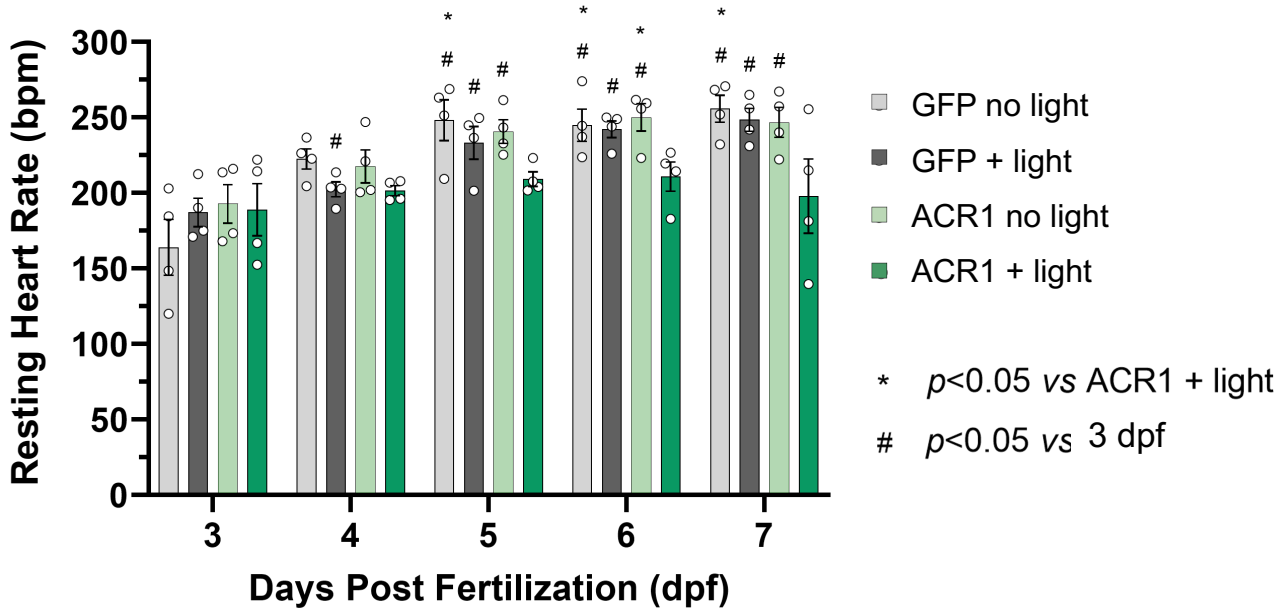

Fig. 29. The average resting heart rate in beats per minute (bpm) of ACR1-expressing zebrafish larvae exposed to optical continuous pacing from 3-7 days post-fertilization (dpf). Error bars represent $\pm$ the standard error from the mean. Clutch size = 2, sample size = 4 for each dpf. The "*" represents statistical significance of the control groups when compared to the treatment group (ACR1 + light) within each dpf. The "#" represents statistical significance of the groups at each dpf when compared to prior to stimulation (3 dpf). Resting heart rate was lower in Myl7:GtACR1-eGFP-expressing stimulated larvae by 6 dpf when compared to the control groups, which were larval zebrafish expressing Myl7:eGFP not exposed to light, Myl7:eGFP exposed to light, and Myl7:GtACR1-eGFP not exposed to light. When compared to prior stimulation (3 dpf), the ACR1-expressing stimulated larva's resting heart rate did not change.

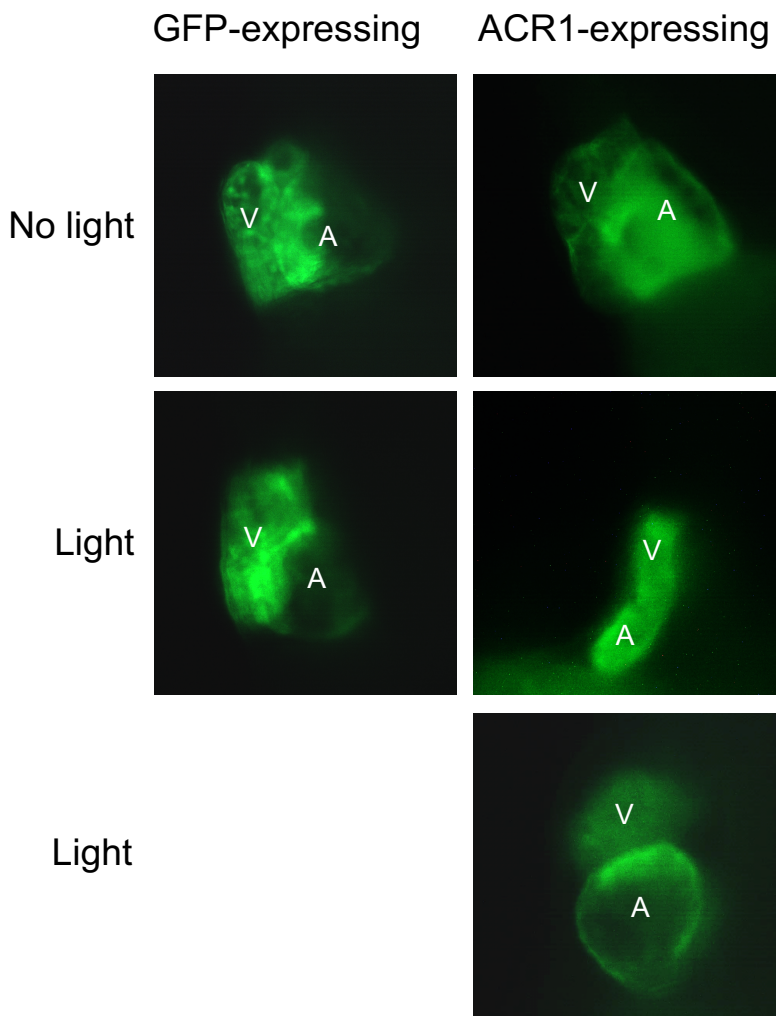

Fig. 30. Fluorescent microscopy images of cardiac morphology in GFP-expressing and ACR1-expressing larvae at 7 post-fertilization (dpf) exposed to the light stimulus. Fluorescent images captured both the ventricle (V) and atrium (A). A tubular heart defect as well as an atrial dilation was found in ACR1-expressing larvae exposed to the light stimulus.

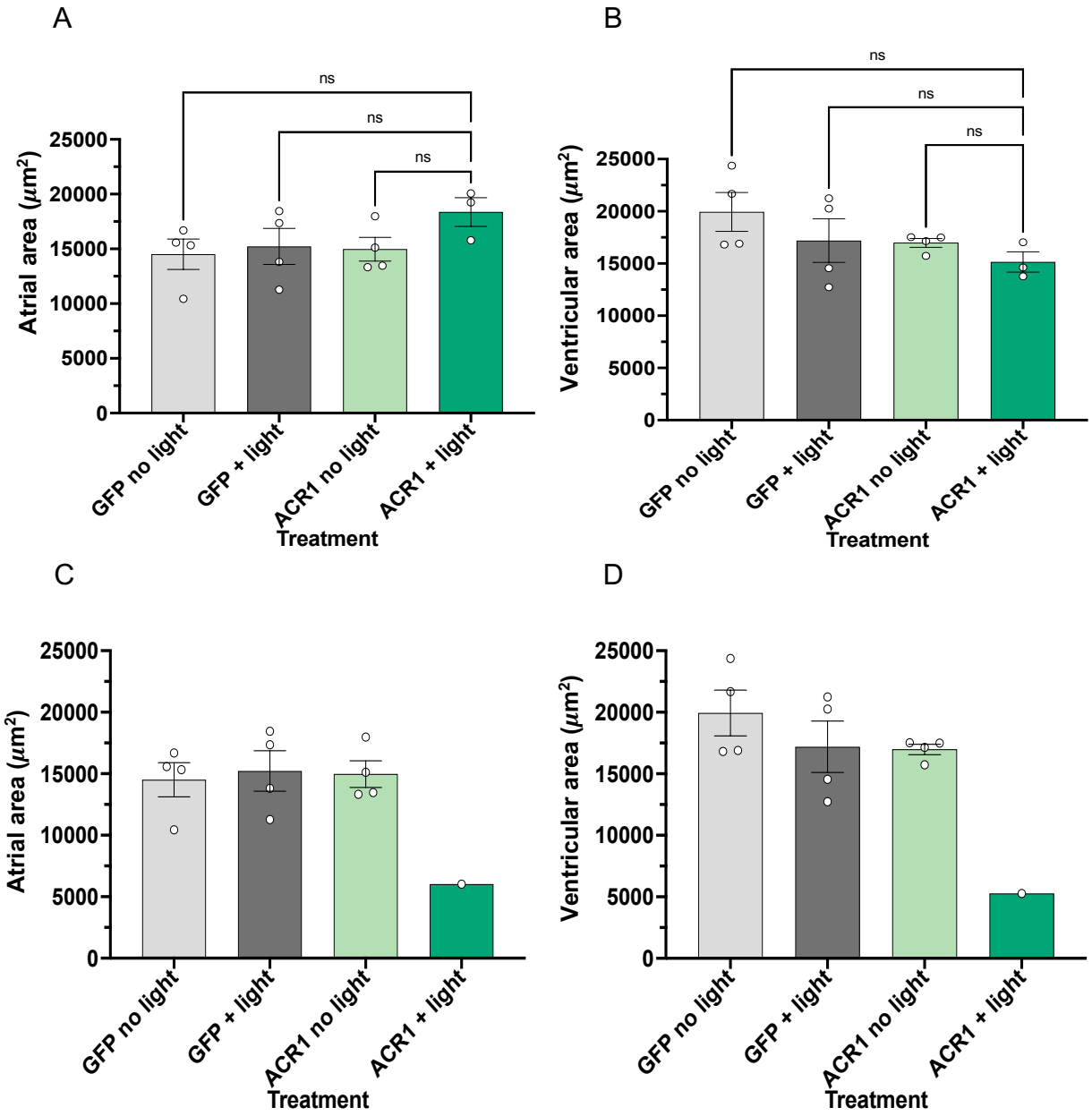

Fig. 31. The average atrial (A,C) and ventricular (B,D) area in μm^2 was determined for ACR1-expressing larvae at 7 post-fertilization (dpf) from fluorescent microscopy images of cardiac morphology. Error bars represent $\pm$ the standard error from the mean. Clutch size = 2, sample size = 4. Area measurements were compared to whether the ACR1-expressing larvae exposed to light presented a chamber dilation (A,B), or tubular defect (C,D). In the tubular defect phenotype, a decline in atrial (C) and ventricular (D) area was observed.

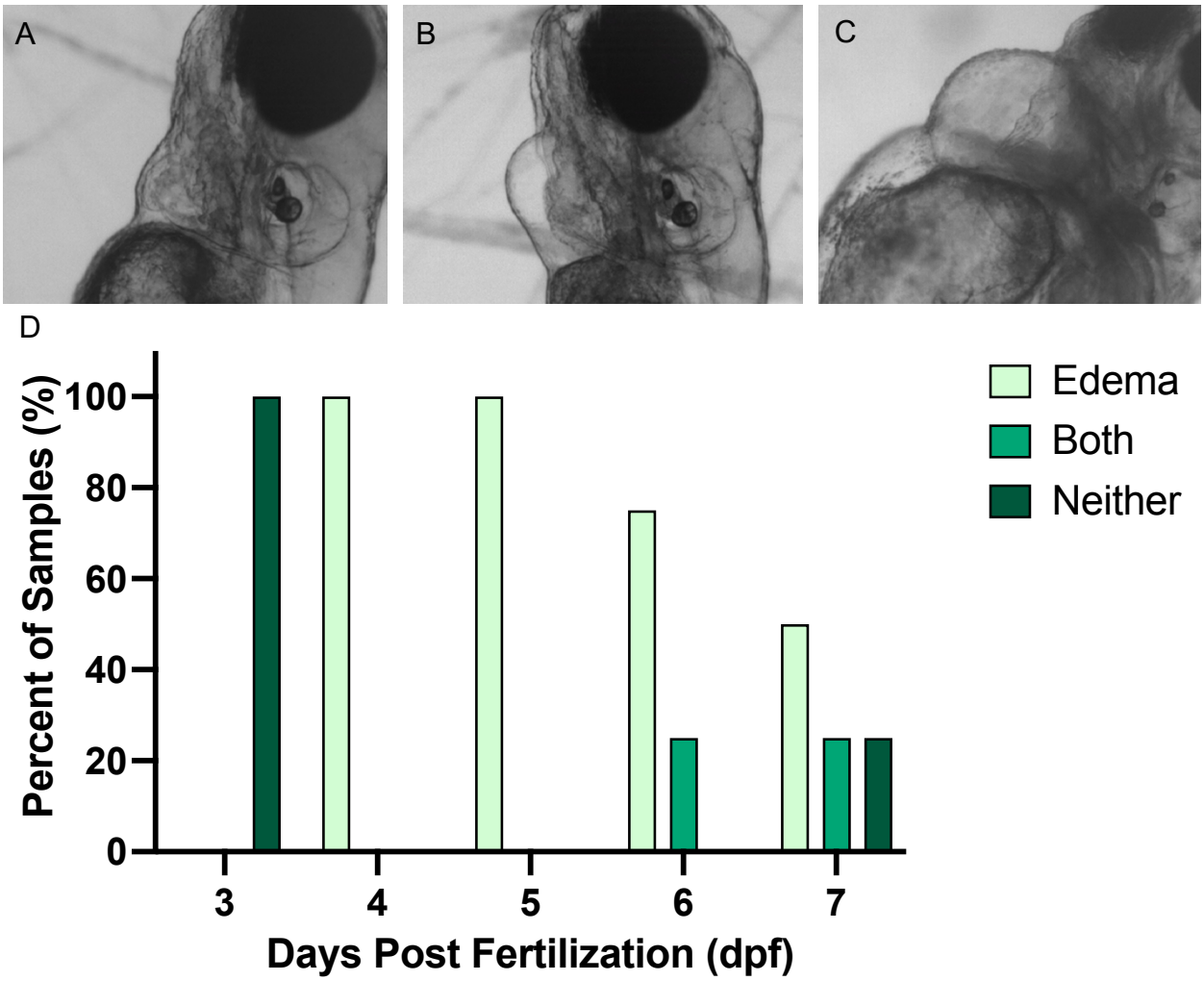

Fig. 32. (A, B, C) Representative images of control (A), and ACR1-expressing zebrafish larvae with a non-tubular (B) or tubular (C) phenotype. In treated larvae, a pericardial edema presented, in which it was mild in the non-tubular groups and severe in those with the tubular defect. Images were acquired at 6 days post-fertilization (dpf) under a brightfield microscope. (D) Percentage of ACR1-expressing larvae exposed to the light stimulus that demonstrated neither an edema or tubular defect, only an edema, or both an edema and tubular defect. Clutch size = 2, sample size = 4. Prior to stimulation, all samples were found to be without a pericardial edema or a tubular defect. After one day of treatment (4 dpf), all samples possessed a pericardial edema. As chronic stimulation progressed, a greater proportion of samples possessed both a tubular defect and a pericardial edema. However, at 7 dpf, one of the treated samples did not possess either an edema or both an edema and tubular defect.

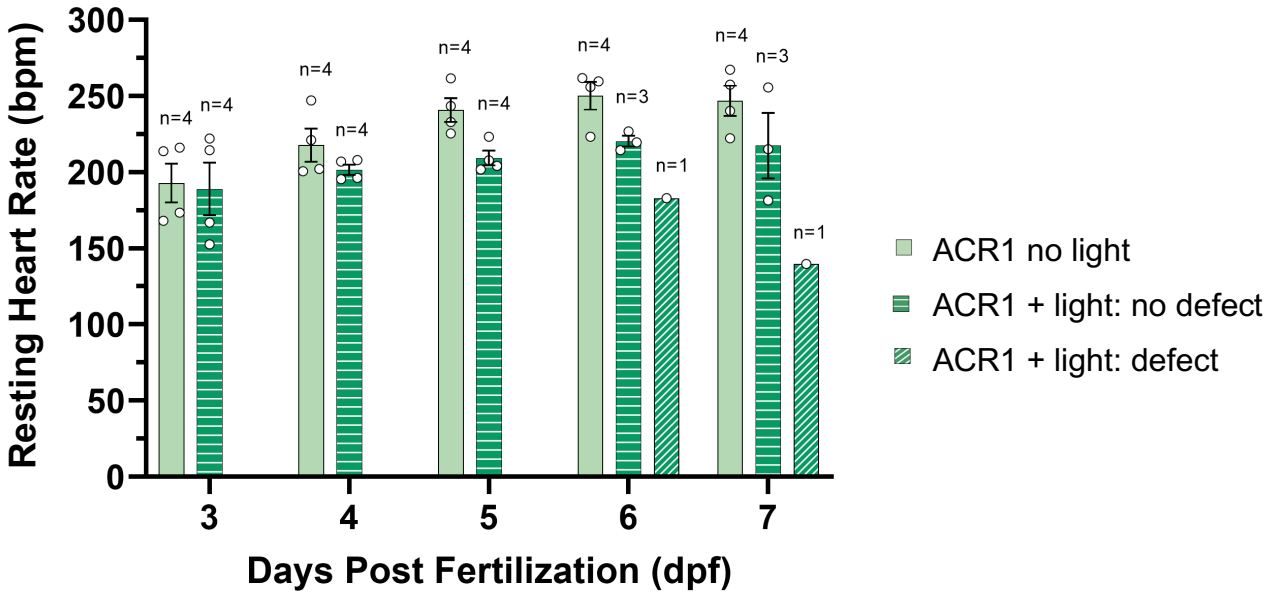

Fig. 33. The average resting heart rate was further interpretated as to whether the ACR1-expressing zebrafish larvae had a tubular heart defect, no tubular defect, or was not exposed to light. Error bars represent ± the standard error from the mean. The decline in resting heart rate appeared to be more pronounced in the ACR1-expressing zebrafish larvae with the tubular heart defect by 6 dpf.

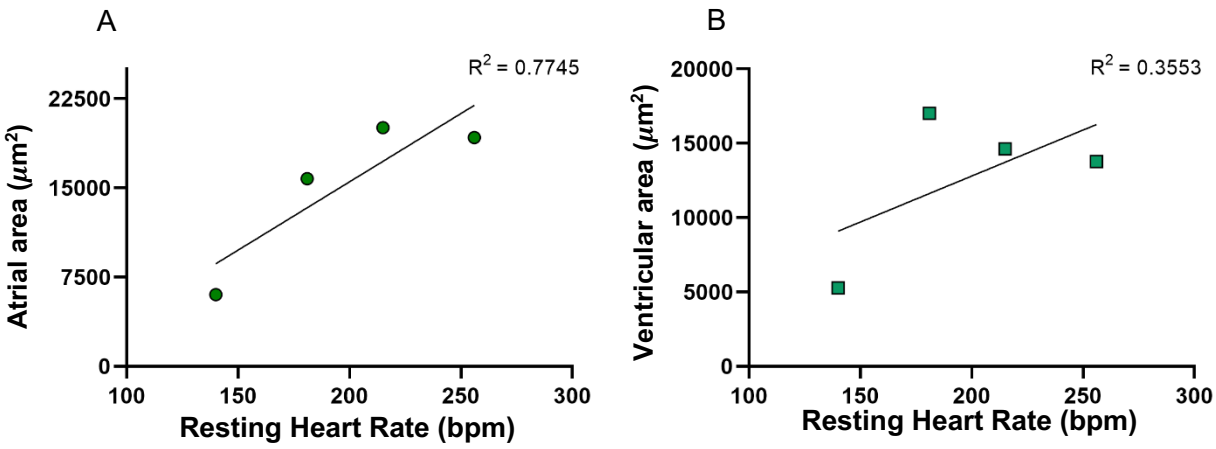

Fig. 34. The average resting heart rate in beats per minute (bpm) was compared to chamber area (μm^2) in continuous light exposed ACR1-expressing larvae at 7 days post fertilization (dpf). Clutch size = 2, sample size = 4. The data was fitted with a simple linear regression to determine the relationship between the two variables. (A) A coefficient of determination (R^2) value of 0.7745 was determined for atrial area when compared to heart rate indicating a strong association between these variables. (B) A R^2 value of 0.3553 was determined when ventricular area was compared to heart rate indicating a weak association.

3.5. Interval Pacing at 4.7 Hz Starting at 2 DPF

3.5.1. Changes in Resting Heart Rate and Morphology in ChR2-expressing Larvae

Due to the fact continuous pacing was producing a tubular defect, as well as potentially leading to the desensitization of the channels, interval pacing was investigated to attempt to mitigate these effects. Exposing ChR2-expressing zebrafish larvae to interval optical pacing beginning at 2 dpf resulted in no changes in resting heart rate (Fig. 35). Fluorescent microscopy images of cardiac morphology revealed an atrial dilation in ChR2-expressing larvae exposed to the light stimulus (Fig. 36). When atrial and ventricular area was measured from fluorescent images, an increase in atrial area was found (Fig. 37).

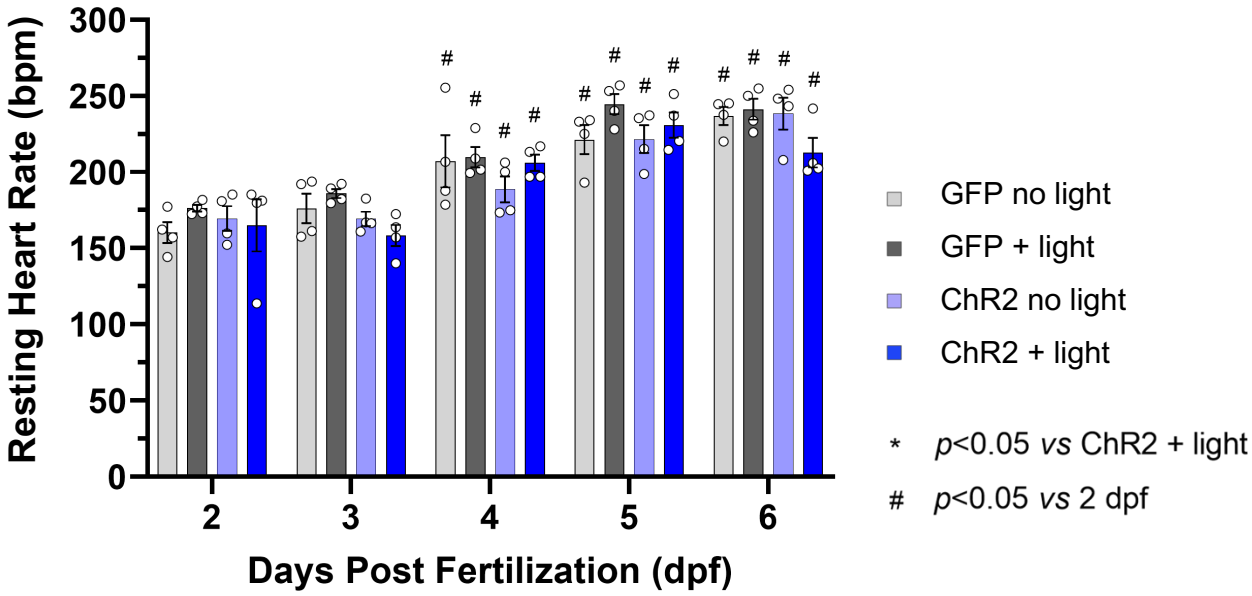

Fig. 35. The average resting heart rate in beats per minute (bpm) of ChR2-expressing zebrafish larvae exposed to optical interval pacing from 2-6 days post-fertilization (dpf). Error bars represent ± the standard error from the mean. Clutch size = 2, sample size = 4 for each dpf. The "*" represents statistical significance of the control groups when compared to the treatment group (ChR2 + light) within each dpf. The "#" represents statistical significance of the groups at each dpf when compared to prior to stimulation (2 dpf). Resting heart rate was unaffected in Myl7:hChR2-eYFP-expressing stimulated larvae when compared to the control groups, which were larval zebrafish expressing Myl7:eGFP not exposed to light, Myl7:eGFP exposed to light, and Myl7:hChR2-eYFP not exposed to light.

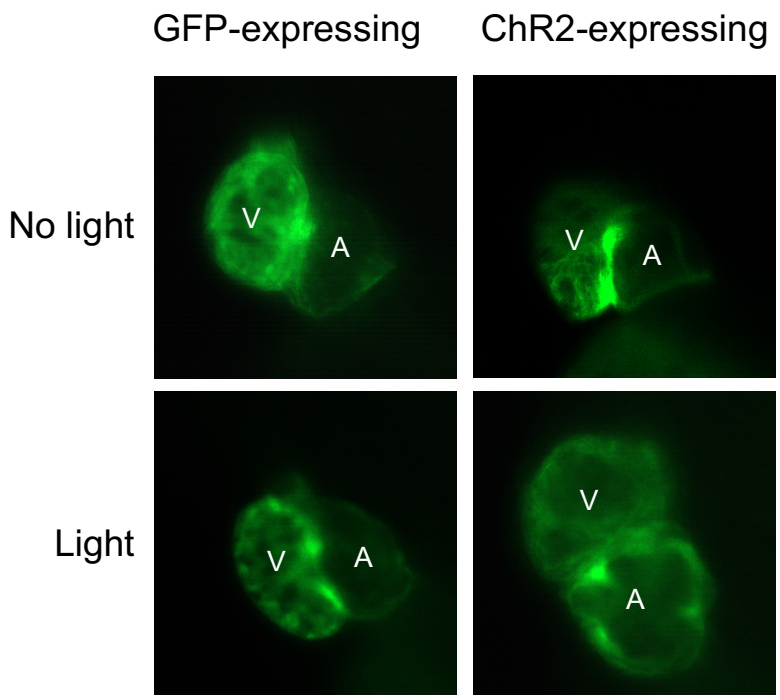

Fig. 36. Fluorescent microscopy images of cardiac morphology in GFP-expressing and ChR2-expressing larvae at 6 post-fertilization (dpf) exposed to the interval light stimulus. Fluorescent images captured both the ventricle (V) and atrium (A). An atrial dilation was observed in the ChR2-expressing larvae exposed to the interval light stimulus.

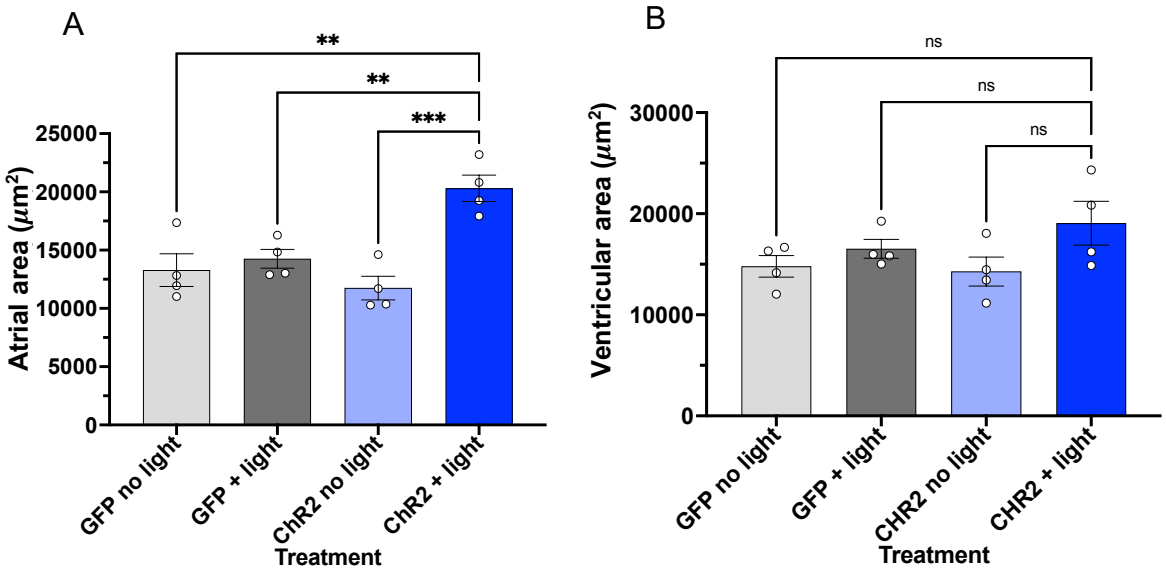

Fig. 37. The average atrial (A) and ventricular (B) area in μm^2 was determined for larvae at 6 post-fertilization (dpf) from fluorescent microscopy images of cardiac morphology. Error bars represent $\pm$ the standard error from the mean. Clutch size = 2, sample size = 4. Atrial area was significantly increased in the ChR2-expressing larval zebrafish exposed to the interval light stimulus.

3.5.1.1. mRNA Expression in Interval Pacing in ChR2-expressing Larvae

Quantitative RT-PCR was used to assess changes in relative mRNA expression of several genes of interest for larvae at 6 dpf (Fig. 38). Atrial and brain natriuretic peptides, Myh6, and TGF-β1 were found to be significantly increased in ChR2-expressing larvae exposed to the interval light stimulation.

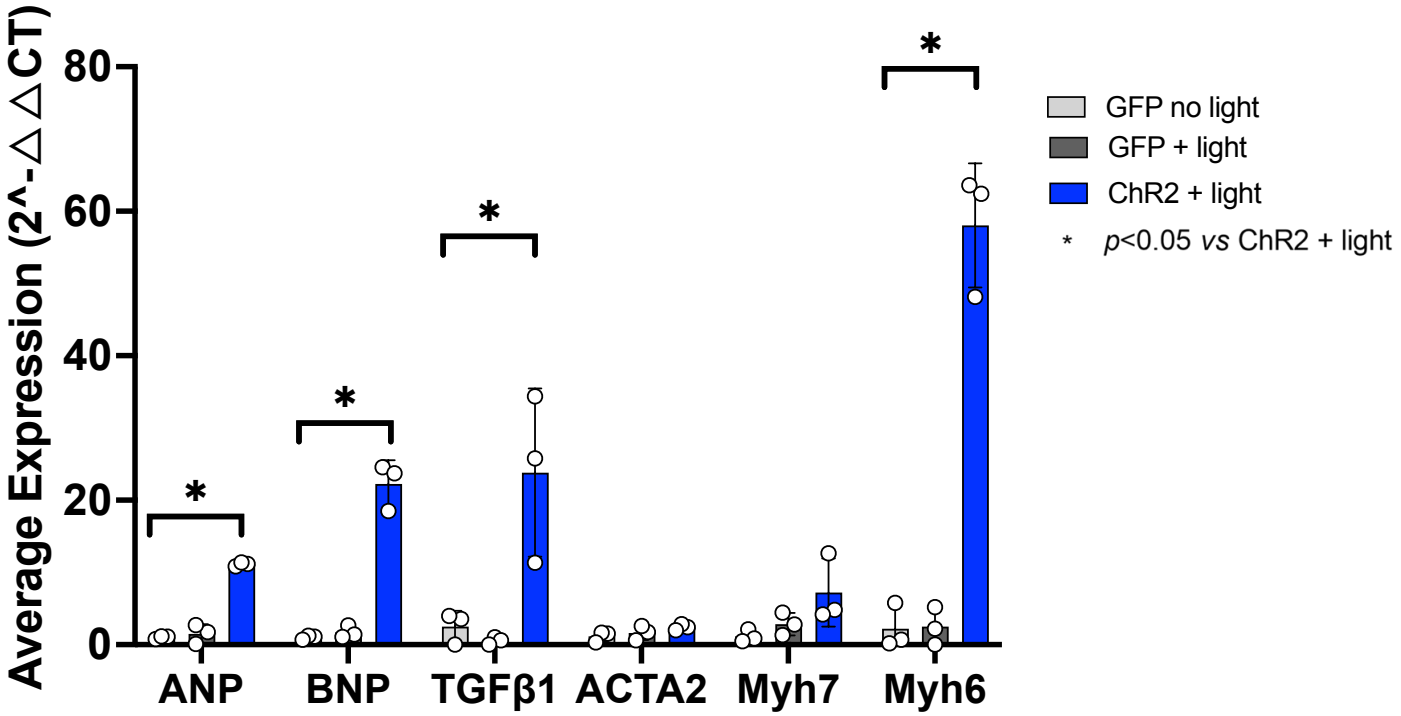

Fig. 38. qRT-PCR relative gene expression of genes of interest determined for ChR2-expressing larvae at 6 days post fertilization (dpf) exposed to interval pacing. The results represent the average from three samples obtained from independent experiments. The results were normalized to two reference genes, Efa1 and Rpl13a. Error bars represent ± the standard error from the mean. Atrial and brain natriuretic peptides, Myh6, and TGF-β1 were found to be significantly increased in ChR2-expressing larvae exposed to the light stimulus.

3.5.2. Changes in Resting Heart Rate and Morphology in ACR1-expressing Larvae

When ACR1-expressing larvae were exposed to interval optical pacing beginning at 2 dpf, resting heart rate was unchanged (Fig. 39). Fluorescent microscopy images of cardiac morphology revealed no changes in ACR1-expressing larvae exposed to the light stimulus (Fig. 40, 41).

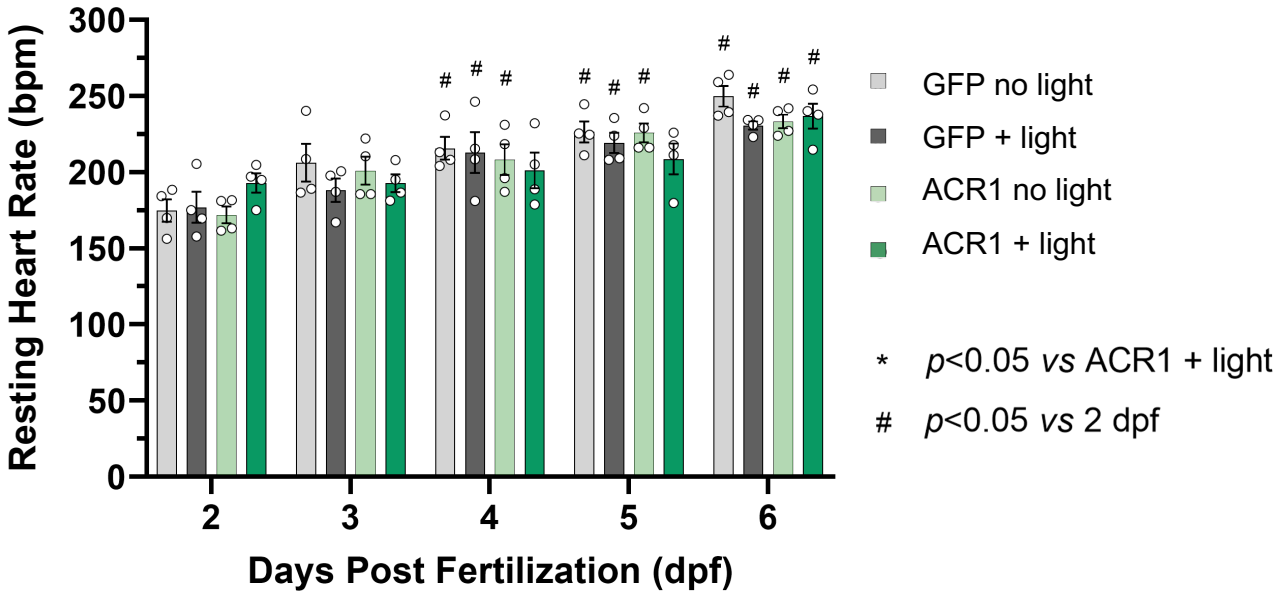

Fig. 39. The average resting heart rate in beats per minute (bpm) of ACR1-expressing zebrafish larvae exposed to optical interval pacing from 2-6 days post-fertilization (dpf). Error bars represent ± the standard error from the mean. Clutch size = 2, sample size = 4 for each dpf. The "*" represents statistical significance of the control groups when compared to the treatment group (ACR1 + light) within each dpf. The "#" represents statistical significance of the groups at each dpf when compared to prior to stimulation (2 dpf). Resting heart rate was unaffected in Myl7:GtACR1-eGFP-expressing stimulated larvae when compared to the control groups, which were larval zebrafish expressing Myl7:eGFP not exposed to light, Myl7:eGFP exposed to light, and Myl7:GtACR1-eGFP not exposed to light.

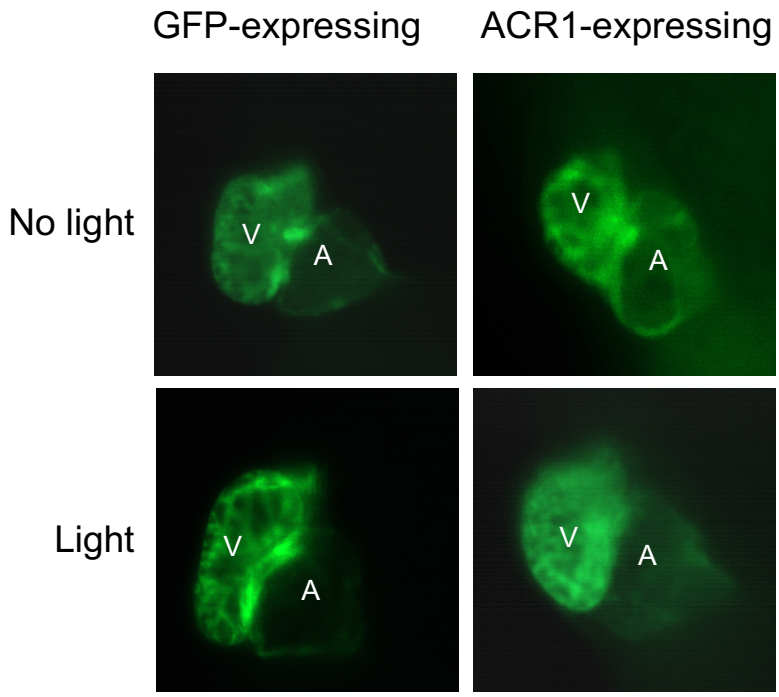

Fig. 40. Fluorescent microscopy images of cardiac morphology in GFP-expressing and ACR1-expressing larvae at 6 post-fertilization (dpf) exposed to the interval light stimulus. Fluorescent images captured both the ventricle (V) and atrium (A). No effects on cardiac morphology were observed at this mode of pacing.

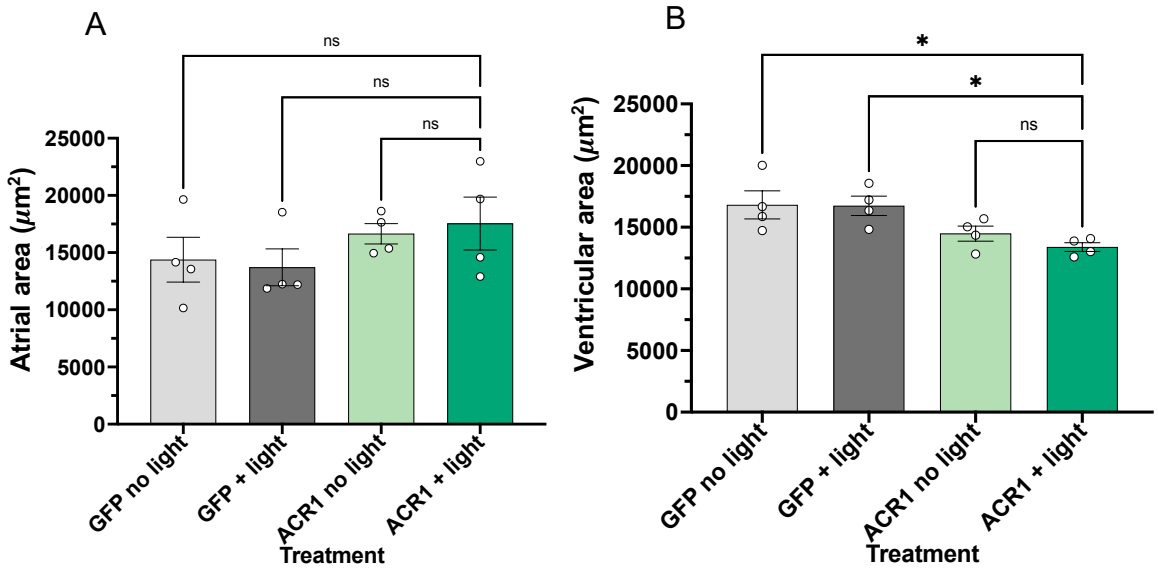

Fig. 41. The average atrial (A) and ventricular (B) area in μm^2 was determined for ACR1-expressing larvae at 6 post-fertilization (dpf) from fluorescent microscopy images of cardiac morphology. Error bars represent $\pm$ the standard error from the mean. Clutch size = 2, sample size = 4. No significant changes in atrial and ventricular area were determined.

3.5.2.1. mRNA Expression in Interval Pacing in ACR1-expressing Larvae

Quantitative RT-PCR was used to assess changes in relative mRNA expression of several genes of interest for larvae at 6 dpf (Fig. 42). Atrial and brain natriuretic peptides, and Myh6 were found to be significantly increased in ACR1-expressing larvae exposed to the interval light stimulation.

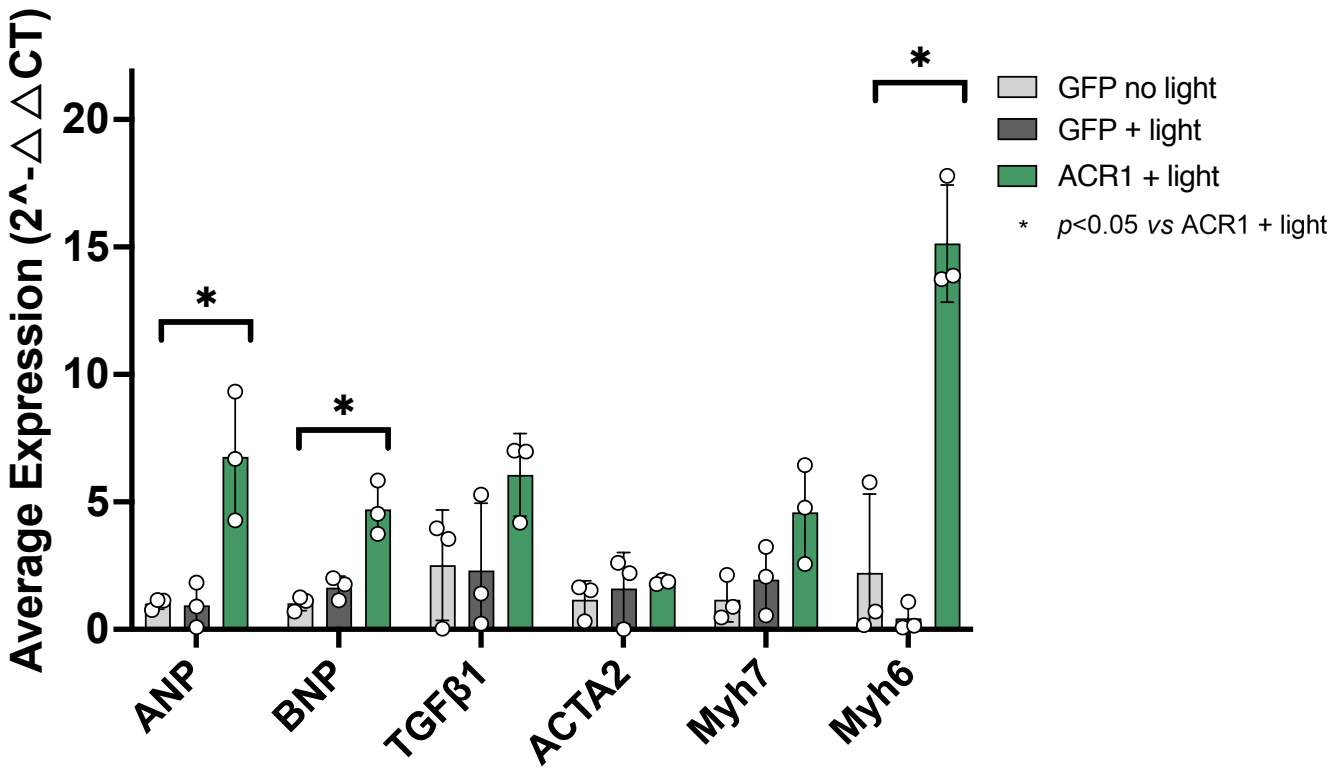

Fig. 42. qRT-PCR relative gene expression of genes of interest determined for ACR1-expressing larvae at 6 days post fertilization (dpf) exposed to interval pacing. The results represent the average from three samples obtained from independent experiments. The results were normalized to two reference genes, Efa1 and Rpl13a. Error bars represent ± the standard error from the mean. Atrial and brain natriuretic peptides, and Myh6 were found to be significantly increased in ACR1-expressing larvae exposed to the light stimulus.

3.6. Interval Pacing at 4.7 Hz Starting at 3 DPF

3.6.1. Changes in Resting Heart Rate and Morphology in ChR2-expressing Larvae

When ChR2-expressing larvae were exposed to interval optical pacing, resting heart rate was unchanged (Fig. 43). Fluorescent microscopy images of cardiac morphology revealed an atrial dilation in ChR2-expressing larvae exposed to the light stimulus, however, no significant changes in chamber area were found (Fig. 44, 45). Due to the lack of effects found, changes in mRNA expression were not investigated for this pacing protocol.

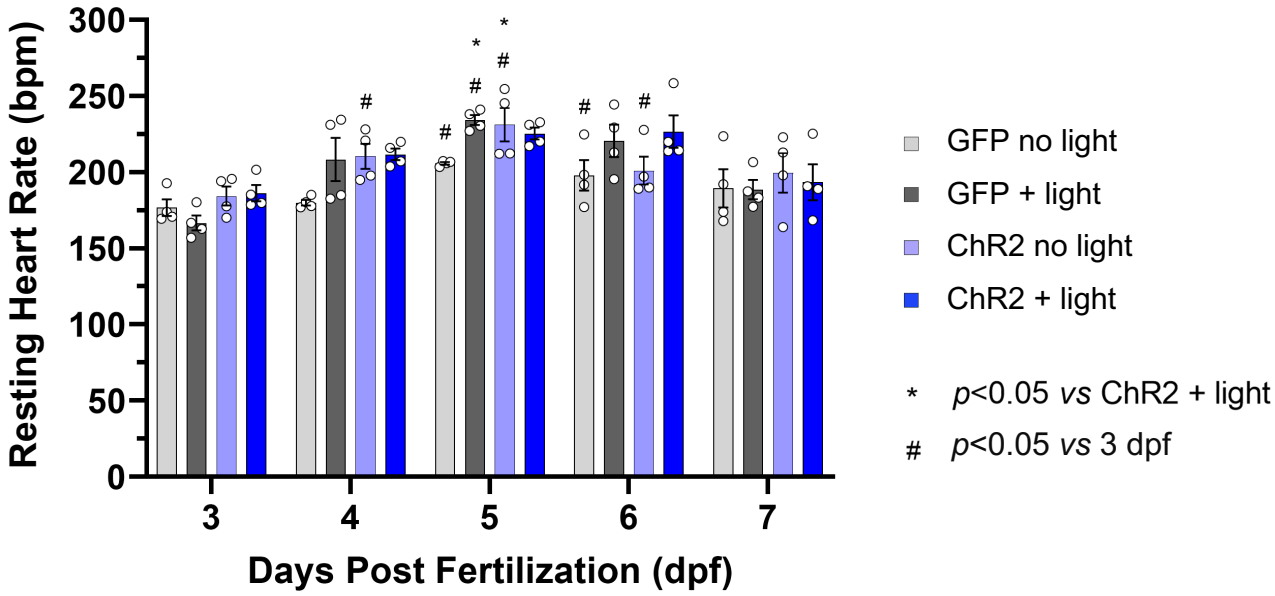

Fig. 43. The average resting heart rate in beats per minute (bpm) of ChR2-expressing zebrafish larvae exposed to optical interval pacing from 3-7 days post-fertilization (dpf). Error bars represent $\pm$ the standard error from the mean. Clutch size = 2, sample size = 4 for each dpf. The "*" represents statistical significance of the control groups when compared to the treatment group (ChR2 + light) within each dpf. The "#" represents statistical significance of the groups at each dpf when compared to prior to stimulation (3 dpf). Resting heart rate was lower unaffected Myl7:hChR2-eGFP-expressing stimulated larvae when compared to the control groups, which were larval zebrafish expressing Myl7:eGFP not exposed to light, Myl7:eGFP exposed to light, and Myl7:hChR2-eYFP not exposed to light.

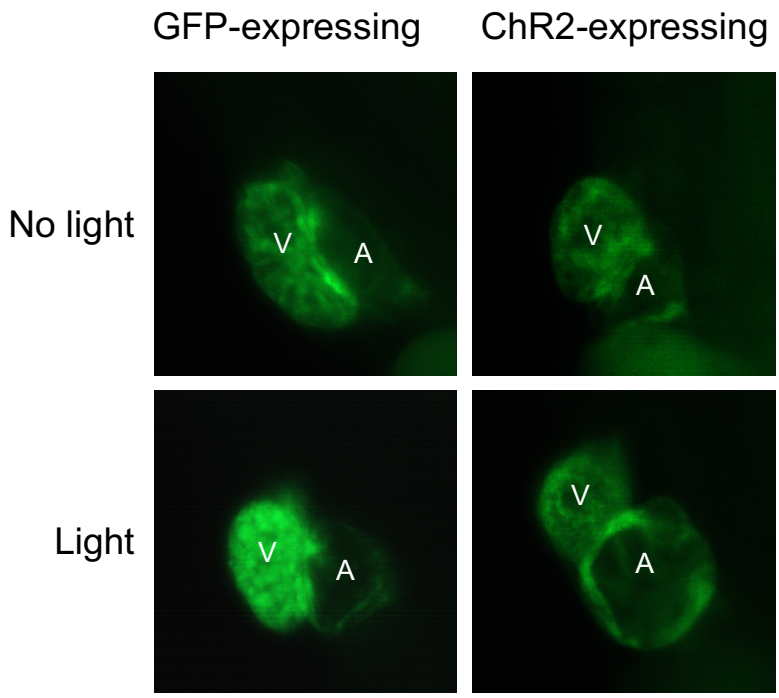

Fig. 44. Fluorescent microscopy images of cardiac morphology in GFP-expressing and ChR2-expressing larvae at 7 days post-fertilization (dpf) exposed to the interval light stimulus. Fluorescent images captured both the ventricle (V) and atrium (A). An atrial dilation was observed in a ChR2-expressing larvae exposed to the light stimulus.

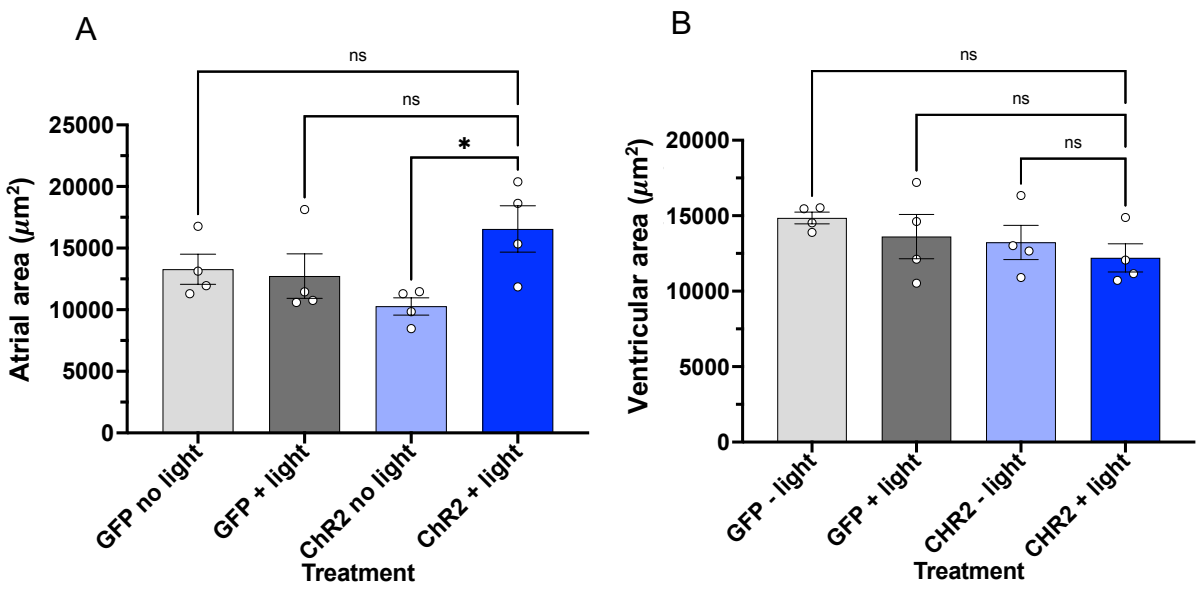

Fig. 45. Average atrial (A) and ventricular (B) area in μm^2 was determined for ChR2-expressing larvae at 7 days post-fertilization (dpf) from fluorescent microscopy images of cardiac morphology. Error bars represent $\pm$ the standard error from the mean. Clutch size = 2, sample size = 4. No significant changes in atrial and ventricular area were determined.

3.6.2. Changes in Resting Heart Rate and Morphology in ACR1-expressing Larvae

When ACR1-expressing larvae were exposed to interval optical pacing, resting heart rate was unchanged (Fig. 46). Fluorescent microscopy images of cardiac morphology revealed no changes in ACR1-expressing larvae exposed to the light stimulus (Fig. 47, 48).

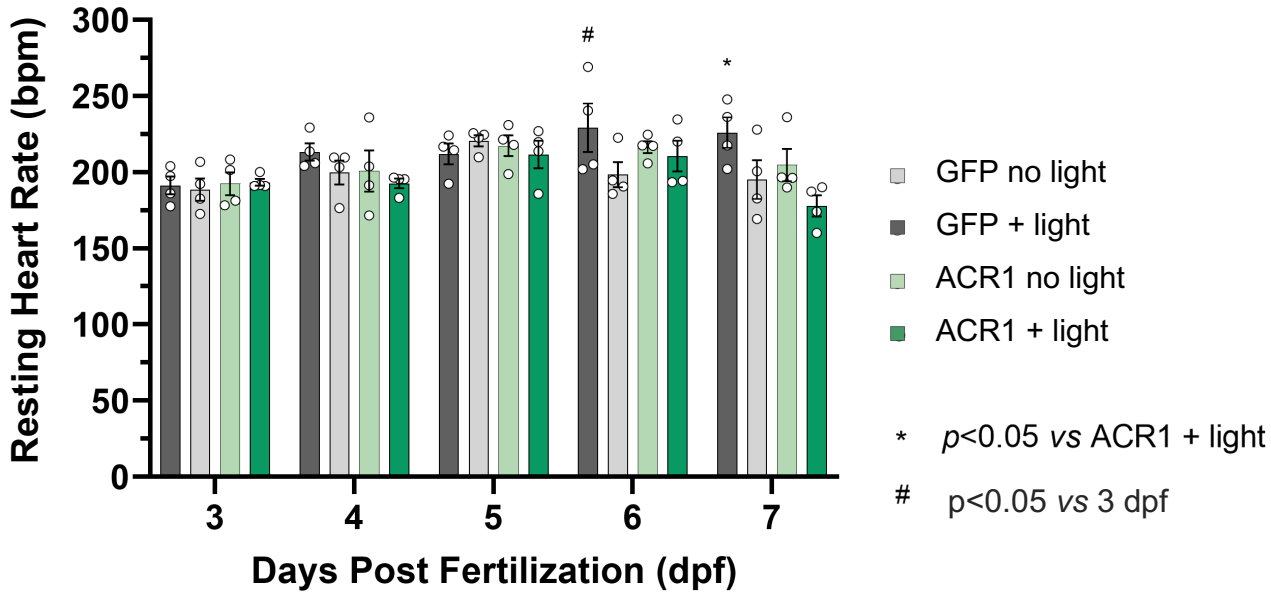

Fig. 46. The average resting heart rate in beats per minute (bpm) of ACR1-expressing zebrafish larvae exposed to optical interval pacing from 3-7 days post-fertilization (dpf). Error bars represent ± the standard error from the mean. Clutch size = 2, sample size = 4 for each dpf. The "*" represents statistical significance of the control groups when compared to the treatment group (ACR1 + light) within each dpf. The "#" represents statistical significance of the groups at each dpf when compared to prior to stimulation (3 dpf). Resting heart rate was unaffected from the light stimulus in the Myl7:GtACR1-eGFP-expressing larvae when compared to the control groups, which were larval zebrafish expressing Myl7:eGFP not exposed to light, Myl7:eGFP exposed to light, and Myl7:GtACR1-eGFP not exposed to light.

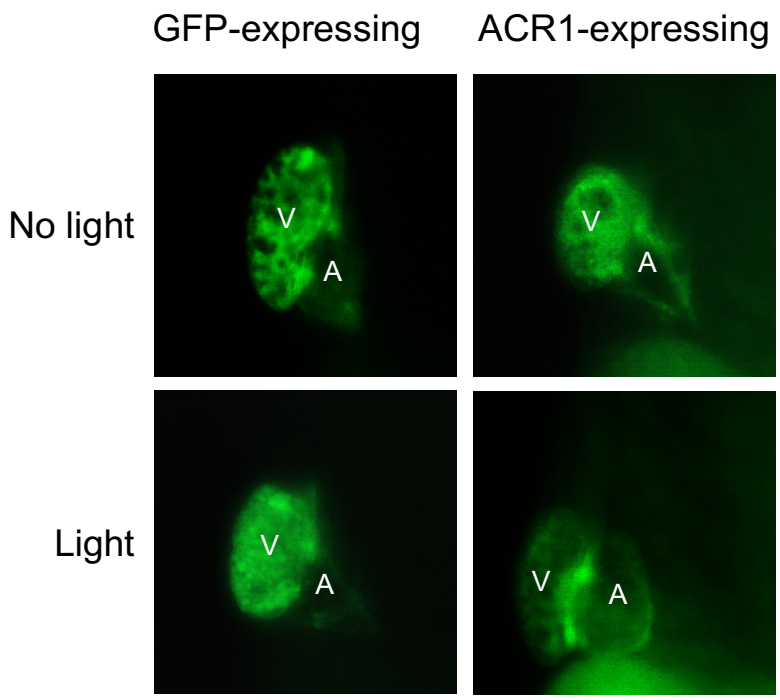

Fig. 47. Fluorescent microscopy images of cardiac morphology in GFP-expressing and ACR1-expressing larvae at 7 days post-fertilization (dpf) exposed to the interval light stimulus. Fluorescent images captured both the ventricle (V) and atrium (A). No changes in cardiac morphology were observed.

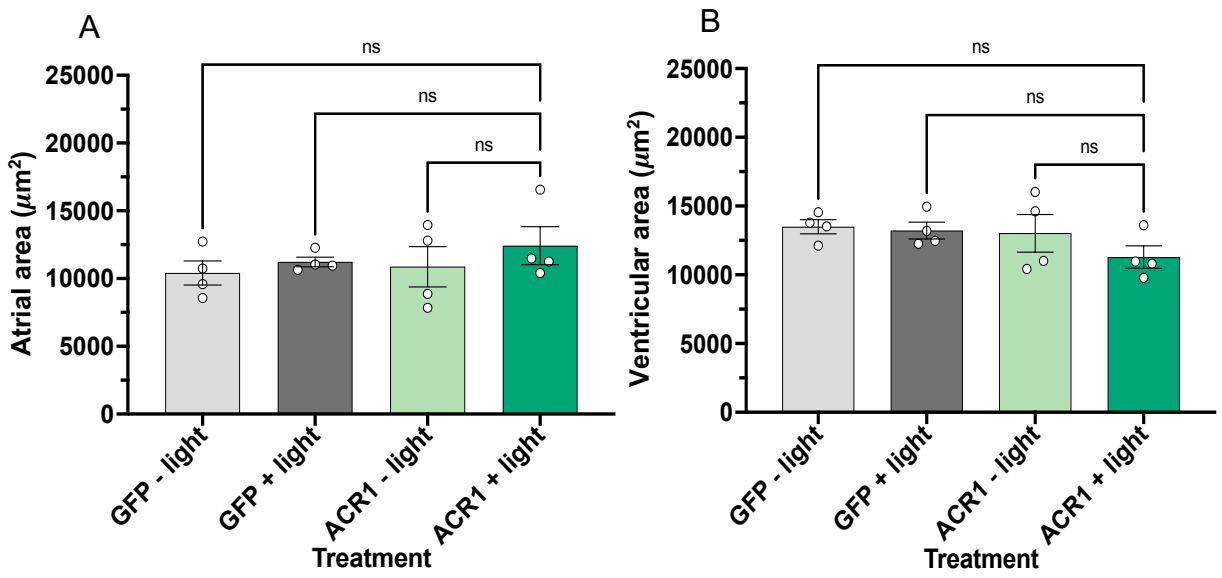

Fig. 48. The average atrial (A) and ventricular (B) area in μm^2 was determined for ACR1-expressing larvae at 7 days post-fertilization (dpf) from fluorescent microscopy images of cardiac morphology. Error bars represent $\pm$ the standard error from the mean. Clutch size = 2, sample size = 4. No significant changes in atrial and ventricular area were determined.

3.7. Results Summary

It was found that chronic continuous pacing beginning at either 2 or 3 dpf, of both ChR2- and ACR1-expressing larvae, produced a tubular heart defect that was associated with a decline in resting heart rate and a decline in atrial and ventricular area (Table 5). The changes in mRNA expression resulting from continuous pacing were associated with ventricular stretch. When chronic continuous pacing was administered a day later in develop (2 compared to 3 dpf), the proportion of samples with the tubular heart defect within the sampled population declined.

Chronic interval pacing of both ChR2- and ACR1-expressing larvae led to no effects on resting heart rate and no production of a tubular heart defect. Starting interval pacing at 2 dpf in ChR2-expressing larvae produced chamber dilation, and changes in mRNA expression for genes related to atrial and ventricular wall stretch, heart failure and inflammation, and atrial hypertrophy. Starting interval pacing at 2 dpf in ACR1-expressing larvae did not produce changes in chamber area. However, changes in mRNA expression for genes related to atrial and ventricular wall stretch, and atrial hypertrophy were observed. When chronic interval pacing was started at 3 dpf in ChR2- and ACR1-expressing larvae, a lack of significant effects on chamber area was observed.

Table 5. Summary of results found across each mode of pacing

Start of Experiment		2 dpf				3 dpf			
Mode of Pacing		Cont.	Interval	Cont.	Interval	Cont.	Interval	Cont.	Interval
Opsin		ChR2		ACR1		ChR2		ACR1	
Heart Rate		↓	NE	↓/NE	NE	↓/NE	NE	↓/NE	NE
Chamber Area	A	↓*	↑	↓/↑	NE	↓/↑	↑*	↓*/NE	NE
	V	↓	↑*	↓/↑	NE	↓/NE	NE	↓*/NE	NE
Gene expression		BNP	ANP, BNP, TGF-ß1, Myh6	BNP, TGF-ß 1	ANP, BNP, Myh6				
Tubular/ Nontubular		4/0	0/4	3/1	0/4	2/2	0/4	2/2	0/4

Legend

- NE: No effect
- *: No significance
- A: Atrium
- V: Ventricle

Chapter 4: Discussion

This study aimed to establish a model of chronic tachypacing-induced HF in larval zebrafish using optogenetics. The effects of chronic optogenetic tachypacing of larval zebrafish hearts with two opsins (ChR2 and ACR1) were compared. Furthermore, the effects of continuous and interval pacing between 2 to 6, and 3 to 7 dpf were investigated. To determine the effects of chronic optical tachypacing, changes in cardiac morphology, function, and mRNA levels of genes associated with cardiac remodelling during HF were assessed. Cardiac morphology and function were measured from *in vivo* brightfield microscopic recordings and morphology was further investigated using fluorescent microscopy. Genetic responses were evaluated by expression changes quantified using qRT-PCR. Continuous chronic tachypacing with ChR2- and ACR1-expressing larvae resulted in cardiac development defects, while interval pacing with ChR2-expressing larvae resulted in morphological changes reminiscent of HR. When changes in mRNA levels were assessed in opsin-expressing larvae exposed to interval pacing, an increase in several markers for HF were elevated, including levels of ANP, BNP, and TGF-ß1, as well as the marker for hypertrophy, Myh6.

4.1. Optical Capture

When the average maximum optical pacing rate was assessed in ChR2-expressing larvae from 2-7 dpf, the samples were found to be successfully paced at a frequency of 4.9 ± 0.2 Hz (Fig. 4B). In ACR1-expressing larvae, a lower average maximal optical pacing rate of 4.2 ± 0.4 Hz was found (Fig. 5B). The differences in ability to capture between the two opsins could be attributed to the different properties of the channels. The ability to capture at higher frequencies is affected by the channel conductance and

kinetics, the channel's reversal potential, and differences in opsin expression. The channel conductance establishes the efficacy of light-induced depolarization, while fast channel kinetics is required for adequate channel recovery between stimuli at high frequencies. Furthermore, ability to depolarize the membrane and initiate cardiac contraction is influenced by the channel's reversal potential, as well as from the opsin expression levels, where low opsin expression reduces the channel's ability to depolarize the membrane (Lin, 2011). While ACR1 possesses greater channel conductance and faster repolarization kinetics, ChR2 has a greater reversal potential, and therefore, might be more effective at depolarizing the membrane (Bergs et al., 2018).

4.2. Changes in Heart Rate

Continuous tachypacing led to a decline in resting heart in ChR2- and ACR1-expressing larvae when pacing was started both 2 and 3 dpf (Fig. 7, 15, 23, 29). However, when changes in heart rate were further examined based upon the resulting phenotype, the decline in resting heart rate was found to be more prominent in samples possessing the tubular heart defect (Fig. 11, 20, 27, 33).

A tubular heart defect has been reported previously in larval zebrafish as a result of interfering with cardiac development through genetic manipulations or exposure to cardiotoxic pharmaceuticals (Huang et al., 2005; Mi et al., 2023; Razaghi et al., 2018). Commonly associated with this defect is a pericardial edema, and a decrease in resting heart rate and contractile function (Du et al., 2015; Duan et al., 2016; Razaghi et al., 2018; Yang et al., 2017).

A possible explanation for the decline in resting heart rate in the defective hearts could be related to the association of the tubular defect with the pericardial edema, as both were observed consistently together (Fig. 10, 17, 26, 32). An increase in pericardial pressure could constrict the heart and affect its pump function. In a study by Maerz et al. (2019), the researchers observed effects on cardiac function and morphology after administrating atorvastatin from 0-2 dpf. Exposure to atorvastatin disrupted cardiac looping and produced a tubular heart defect, bradycardia, and a pericardial edema. The researchers were able to prevent the formation of the pericardial edema through the administration of water-soluble cholesterol. While the tubular defect persisted without the pericardial edema, the heart rate was rescued, indicating a possible effect of the edema on heart rate but not morphology. Future work could similarly prevent the pericardial edema formation to address the possible effects of the pericardial edema on the bradycardia recorded in our study.

Furthermore, bradycardia in the tubular defect group could result from the chronic continuous optogenetic stimulation interfering with the development of the cardiac conduction system. The zebrafish cardiac conduction system firstly forms at 24 hours post-fertilization (hpf), where it exists as a linear conduction pattern slowly travelling from the sinus venosus to the outflow track, with a primitive sinoatrial node covering a large area on the venous pole of the heart tube (Chi et al., 2008; Fishman, 2005; Martin & Waxman, 2021). At 36-48 hpf, the atrioventricular conduction delay forms, and the sinoatrial node condenses into a ring around the venous pole (Martin & Waxman, 2021; Pashmforoush et al., 2004). At 72 hpf, a more mature pacemaker has formed as the sinoatrial node narrows into a small cluster of cells in the right dorsal region of the

atrium (K. E. Martin & Waxman, 2021). Additionally, from 72-96 hpf the ventricle develops trabeculation, which serves as a fast conduction network for zebrafish**,** functionally similar to the Purkinje fibre network in mammals (Sedmera et al., 2003). As our treatments began at either 2 or 3 dpf, it is possible that the continuous pacing interferes with these critical points of conduction system development, like through the interference of the development of the mature sinoatrial node, and results in bradycardia.

When chronic interval pacing was applied, no changes in resting heart rate occurred in the ChR2- and ACR1-expressing larvae (Fig. 35, 39, 42, 45). This finding is consistent with a previous study by Lemme et al. (2019), in which engineered heart tissue expressing ChR2 experienced chronic optical interval tachypacing. In this study, no effect was found on the resting beating rate, and the researchers believed this was due to the electrical remodeling observed. Faster diastolic depolarization was recorded, which should increase the resting beating rate. However, a slower upstroke velocity was also reported. The slower upstroke velocity was suspected to be mediated by the depolarized take-off potential, which the researchers predicted affected sodium channel availability. Therefore, the changes in take-off potential are likely involved in maintaining physiological beating rates. Alternatively, the lack of effects on resting beating rate reported in the study by Lemme et al. (2019) could also be attributed to the use of engineered heart tissue, as tissue models lacks the neurohormonal influences present in a whole organism model. However, in models of electrical tachypacing-induced cardiomyopathies, it is frequently reported that resting heart rate increases, which is inconsistent with our findings (Spinale et al., 1991, 1992, 1994).

4.3. Changes in Cardiac Morphology

Chronic continuous tachypacing led to a tubular defect in ChR2- and ACR1-expressing larvae when pacing started at both 2 and 3 dpf (Fig. 8, 16, 23, 30). The defect appeared 24 hours after pacing and was present in greater proportions as the duration of the treatment increased (Fig. 9, 18, 26, 32).

Disruptions to early cardiac development can lead to a tubular heart appearance, in which the ventricle is positioned anterior to the atrium, similar to what was observed in our study (Antkiewicz et al., 2005; Bello et al., 2004; Wang et al., 2006). In a study by Antkiewicz et al. (2005), the authors described a tubular defect that progressed by 72 hpf after exposure to 2, 3, 7, 8-tetrachlorodibenzodioxin (TCDD). The authors hypothesized that the resulting defect was due to the disrupted development of the common cardinal vein. In physiological zebrafish cardiac development between 72 and 96 hpf, the common cardinal vein attaches to the heart at the sinus venosus and migrates dorsally, which leads to further cardiac looping (Bello et al., 2004). As a result of disrupting cardiac development, there is mechanical stretching and elongation of the heart, producing a tubular appearance (Antkiewicz et al., 2005). Therefore, beginning chronic continuous optical pacing at 2 and 3 dpf may have disrupted this process in cardiac development, leading to an elongated heart defect.

An additional phenotype was observed as an effect of chronic optogenetic tachypacing, which was a dilation of the chambers. When opsin-expressing larvae were continuously paced, those that did not develop a tubular defect, demonstrated a dilation in the atrium at the experimental endpoint (Fig. 16, 23, 36).

Chamber dilation is a common morphological effect as a result of chronic tachypacing (Damiano et al., 1987; Shannon et al., 1991; Tanaka et al., 1992). During chronic tachypacing, there is a discrepancy between metabolic supply and demand, and the hemodynamic capabilities of the heart (Raymond-Paquin et al., 2018; Yamamoto et al., 2006). As a result, the RAAS is activated, which increases salt and water retention to raise blood volume and improve cardiac output. However, the volume overload leads to a stretching force on the myocardium and consequently, the heart undergoes eccentric hypertrophy (Mihl et al., 2008). It is likely then that in our study the hearts experienced eccentric hypertrophy. To assess this effect, treated larval hearts could be isolated, sectioned and stained to observe structural changes at a cellular level.

Lastly, differences in morphology were found between ChR2- and ACR1-expressing larvae exposed to interval pacing. When samples were paced in 15-second intervals, a dilation was observed in ChR2-expressing samples and not ACR1-expressing samples at the experimental endpoints (Fig. 36, 40). One possible explanation could be differences in the ability to capture at 4.7 Hz. It was found that a greater proportion of ChR2-expressing samples were captured at 4.7 Hz than ACR1 (Fig. 4B, 5B). As a result of ability to capture, ChR2-expressing samples could have been more affected by the treatment. Secondly, differences in the effects of pacing the different opsin-expressing larvae could be related to the fact that the opsins are selective for the passage of different ions. For instance, it is supported that tachypacing can cause calcium mishandling, which can have pathological effects on cardiac function and structure (Perreault et al., 1992). Since ChR2 is selective for cations, chronic activation of this channel could enhance this pathway towards dysfunction.

4.4. Changes in mRNA expression

It was found that continuous pacing of ChR2-expressing larvae led to increased mRNA expression of BNP, and in ACR1-expressing larvae there was an increase in BNP and TGF-β1 (Fig. 14, 22). It has been commonly supported that BNP is elevated during HF (Becker et al., 2012; Nadrowski et al., 2013; Weber & Hamm, 2006). The natriuretic peptides are believed to be cardioprotective during HF by balancing the effects of RAAS and TGF-β1 signaling and promoting natriuresis, which prevent hypertrophy and fibrosis (Nishikimi et al., 2006). Due to their significant role in HF, ANP and BNP are commonly used as biomarkers for the progression of HF (Gaggin & Januzzi, 2013).

Interestingly, ANP was not significantly elevated from continuous pacing (Fig 14, 22). This finding is contrary to most studies of HF, in which ANP levels are elevated (Agnoletti et al., 1990; Becker et al., 2012; Moe et al., 1990). However, several reports of chronic tachypacing-induced HF have reported ANP plasma levels returning to baseline, potentially due to ANP stores becoming depleted (Khasnis et al., 2005; Moe et al., 1990, 1991). A possible method to observe if ANP levels are plateauing in our study would be to perform measurements of ANP mRNA expression at multiple time points.

An additional explanation for the lack of increase in ANP could be related to possible effects on atrial integrity from our treatment. An increase in atrial fibrosis reduces atrial cardiomyocytes and the chamber's ability to stretch, leading to a decline in ANP production (van den Berg et al., 2004). In a study by Ogawa et al. (2018), the researchers developed an ANP/BNP index to represent atrial integrity throughout HF. The study proposed that in more severe conditions of HF, the ANP/BNP index should

be low as BNP will remain elevated, while ANP is reduced due to an increase in atrial fibrosis. In our study, if the tubular defect produced was associated with atrial fibrosis, it would explain why ANP levels were depleted but not BNP. In a study by Sarmah & Marrs (2017), the researchers studied the relationship between fibrosis and tubular heart defects in larval zebrafish after early exposure to ethanol. Within this study, histological analysis revealed changes in myocardial structure indicative of cardiac fibrosis.

In ACR1-expressing samples, there was an increase in mRNA of TGF-β1, a genetic marker for cardiac hypertrophy and fibrosis. However, TGF-β1 is involved in numerous signaling pathways in many different tissue types, and due to the fact RNA samples were isolated from whole embryos, it may be elevated due to noncardiac specific factors. Furthermore, mRNA levels of ACTA2, an additional fibrotic marker, was unaffected in both opsin-expressing samples. Nevertheless, the role of fibrosis within the tubular heart defect presented in our study should be further examined through additional techniques like histological analysis.

Similar to continuous pacing, chronic interval pacing of opsin-expressing larvae led to an increase in mRNA expression of BNP and TGF-β1 (Fig. 38, 41). Additionally, interval tachypacing led to an elevation of ANP and Myh6, markers for atrial wall stretch, and hypertrophy, respectively. This finding was intriguing due to the reported atrial dilation in the ChR2-expressing larvae exposed to interval pacing. An interpretation of these findings could be that interval tachypacing of ChR2-expressing larvae increases atrial wall stretch, which increases ANP production and leads to eccentric hypertrophic growth of the atrium.

However, Myh7, the additional studied hypertrophy marker, was not found to be elevated. A possible explanation for the elevation of Myh6 and not Myh7 could be due to the greater expression of Myh6 within the atrium, where the majority of the dilation was reported. The elevation of these markers in ACR1-expressing samples did not agree with the observed lack of effects on cardiac morphology and function. However, ANP and BNP could be elevated in a state of compensatory HF, preceding obvious changes in cardiac function and morphology. Furthermore, while at 6 dpf there were no measured changes in morphology, brightfield recordings from earlier time points revealed samples possessing possible chamber dilation. It is possible, then, that the pooled samples for mRNA extraction possess larvae that have been morphologically affected by the treatment; however, due to low sample sizes, effects on morphology were not discovered when the images were acquired.

4.5. Limitations

A limitation of this study was its low sample size. For instance, since differential phenotypes emerged due to the continuous tachypacing, sample sizes of some phenotypes were too low to perform statistics (n=1); it would be beneficial to increase sample sizes to observe more definitive trends.

Additionally, using larval zebrafish as a model species could cause confounding effects due to the ongoing maturation of the model. For instance, while chronic continuous tachypacing led to dilated chambers and elevated markers of HF, the mode of pacing also produced a tubular heart defect that is not representative of human HF but of irregular cardiac development. However, the results highlight the potential for this

model for circumstances where cardiac development and dysfunction are confounded, like for the study of congenital heart defects or pediatric HF.

Furthermore, while qRT-PCR measures changes in mRNA expression, it cannot directly infer changes in protein levels as several factors can create discrepancies. For instance, translational regulation, differences in protein half-lives, and experimental error are all believed to contribute to inconsistencies. While the qRT-PCR results provide intriguing preliminary data for the study, confirming the upregulation of these proteins using additional techniques such as immunohistochemistry and western blot analysis would be beneficial (Beyer et al., 2004; Greenbaum et al., 2003).

4.6. Conclusions

In conclusion, we established a putative model of chronic optogenetic tachypacing-induced HF in larval zebrafish. When the use of two opsins, ChR2 and ACR1, were compared, we observed differences in the effects of chronic optical pacing. Furthermore, chronic optogenetic tachypacing resulted in changes in resting heart rate and cardiac morphology, and mRNA expression, which were dependent on the developmental period of stimulus application, and whether continuous or interval pacing was used.

4.7. Future Directions

Future studies could study alterations in recognized markers for cardiac development, like Nkx2.5, Tbx20, and Hand2, to discern potential confounding effects on the progression of HF from disrupted cardiac development (Lu et al., 2016). Alternatively, pacing could be performed later within larval zebrafish development so that they have further completed cardiac development.

Additionally, while HF can occur in a pediatric setting, the condition is most prevalent in adults. Therefore, it would be beneficial to establish the model in more developed zebrafish. The use of more mature zebrafish would allow for further cardiac development which could mitigate possible confounding effects of disrupted development. Furthermore, due to the immature organ systems in the larvae, mature zebrafish may have mechanisms towards the progression of HF that are more similar to clinical HF.

Furthermore, it is well supported that chronic tachypacing leads to dysfunction primarily through altered hemodynamic properties and energetic starvation (Raymond-Paquin et al., 2018). It would be beneficial to pursue measurements of altered hemodynamic and metabolic activity to establish this model and demonstrate that it leads to dysfunction in similar mechanisms.

Lastly, it may be interesting to simulate chronic tachyarrhythmia. While chronic rhythmic tachypacing can occur clinically, cardiomyopathies are most commonly the result of a chronic tachyarrhythmia, with atrial fibrillation being the most common cause (Bozkurt et al., 2016). In a study by Wijffels et al. (1995), atrial fibrillation was artificially maintained in goats using implanted atrial leads. In this study, the atrium was burst paced for one second at 64 Hz and then allowed to slow to sinus rhythm before an

automated administration of another set of burst pacing. This pacing procedure sufficiently captured the progressive nature of AF, as over time, the episodes of non-sustained atrial fibrillation lengthened until sustained atrial fibrillation was achieved. The electrical pacing patterns described in models of tachyarrhythmias, like the study discussed, could be modelled to deliver a noninvasive optogenetic stimulus in larval zebrafish to create a more clinically relevant model of HF.

References

Ackerman, M. J., Priori, S. G., Willems, S., Berul, C., Brugada, R., Calkins, H., Camm, A. J., Ellinor, P. T., Gollob, M., Hamilton, R., Hershberger, R. E., Judge, D. P., Le Marec, H., McKenna, W. J., Schulze-Bahr, E., Semsarian, C., Towbin, J. A., Watkins, H., Wilde, A., … Zipes, D. P. (2011). HRS/EHRA Expert Consensus Statement on the State of Genetic Testing for the Channelopathies and Cardiomyopathies: This document was developed as a partnership between the Heart Rhythm Society (HRS) and the European Heart Rhythm Association (EHRA). *Heart Rhythm*, *8*(8), 1308–1339. https://doi.org/10.1016/j.hrthm.2011.05.020

Agnoletti, G., Cornacchiari, A., Panzali, A. F., Ghielmi, S., De Giuli, F., & Ferrari, R. (1990). Effect of congestive heart failure on rate of atrial natriuretic factor release in response to stretch and isoprenaline. *Cardiovascular Research*, *24*(11), 938–945. https://doi.org/10.1093/cvr/24.11.938

Ahmad, F., Seidman, J. G., & Seidman, C. E. (2005). The Genetic Basis for Cardiac Remodeling. *Annual Review of Genomics and Human Genetics*, *6*(1), 185–216. https://doi.org/10.1146/annurev.genom.6.080604.162132

Aldor, Erd, Gaul, Kuh, Leisch, Lenzhofer, Mlczoch, Peschorn, Tiso, Block, & Balthazar. (2000). Effect of 48-h intravenous trimetazidine on short- and long-term outcomes of patients with acute myocardial infarction, with and without thrombolytic therapy. A double-blind, placebo-controlled, randomized trial. *European Heart Journal*, *21*(18), 1537–1546. https://doi.org/10.1053/euhj.1999.2439

Alousi, A. A., Canter, J. M., & Fort, D. J. (1985). The beneficial effect of amrinone on acute drug-induced heart failure in the anaesthetised dog. *Cardiovascular Research*, *19*(8), 483–494. https://doi.org/10.1093/cvr/19.8.483

Ambrosi, C. M., Williams, J. C., & Entcheva, E. (2014). Abstract 19856: Optogenetic Modulation of Pacemaking, Arrhythmia Generation, and Inhibition with Sustained (Non-pulsed) Light. *Circulation*, *130*(suppl_2), A19856–A19856. https://doi.org/10.1161/circ.130.suppl_2.19856

Ammarguellat, F., Larouche, I., & Schiffrin, E. L. (2001). Myocardial Fibrosis in DOCA-Salt Hypertensive Rats. *Circulation*, *103*(2), 319–324. https://doi.org/10.1161/01.CIR.103.2.319

Amores, A., Catchen, J., Ferrara, A., Fontenot, Q., & Postlethwait, J. H. (2011). Genome Evolution and Meiotic Maps by Massively Parallel DNA Sequencing: Spotted Gar, an Outgroup for the Teleost Genome Duplication. *Genetics*, *188*(4), 799–808. https://doi.org/10.1534/genetics.111.127324

Amores, A., Force, A., Yan, Y.-L., Joly, L., Amemiya, C., Fritz, A., Ho, R. K., Langeland, J., Prince, V., Wang, Y.-L., Westerfield, M., Ekker, M., & Postlethwait, J. H. (1998). Zebrafish hox Clusters and Vertebrate Genome Evolution. *Science*, *282*(5394), 1711–1714. https://doi.org/10.1126/science.282.5394.1711

Andersen, C. L., Jensen, J. L., & Ørntoft, T. F. (2004). Normalization of Real-Time Quantitative Reverse Transcription-PCR Data: A Model-Based Variance Estimation Approach to Identify Genes Suited for Normalization, Applied to Bladder and Colon Cancer Data Sets. *Cancer Research*, *64*(15), 5245–5250. https://doi.org/10.1158/0008-5472.CAN-04-0496

Anderson, P. G., Bishop, S. P., & Peterson, J. T. (2006). Chapter 26—Cardiovascular Research. In M. A. Suckow, S. H. Weisbroth, & C. L. Franklin (Eds.), *The Laboratory Rat (Second Edition)* (pp. 773–802). Academic Press. https://doi.org/10.1016/B978-012074903-4/50029-7

Antkiewicz, D. S., Burns, C. G., Carney, S. A., Peterson, R. E., & Heideman, W. (2005). Heart Malformation Is an Early Response to TCDD in Embryonic Zebrafish. *Toxicological Sciences*, *84*(2), 368–377. https://doi.org/10.1093/toxsci/kfi073

Apitz, C., Honjo, O., Friedberg, M. K., Assad, R. S., Arsdell, G. V., Humpl, T., & Redington, A. N. (2012). Beneficial Effects of Vasopressors on Right Ventricular Function in Experimental Acute Right Ventricular Failure in a Rabbit Model. *The Thoracic and Cardiovascular Surgeon*, 17–23. https://doi.org/10.1055/s-0031-1298058

Arber, S., Hunter, J. J., Ross, J., Hongo, M., Sansig, G., Borg, J., Perriard, J.-C., Chien, K. R., & Caroni, P. (1997). MLP-Deficient Mice Exhibit a Disruption of Cardiac Cytoarchitectural Organization, Dilated Cardiomyopathy, and Heart Failure. *Cell*, *88*(3), 393–403. https://doi.org/10.1016/S0092-8674(00)81878-4

Arrenberg, A. B., Stainier, D. Y. R., Baier, H., & Huisken, J. (2010). Optogenetic Control of Cardiac Function. *Science*, *330*(6006), 971–974. https://doi.org/10.1126/science.1195929

Ayitey-Smith, E., & Kalsner, S. (1977). Increased monoamine oxidase activity in cardiovascular and central nervous systems of DOCA-NaCl hypertensive rabbits. *Life Sciences*, *20*(8), 1341–1345. https://doi.org/10.1016/0024-3205(77)90359-9

Baillie, J. S., Stoyek, M. R., & Quinn, T. A. (2021). Seeing the Light: The Use of Zebrafish for Optogenetic Studies of the Heart. *Frontiers in Physiology*, *12*, 748570. https://doi.org/10.3389/fphys.2021.748570

Bakkers, J. (2011). Zebrafish as a model to study cardiac development and human cardiac disease. *Cardiovascular Research*, *91*(2), 279–288. https://doi.org/10.1093/cvr/cvr098

Basting, T., & Lazartigues, E. (2017). DOCA-Salt Hypertension: An Update. *Current Hypertension Reports*, *19*(4), 32. https://doi.org/10.1007/s11906-017-0731-4

Battista, N., Douglas, D., Lane, A., Samsa, L., Liu, J., & Miller, L. (2019). Vortex Dynamics in Trabeculated Embryonic Ventricles. *Journal of Cardiovascular Development and Disease*, *6*, 6. https://doi.org/10.3390/jcdd6010006

Becker, J. R., Robinson, T. Y., Sachidanandan, C., Kelly, A. E., Coy, S., Peterson, R. T., & MacRae, C. A. (2012). In vivo natriuretic peptide reporter assay identifies chemical modifiers of hypertrophic cardiomyopathy signalling. *Cardiovascular Research*, *93*(3), 463–470. https://doi.org/10.1093/cvr/cvr350

Bello, S. M., Heideman, W., & Peterson, R. E. (2004). 2,3,7,8-Tetrachlorodibenzo-p-dioxin inhibits regression of the common cardinal vein in developing zebrafish. *Toxicological Sciences: An Official Journal of the Society of Toxicology*, *78*(2), 258–266. https://doi.org/10.1093/toxsci/kfh065

Belmonte, S. L., & Blaxall, B. C. (2011). G protein coupled receptor kinases as therapeutic targets in cardiovascular disease. *Circulation Research*, *109*(3), 309–319. Scopus. https://doi.org/10.1161/CIRCRESAHA.110.231233

Bergs, A., Schultheis, C., Fischer, E., Tsunoda, S. P., Erbguth, K., Husson, S. J., Govorunova, E., Spudich, J. L., Nagel, G., Gottschalk, A., & Liewald, J. F. (2018). Rhodopsin optogenetic toolbox v2.0 for light-sensitive excitation and inhibition in Caenorhabditis elegans. *PLOS ONE*, *13*(2), e0191802. https://doi.org/10.1371/journal.pone.0191802

Bertero, E., & Maack, C. (2018). Metabolic remodelling in heart failure. *Nature Reviews Cardiology*, *15*(8), 457–470. https://doi.org/10.1038/s41569-018-0044-6

Beyer, A., Hollunder, J., Nasheuer, H.-P., & Wilhelm, T. (2004). Post-transcriptional Expression Regulation in the Yeast Saccharomyces cerevisiae on a Genomic Scale *. *Molecular & Cellular Proteomics*, *3*(11), 1083–1092. https://doi.org/10.1074/mcp.M400099-MCP200

Bourdier, G., & Robelet, S. (2019). Isoproterenol-induced heart failure in rat heart: Evaluation and cardioprotective strategy. *Archives of Cardiovascular Diseases Supplements*, *11*(2), 230. https://doi.org/10.1016/j.acvdsp.2019.02.107

Bovo, E., Dvornikov, A. V., Mazurek, S. R., de Tombe, P. P., & Zima, A. V. (2013). Mechanisms of Ca2+ handling in zebrafish ventricular myocytes. *Pflügers Archiv - European Journal of Physiology*, *465*(12), 1775–1784. https://doi.org/10.1007/s00424-013-1312-2

Boyden, E. S., Zhang, F., Bamberg, E., Nagel, G., & Deisseroth, K. (2005). Millisecond-timescale, genetically targeted optical control of neural activity. *Nature Neuroscience*, *8*(9), 1263–1268. https://doi.org/10.1038/nn1525

Bozkurt, B., Colvin, M., Cook, J., Cooper, L. T., Deswal, A., Fonarow, G. C., Francis, G. S., Lenihan, D., Lewis, E. F., McNamara, D. M., Pahl, E., Vasan, R. S., Ramasubbu, K., Rasmusson, K., Towbin, J. A., & Yancy, C. (2016). Current Diagnostic and Treatment Strategies for Specific Dilated Cardiomyopathies: A Scientific Statement From the American Heart Association. *Circulation*, *134*(23), e579–e646. https://doi.org/10.1161/CIR.0000000000000455

Brette, F., Luxan, G., Cros, C., Dixey, H., Wilson, C., & Shiels, H. A. (2008). Characterization of isolated ventricular myocytes from adult zebrafish (Danio rerio). *Biochemical and Biophysical Research Communications*, *374*(1), 143–146. https://doi.org/10.1016/j.bbrc.2008.06.109

Brilla, C. G., & Weber, K. T. (1992). Mineralocorticoid excess, dietary sodium, and myocardial fibrosis. *The Journal of Laboratory and Clinical Medicine*, *120*(6), 893–901. https://doi.org/10.5555/uri:pii:002221439290267O

Briston, S., Caldwell, J., Horn, M., Clarke, J., Richards, M., Greensmith, D., Graham, H., Hall, M., Eisner, D., Dibb, K., & Trafford, A. (2011). Impaired β-adrenergic responsiveness accentuates dysfunctional excitation–contraction coupling in an ovine model of tachypacing-induced heart failure. *The Journal of Physiology*, *589*(6), 1367–1382.

Bristow, M. R., Sageman, W. S., Scott, R. H., Billingham, M. E., Bowden, R. E., Kernoff, R. S., Snidow, G. H., & Daniels, J. R. (1980). Acute and chronic cardiovascular

effects of doxorubicin in the dog: The cardiovascular pharmacology of drug-induced histamine release. *Journal of Cardiovascular Pharmacology*, *2*(5), 487–515. https://doi.org/10.1097/00005344-198009000-00002

Burchell, S. A., Spinale, F. G., Crawford, F. A., Tanaka, R., & Zile, M. R. (1992). Effects of chronic tachycardia-induced cardiomyopathy on the beta-adrenergic receptor system. *The Journal of Thoracic and Cardiovascular Surgery*, *104*(4), 1006–1012.

Byrne, M. J., Raman, J. S., Alferness, C. A., Esler, M. D., Kaye, D. M., & Power, J. M. (2002). An ovine model of tachycardia-induced degenerative dilated cardiomyopathy and heart failure with prolonged onset. *Journal of Cardiac Failure*, *8*(2), 108–115. https://doi.org/10.1054/jcaf.2002.32323

Cao, G., Xuan, X., Zhang, R., Hu, J., & Dong, H. (2021). Gene Therapy for Cardiovascular Disease: Basic Research and Clinical Prospects. *Frontiers in Cardiovascular Medicine*, *8*. https://www.frontiersin.org/articles/10.3389/fcvm.2021.760140

Cao, H.-J., Fang, J., Zhang, Y.-L., Zou, L.-X., Han, X., Yang, J., Yan, X., Li, P., Wang, H.-X., Guo, S.-B., & Li, H.-H. (2019). Genetic ablation and pharmacological inhibition of immunosubunit β5i attenuates cardiac remodeling in deoxycorticosterone-acetate (DOCA)-salt hypertensive mice. *Journal of Molecular and Cellular Cardiology*, *137*, 34–45. https://doi.org/10.1016/j.yjmcc.2019.09.010

Cardin, S., Pelletier, P., Libby, E., Le Bouter, S., Xiao, L., Kääb, S., Demolombe, S., Glass, L., & Nattel, S. (2008). Marked differences between atrial and ventricular gene-expression remodeling in dogs with experimental heart failure. *Journal of Molecular and Cellular Cardiology*, *45*(6), 821–831. https://doi.org/10.1016/j.yjmcc.2008.08.007

Castranova, D., Lawton, A., Lawrence, C., Baumann, D. P., Best, J., Coscolla, J., Doherty, A., Ramos, J., Hakkesteeg, J., Wang, C., Wilson, C., Malley, J., & Weinstein, B. M. (2011). The Effect of Stocking Densities on Reproductive Performance in Laboratory Zebrafish (Danio rerio). *Zebrafish*, *8*(3), 141–146. https://doi.org/10.1089/zeb.2011.0688

Chekanov, V. S. (1999). A stable model of chronic bilateral ventricular insufficiency (dilated cardiomyopathy) induced by arteriovenous anastomosis and doxorubicin administration in sheep. *The Journal of Thoracic and Cardiovascular Surgery*, *117*(1), 198–199. https://doi.org/10.1016/s0022-5223(99)70494-0

Chen, J.-N., Eeden, F. J. M. van, Warren, K. S., Chin, A., Nüsslein-Volhard, C., Haffter, P., & Fishman, M. C. (1997). Left-right pattern of cardiac BMP4 may drive asymmetry of the heart in zebrafish. *Development*, *124*(21), 4373–4382. https://doi.org/10.1242/dev.124.21.4373

Chen, Y., Pai, C., Huang, S., Chang, S., Lin, L., Chiang, F., Lin, J., Hwang, J., & Tsai, C. (2013). Inactivation of Myosin Binding Protein C Homolog in Zebrafish as a Model for Human Cardiac Hypertrophy and Diastolic Dysfunction. *Journal of the American Heart Association*, *2*(5), e000231. https://doi.org/10.1161/JAHA.113.000231

Chi, N. C., Shaw, R. M., Jungblut, B., Huisken, J., Ferrer, T., Arnaout, R., Scott, I., Beis, D., Xiao, T., Baier, H., Jan, L. Y., Tristani-Firouzi, M., & Stainier, D. Y. R. (2008). Genetic and Physiologic Dissection of the Vertebrate Cardiac Conduction System. *PLOS Biology*, *6*(5), e109. https://doi.org/10.1371/journal.pbio.0060109

Chouchani, E. T., Pell, V. R., Gaude, E., Aksentijević, D., Sundier, S. Y., Robb, E. L., Logan, A., Nadtochiy, S. M., Ord, E. N. J., Smith, A. C., Eyassu, F., Shirley, R., Hu, C.-H., Dare, A. J., James, A. M., Rogatti, S., Hartley, R. C., Eaton, S., Costa, A. S. H., … Murphy, M. P. (2014). Ischaemic accumulation of succinate controls reperfusion injury through mitochondrial ROS. *Nature*, *515*(7527), Article 7527. https://doi.org/10.1038/nature13909

Citerni, C., Kirchhoff, J., Olsen, L. H., Sattler, S. M., Gentilini, F., Forni, M., Zannoni, A., Grunnet, M., Edvardsson, N., Bentzen, B. H., & Diness, J. G. (2020). Characterization of Atrial and Ventricular Structural Remodeling in a Porcine Model of Atrial Fibrillation Induced by Atrial Tachypacing. *Frontiers in Veterinary Science*, *7*. https://www.frontiersin.org/articles/10.3389/fvets.2020.00179

Ciuffreda, M. C., Tolva, V., Casana, R., Gnecchi, M., Vanoli, E., Spazzolini, C., Roughan, J., & Calvillo, L. (2014). Rat Experimental Model of Myocardial Ischemia/Reperfusion Injury: An Ethical Approach to Set up the Analgesic Management of Acute Post-Surgical Pain. *PLoS ONE*, *9*(4), e95913. https://doi.org/10.1371/journal.pone.0095913

Clemo, H. F., Stambler, B. S., & Baumgarten, C. M. (1999). Swelling-activated chloride current is persistently activated in ventricular myocytes from dogs with tachycardia-induced congestive heart failure. *Circulation Research*, *84*(2), 157–165. https://doi.org/10.1161/01.res.84.2.157

Cohen, M., Boiangiu, C., & Abidi, M. (2010). Therapy for ST-Segment Elevation Myocardial Infarction Patients Who Present Late or Are Ineligible for Reperfusion

Therapy. *Journal of the American College of Cardiology*, *55*(18), 1895–1906. https://doi.org/10.1016/j.jacc.2009.11.087

Cohn, J. N., Ferrari, R., Sharpe, N., & null, null. (2000). Cardiac remodeling—concepts and clinical implications: A consensus paper from an international forum on cardiac remodeling. *Journal of the American College of Cardiology*, *35*(3), 569–582. https://doi.org/10.1016/S0735-1097(99)00630-0

Coleman, H. N., Taylor, R. R., Pool, P. E., Whipple, G. H., Covell, J. W., Ross, J., & Braunwald, E. (1971). Congestive heart failure following chronic tachycardia. *American Heart Journal*, *81*(6), 790–798. https://doi.org/10.1016/0002-8703(71)90083-4

Collister, J. P., Nahey, D. B., Hartson, R., Wiedmeyer, C. E., Banek, C. T., & Osborn, J. W. (2018). Lesion of the OVLT markedly attenuates chronic DOCA-salt hypertension in rats. *American Journal of Physiology-Regulatory, Integrative and Comparative Physiology*, *315*(3), R568–R575. https://doi.org/10.1152/ajpregu.00433.2017

Culp, P., Nüsslein-Volhard, C., & Hopkins, N. (1991). High-frequency germ-line transmission of plasmid DNA sequences injected into fertilized zebrafish eggs. *Proceedings of the National Academy of Sciences of the United States of America*, *88*(18), 7953–7957.

Curtis, A. B., Karki, R., Hattoum, A., & Sharma, U. C. (2018). Arrhythmias in Patients ≥80 Years of Age. *Journal of the American College of Cardiology*, *71*(18), 2041–2057. https://doi.org/10.1016/j.jacc.2018.03.019

Damiano, R. J., Tripp, H. F., Asano, T., Small, K. W., Jones, R. H., & Lowe, J. E. (1987). Left ventricular dysfunction and dilatation resulting from chronic supraventricular tachycardia. *The Journal of Thoracic and Cardiovascular Surgery*, *94*(1), 135–143. https://doi.org/10.1016/S0022-5223(19)36329-9

Das, U. N. (2000). Free radicals, cytokines and nitric oxide in cardiac failure and myocardial infarction. *Molecular and Cellular Biochemistry*, *215*(1), 145–152. https://doi.org/10.1023/A:1026579422132

Dassanayaka, S., & Jones, S. (2015). Recent Developments in Heart Failure. *Circulation Research*, *117*(7), e58–e63. https://doi.org/10.1161/CIRCRESAHA.115.305765

Davey, B., Szwast, A., & Rychik, J. (2012). Diagnosis and management of heart failure in the fetus. *Minerva Pediatrica*, *64*(5), 471–492.

de Graeff, N., Jongsma, K. R., Johnston, J., Hartley, S., & Bredenoord, A. L. (2019). The ethics of genome editing in non-human animals: A systematic review of reasons reported in the academic literature. *Philosophical Transactions of the Royal Society B: Biological Sciences*, *374*(1772), 20180106. https://doi.org/10.1098/rstb.2018.0106

De Villiers, C., & Riley, P. R. (2020). Mouse models of myocardial infarction: Comparing permanent ligation and ischaemia-reperfusion. *Disease Models & Mechanisms*, *13*(11), dmm046565. https://doi.org/10.1242/dmm.046565

deAlmeida, A. C., van Oort, R. J., & Wehrens, X. H. T. (2010). Transverse Aortic Constriction in Mice. *Journal of Visualized Experiments : JoVE*, *38*, 1729. https://doi.org/10.3791/1729

Degabriele, N. M., Griesenbach, U., Sato, K., Post, M. J., Zhu, J., Williams, J., Jeffery, P. K., Geddes, D. M., & Alton, E. W. F. W. (2004). Critical appraisal of the mouse model of myocardial infarction. *Experimental Physiology*, *89*(4), 497–505. https://doi.org/10.1113/expphysiol.2004.027276

Denvir, M. A., Tucker, C. S., & Mullins, J. J. (2008). Systolic and diastolic ventricular function in zebrafish embryos: Influence of norepenephrine, MS-222 and temperature. *BMC Biotechnology*, *8*(1), 21. https://doi.org/10.1186/1472-6750-8-21

Dietrich, A.-C., Lombardo, V. A., Veerkamp, J., Priller, F., & Abdelilah-Seyfried, S. (2014). Blood Flow and Bmp Signaling Control Endocardial Chamber Morphogenesis. *Developmental Cell*, *30*(4), 367–377. https://doi.org/10.1016/j.devcel.2014.06.020

Dixon, J. A., & Spinale, F. G. (2009). Large animal models of heart failure: A critical link in the translation of basic science to clincial practice. *Circulation. Heart Failure*, *2*(3), 262–271. https://doi.org/10.1161/CIRCHEARTFAILURE.108.814459

Du, Z., Wang, G., Gao, S., & Wang, Z. (2015). Aryl organophosphate flame retardants induced cardiotoxicity during zebrafish embryogenesis: By disturbing expression of the transcriptional regulators. *Aquatic Toxicology (Amsterdam, Netherlands)*, *161*, 25–32. https://doi.org/10.1016/j.aquatox.2015.01.027

Duan, J., Yu, Y., Li, Y., Li, Y., Liu, H., Jing, L., Yang, M., Wang, J., Li, C., & Sun, Z. (2016). Low-dose exposure of silica nanoparticles induces cardiac dysfunction via neutrophil-mediated inflammation and cardiac contraction in zebrafish

embryos. *Nanotoxicology*, *10*(5), 575–585. https://doi.org/10.3109/17435390.2015.1102981

Dzau, V., Colucci, W., Hollenberg, N., & Williams, G. (1981). Relation of the renin-angiotensin-aldosterone system to clinical state in congestive heart failure. | Circulation. *Circulation*, *63*, 645–651.

Eaton, L. W., & Bulkley, B. H. (1981). Expansion of acute myocardial infarction: Its relationship to infarct morphology in a canine model. *Circulation Research*, *49*(1), 80–88. https://doi.org/10.1161/01.RES.49.1.80

Eisenhofer, G., Friberg, P., Rundqvist, B., Quyyumi, A., Lambert, G., Kaye, D., Kopin, I., Goldstein, D., & Esler, M. (1996). Cardiac Sympathetic Nerve Function in Congestive Heart Failure | Circulation. *Circulation*, *93*(9), 1667–1676.

Ellis, E. R., & Josephson, M. E. (2013). What About Tachycardia-induced Cardiomyopathy? *Arrhythmia & Electrophysiology Review*, *2*(2), 82–90. https://doi.org/10.15420/aer.2013.2.2.82

Entcheva, E., & Kay, M. W. (2021). Cardiac optogenetics: A decade of enlightenment. *Nature Reviews Cardiology*, *18*(5), Article 5. https://doi.org/10.1038/s41569-020-00478-0

Fan, G., Jiang, Y.-P., Lu, Z., Martin, D. W., Kelly, D. J., Zuckerman, J. M., Ballou, L. M., Cohen, I. S., & Lin, R. Z. (2005). A Transgenic Mouse Model of Heart Failure Using Inducible Gαq*. *Journal of Biological Chemistry*, *280*(48), 40337–40346. https://doi.org/10.1074/jbc.M506810200

Fang, Y., Sun, Y., Luo, C., Gu, J., Shi, Z., Lu, G., Silvestre, J.-S., & Chen, Z. (2020). Evaluation of cardiac dysfunction in adult zebrafish using high frequency echocardiography. *Life Sciences*, *253*, 117732. https://doi.org/10.1016/j.lfs.2020.117732

Farrell, A. P., & Pieperhoff, S. (2011). Design and physiology of the heart | Cardiac Anatomy in Fishes. *Encyclopedia of Fish Physiology*, *2*, 998–1005. https://doi.org/10.1016/B978-0-12-374553-8.00139-8

Finckh, M., Hellmann, W., Ganten, D., Furtwängler, A., Allgeier, J., Boltz, M., & Holtz, J. (1991). Enhanced cardiac angiotensinogen gene expression and angiotensin converting enzyme activity in tachypacing-induced heart failure in rats. *Basic Research in Cardiology*, *86*(4), 303–316. https://doi.org/10.1007/BF02191528

Fink, M., Callol-Massot, C., Chu, A., Ruiz-Lozano, P., Belmonte, J. C. I., Giles, W., Bodmer, R., & Ocorr, K. (2009). A new method for detection and quantification of heartbeat parameters in Drosophila, zebrafish, and embryonic mouse hearts. *BioTechniques*, *46*(2), 101–113. https://doi.org/10.2144/000113078

Firoozan, S., Wei, K., Linka, A., Skyba, D., Goodman, N. C., & Kaul, S. (1999). A canine model of chronic ischemic cardiomyopathy: Characterization of regional flow-function relations. *The American Journal of Physiology*, *276*(2), H446-455. https://doi.org/10.1152/ajpheart.1999.276.2.H446

Fishman, G. I. (2005). Understanding Conduction System Development. *Circulation Research*, *96*(8), 809–811. https://doi.org/10.1161/01.RES.0000165653.83279.20

Flaherty, J. T., Pitt, B., Gruber, J. W., Heuser, R. R., Rothbaum, D. A., Burwell, L. R., George, B. S., Kereiakes, D. J., Deitchman, D., & Gustafson, N. (1994). Recombinant human superoxide dismutase (h-SOD) fails to improve recovery of ventricular function in patients undergoing coronary angioplasty for acute myocardial infarction. *Circulation*, *89*(5), 1982–1991. https://doi.org/10.1161/01.cir.89.5.1982

Force, A., Lynch, M., Pickett, F. B., Amores, A., Yan, Y., & Postlethwait, J. (1999). Preservation of Duplicate Genes by Complementary, Degenerative Mutations. *Genetics*, *151*(4), 1531–1545. https://doi.org/10.1093/genetics/151.4.1531

Frank, A., Bonney, M., Bonney, S., Weitzel, L., Koeppen, M., & Eckle, T. (2012). Myocardial ischemia reperfusion injury—From basic science to clinical bedside. *Seminars in Cardiothoracic and Vascular Anesthesia*, *16*(3), 123–132. https://doi.org/10.1177/1089253211436350

Fröhlich, G. M., Meier, P., White, S. K., Yellon, D. M., & Hausenloy, D. J. (2013). Myocardial reperfusion injury: Looking beyond primary PCI. *European Heart Journal*, *34*(23), 1714–1722. https://doi.org/10.1093/eurheartj/eht090

Fujita, M., Morimoto, Y., Ishihara, M., Shimizu, M., Takase, B., Maehara, T., & Kikuchi, M. (2004). A new rabbit model of myocardial infarction without endotracheal intubation. *Journal of Surgical Research*, *116*(1), 124–128. https://doi.org/10.1016/S0022-4804(03)00304-4

Gaggin, H. K., & Januzzi, J. L. (2013). Biomarkers and diagnostics in heart failure. *Biochimica et Biophysica Acta (BBA) - Molecular Basis of Disease*, *1832*(12), 2442–2450. https://doi.org/10.1016/j.bbadis.2012.12.014

Gaide, M. S., Cameron, J. S., Altman, C. B., Myerburg, R. J., & Bassett, A. L. (1985). Myocardial infarction in the guinea pig: Cellular electrophysiology. *Life Sciences*, *36*(25), 2391–2401. https://doi.org/10.1016/0024-3205(85)90343-1

Gao, B., Qu, Y., Sutherland, W., Chui, R. W., Hoagland, K., & Vargas, H. M. (2018). Decreased contractility and altered responses to inotropic agents in myocytes from tachypacing-induced heart failure canines. *Journal of Pharmacological and Toxicological Methods*, *93*, 98–107. https://doi.org/10.1016/j.vascn.2018.06.001

Gao, X.-Q., Li, H.-W., Ling, X., Qiu, Y.-H., Gao, Y., & Zhang, Y. (2013). Effect of rosiglitazone on rabbit model of myocardial ischemia-reperfusion injury. *Asian Pacific Journal of Tropical Medicine*, *6*(3), 228–231. https://doi.org/10.1016/S1995-7645(13)60029-2

Garcia-Dorado, D., Therox, P., Elzage, J., Galinanes, M., Solares, J., Riesgo, M., Gomez, M., Garcia-Dorado, A., & Aviles, F. (1987). Myocardial reperfusion in the pig heart model: Infarct size and duration of coronary occlusion. *Cardiovascular Research*, *21*(7), 537–544. https://doi.org/10.1093/cvr/21.7.537

Gharacholou, S. M., Alexander, K. P., Chen, A. Y., Wang, T. Y., Melloni, C., Gibler, W. B., Pollack, C. V., Ohman, E. M., Peterson, E. D., & Roe, M. T. (2010). Implications and reasons for the lack of use of reperfusion therapy in patients with ST-segment elevation myocardial infarction: Findings from the CRUSADE initiative. *American Heart Journal*, *159*(5), 757–763. https://doi.org/10.1016/j.ahj.2010.02.009

Giardoglou, P., & Beis, D. (2019). On Zebrafish Disease Models and Matters of the Heart. *Biomedicines*, *7*(1), 15. https://doi.org/10.3390/biomedicines7010015

Govorunova, E. G., Sineshchekov, O. A., Janz, R., Liu, X., & Spudich, J. L. (2015). Natural light-gated anion channels: A family of microbial rhodopsins for advanced optogenetics. *Science*, *349*(6248), 647–650. https://doi.org/10.1126/science.aaa7484

Granger, D. N., & Kvietys, P. R. (2015). Reperfusion injury and reactive oxygen species: The evolution of a concept. *Redox Biology*, *6*, 524–551. https://doi.org/10.1016/j.redox.2015.08.020

Greenbaum, D., Colangelo, C., Williams, K., & Gerstein, M. (2003). Comparing protein abundance and mRNA expression levels on a genomic scale. *Genome Biology*, *4*(9), 117. https://doi.org/10.1186/gb-2003-4-9-117

Grimm, D., Elsner, D., Schunkert, H., Pfeifer, M., Griese, D., Bruckschlegel, G., Muders, F., Riegger, G. A. J., & Kromer, E. P. (1998). Development of heart failure following isoproterenol administration in the rat: Role of the renin–angiotensin system. *Cardiovascular Research*, *37*(1), 91–100. https://doi.org/10.1016/S0008-6363(97)00212-5

Gu, G., Na, Y., Chung, H., Seok, S. H., & Lee, H.-Y. (2017). Zebrafish Larvae Model of Dilated Cardiomyopathy Induced by Terfenadine. *Korean Circulation Journal*, *47*(6), 960–969. https://doi.org/10.4070/kcj.2017.0080

Guild, S.-J., Han, J.-C., Power, A., Ward, M.-L., Nisbet, L. A., & Loiselle, D. S. (2016). The Effect of Monocrotaline-Induced Heart Failure on Left- and Right-Ventricular Function. *The FASEB Journal*, *30*(S1), 958.6-958.6. https://doi.org/10.1096/fasebj.30.1_supplement.958.6

Guru, A., Post, R. J., Ho, Y.-Y., & Warden, M. R. (2015). Making Sense of Optogenetics. *International Journal of Neuropsychopharmacology*, *18*(11), pyv079. https://doi.org/10.1093/ijnp/pyv079

Gut, P., Reischauer, S., Stainier, D. Y. R., & Arnaout, R. (2017). Little Fish, Big Data: Zebrafish as a Model for Cardiovascular and Metabolic Disease. *Physiological Reviews*, *97*(3), 889–938. https://doi.org/10.1152/physrev.00038.2016

Guzman, R. J., Krystkowiak, A., & Zarins, C. K. (2002). Early and Sustained Medial Cell Activation after Aortocaval Fistula Creation in Mice. *Journal of Surgical Research*, *108*(1), 112–121. https://doi.org/10.1006/jsre.2002.6530

Haack, T., & Abdelilah-Seyfried, S. (2016). The force within: Endocardial development, mechanotransduction and signalling during cardiac morphogenesis. *Development*, *143*(3), 373–386. https://doi.org/10.1242/dev.131425

Habets, P. E. M. H., Clout, D. E. W., Lekanne Deprez, R. H., Van Roon, M. A., Moorman, A. F. M., & Christoffels, V. M. (2003). Cardiac expression of Gal4 causes cardiomyopathy in a dose-dependent manner. *Journal of Muscle Research & Cell Motility*, *24*(2), 205–209. https://doi.org/10.1023/A:1026055612227

Haesemeyer, M. (2020). Thermoregulation in fish. *Molecular and Cellular Endocrinology*, *518*, 110986. https://doi.org/10.1016/j.mce.2020.110986

Halestrap, A. P. (2009). Mitochondria and reperfusion injury of the heart—A holey death but not beyond salvation. *Journal of Bioenergetics and Biomembranes*, *41*(2), 113–121. https://doi.org/10.1007/s10863-009-9206-x

Hamed, A. T., & Lokhandwala, M. F. (1981). Control of Hindlimb Vascular Resistance and Vascular Responsiveness in Doca-Salt Hypertensive Dogs. *Clinical and Experimental Hypertension*, *3*(1), 85–101. https://doi.org/10.3109/10641968109037170

Harrison, M. R. M., Bussmann, J., Huang, Y., Zhao, L., Osorio, A., Burns, C. G., Burns, C. E., Sucov, H. M., Siekmann, A. F., & Lien, C.-L. (2015). Chemokine-Guided Angiogenesis Directs Coronary Vasculature Formation in Zebrafish. *Developmental Cell*, *33*(4), 442–454. https://doi.org/10.1016/j.devcel.2015.04.001

Hartner, A., Cordasic, N., Klanke, B., Veelken, R., & Hilgers, K. F. (2003). Strain differences in the development of hypertension and glomerular lesions induced by deoxycorticosterone acetate salt in mice. *Nephrology Dialysis Transplantation*, *18*(10), 1999–2004. https://doi.org/10.1093/ndt/gfg299

Hartupee, J., & Mann, D. L. (2017). Neurohormonal activation in heart failure with reduced ejection fraction. *Nature Reviews. Cardiology*, *14*(1), 30–38. https://doi.org/10.1038/nrcardio.2016.163

Hau, J., & Schapiro, S. J. (Eds.). (2010). Physiological, Hematological, and Clinical Chemistry Parameters, Including Conversion Factors. In *Handbook of Laboratory Animal Science, Volume I* (3rd ed.). CRC Press.

Haverinen, J., Dzhumaniiazova, I., Abramochkin, D. V., Hassinen, M., & Vornanen, M. (2021). Effects of Na+ channel isoforms and cellular environment on temperature tolerance of cardiac Na+ current in zebrafish (Danio rerio) and rainbow trout (Oncorhynchus mykiss). *Journal of Experimental Biology*, *224*(8), jeb241067. https://doi.org/10.1242/jeb.241067

Hołda, M. K., Szczepanek, E., Bielawska, J., Palka, N., Wojtysiak, D., Frączek, P., Nowakowski, M., Sowińska, N., Arent, Z., Podolec, P., & Kopeć, G. (2020). Changes in heart morphometric parameters over the course of a monocrotaline-induced pulmonary arterial hypertension rat model. *Journal of Translational Medicine*, *18*, 262. https://doi.org/10.1186/s12967-020-02440-7

Hon, J. K. F., Steendijk, P., Khan, H., Wong, K., & Yacoub, M. (2001). Acute effects of pulmonary artery banding in sheep on right ventricle pressure–volume relations: Relevance to the arterial switch operation. *Acta Physiologica Scandinavica*, *172*(2), 97–106. https://doi.org/10.1046/j.1365-201X.2001.00844.x

Hood, W. B., Mccarthy, B., & Lown, B. (1967). Myocardial Infarction Following Coronary Ligation in Dogs. *Circulation Research*, *21*(2), 191–200. https://doi.org/10.1161/01.RES.21.2.191

Hornyik, T., Rieder, M., Castiglione, A., Major, P., Baczko, I., Brunner, M., Koren, G., & Odening, K. E. (2022). Transgenic rabbit models for cardiac disease research. *British Journal of Pharmacology*, *179*(5), 938–957. https://doi.org/10.1111/bph.15484

Howard, R. J., Moe, G. W., & Armstrong, P. W. (1991). Sequential echocardiographic-Doppler assessment of left ventricular remodelling and mitral regurgitation during evolving experimental heart failure. *Cardiovascular Research*, *25*(6), 468–474. https://doi.org/10.1093/cvr/25.6.468

Howe, K., Clark, M. D., Torroja, C. F., Torrance, J., Berthelot, C., Muffato, M., Collins, J. E., Humphray, S., McLaren, K., Matthews, L., McLaren, S., Sealy, I., Caccamo, M., Churcher, C., Scott, C., Barrett, J. C., Koch, R., Rauch, G.-J., White, S., … Stemple, D. L. (2013). The zebrafish reference genome sequence and its relationship to the human genome. *Nature*, *496*(7446), Article 7446. https://doi.org/10.1038/nature12111

Huang, H., Zhang, B., Hartenstein, P. A., Chen, J., & Lin, S. (2005). NXT2 is required for embryonic heart development in zebrafish. *BMC Developmental Biology*, *5*(1), 7. https://doi.org/10.1186/1471-213X-5-7

Hulsmans, M., Aguirre, A. D., Bonner, M. D., Bapat, A., Cremer, S., Iwamoto, Y., King, K. R., Swirski, F. K., Milan, D. J., Weissleder, R., & Nahrendorf, M. (2018). A Miniaturized, Programmable Pacemaker for Long-Term Studies in the Mouse. *Circulation Research*, *123*(11), 1208–1219. https://doi.org/10.1161/CIRCRESAHA.118.313429

Ishikawa, K., Aguero, J., Tilemann, L., Ladage, D., Hammoudi, N., Kawase, Y., Santos-Gallego, C. G., Fish, K., Levine, R. A., & Hajjar, R. J. (2014). Characterizing preclinical models of ischemic heart failure: Differences between LAD and LCx infarctions. *American Journal of Physiology - Heart and Circulatory Physiology*, *307*(10), H1478–H1486. https://doi.org/10.1152/ajpheart.00797.2013

Iyer, A., Chan, V., & Brown, L. (2010). The DOCA-Salt Hypertensive Rat as a Model of Cardiovascular Oxidative and Inflammatory Stress. *Current Cardiology Reviews*, *6*(4), 291–297. https://doi.org/10.2174/157340310793566109

Jennings, R. B., Sommers, H. M., Smyth, G. A., Flack, H. A., & Linn, H. (1960). Myocardial necrosis induced by temporary occlusion of a coronary artery in the dog. *Archives of Pathology*, *70*, 68–78.

Katz, M. G., Hadas, Y., Vincek, A. S., Shtraizent, N., Schadt, E., & Eliyahu, E. (2022). Cardiac Targeted Adeno-Associated Virus Injection in Rats. In K. Ishikawa (Ed.), *Cardiac Gene Therapy: Methods and Protocols* (pp. 135–145). Springer US. https://doi.org/10.1007/978-1-0716-2707-5_10

Kerbaul, F., Rondelet, B., Motte, S., Fesler, P., Hubloue, I., Ewalenko, P., Naeije, R., & Brimioulle, S. (2004). Effects of norepinephrine and dobutamine on pressure load-induced right ventricular failure*. *Critical Care Medicine*, *32*(4), 1035. https://doi.org/10.1097/01.CCM.0000120052.77953.07

Keshmiri Neghab, H., Soheilifar, M. H., Saboury, A. A., Goliaei, B., Hong, J., & Esmaeeli Djavid, G. (2021). Optogenetic Stimulation of Primary Cardiomyocytes Expressing ChR2. *Journal of Lasers in Medical Sciences*, *12*, e32. https://doi.org/10.34172/jlms.2021.32

Khasnis, A., Jongnarangsin, K., Abela, G., Veerareddy, S., Reddy, V., & Thakur, R. (2005). Tachycardia-Induced Cardiomyopathy: A Review of Literature. *Pacing and Clinical Electrophysiology*, *28*(7), 710–721. https://doi.org/10.1111/j.1540-8159.2005.00143.x

Kim, J.-H., Chung, H.-S., Antonisamy, P., Lee, S. R., & Bae, H. (2014). Cardioprotective Effect of Rhizomes of Acorus gramineus Against Isoproterenol-Induced Cardiac Damage in Pigs. *Cardiovascular Toxicology*, *14*(2), 183–192. https://doi.org/10.1007/s12012-014-9243-5

Kopton, R. A., Baillie, J. S., Rafferty, S. A., Moss, R., Zgierski-Johnston, C. M., Prykhozhij, S. V., Stoyek, M. R., Smith, F. M., Kohl, P., Quinn, T. A., & Schneider-Warme, F. (2018). Cardiac Electrophysiological Effects of Light-Activated Chloride Channels. *Frontiers in Physiology*, *9*, 1806. https://doi.org/10.3389/fphys.2018.01806

Kossack, M., Hein, S., Juergensen, L., Siragusa, M., Benz, A., Katus, H. A., Most, P., & Hassel, D. (2017). Induction of cardiac dysfunction in developing and adult zebrafish by chronic isoproterenol stimulation. *Journal of Molecular and Cellular Cardiology*, *108*, 95–105. https://doi.org/10.1016/j.yjmcc.2017.05.011

Kothari, D. S., & Skinner, J. R. (2006). Neonatal tachycardias: An update. *Archives of Disease in Childhood. Fetal and Neonatal Edition*, *91*(2), F136–F144. https://doi.org/10.1136/adc.2004.049049

Langenbacher, A. D., Shimizu, H., Hsu, W., Zhao, Y., Borges, A., Koehler, C., & Chen, J.-N. (2020). Mitochondrial Calcium Uniporter Deficiency in Zebrafish Causes Cardiomyopathy With Arrhythmia. *Frontiers in Physiology*, *11*. https://www.frontiersin.org/articles/10.3389/fphys.2020.617492

Lemme, M., Braren, I., Prondzynski, M., Aksehirlioglu, B., Ulmer, B., Schulze, M., Ismaili, D., Meyer, C., Hansen, A., Christ, T., Lemoine, M., & Eschenhagen, T. (2019). Chronic intermittent tachypacing by an optogenetic approach induces arrhythmia vulnerability in human engineered heart tissue. *Cardiovascular Research*, *116*. https://doi.org/10.1093/cvr/cvz245

Lemoine, M. D., Lemme, M., Ulmer, B. M., Braren, I., Krasemann, S., Hansen, A., Kirchhof, P., Meyer, C., Eschenhagen, T., & Christ, T. (2020). Intermittent Optogenetic Tachypacing of Atrial Engineered Heart Tissue Induces Only Limited Electrical Remodelling. *Journal of Cardiovascular Pharmacology*, *77*(3), 291–299. https://doi.org/10.1097/FJC.0000000000000951

Lewis, E. F., Moye, L. A., Rouleau, J. L., Sacks, F. M., Arnold, J. M. O., Warnica, J. W., Flaker, G. C., Braunwald, E., & Pfeffer, M. A. (2003). Predictors of late development of heart failure in stable survivors of myocardial infarction: The CARE study. *Journal of the American College of Cardiology*, *42*(8), 1446–1453. https://doi.org/10.1016/S0735-1097(03)01057-X

Li, R., Weisel, R. D., Mickle, D. A., Jia, Z. Q., Kim, E. J., Sakai, T., Tomita, S., Schwartz, L., Iwanochko, M., Husain, M., Cusimano, R. J., Burns, R. J., & Yau, T. M. (2000). Autologous porcine heart cell transplantation improved heart function after a myocardial infarction. *The Journal of Thoracic and Cardiovascular Surgery*, *119*(1), 62–68. https://doi.org/10.1016/s0022-5223(00)70218-2

Li, R.-K., Jia, Z.-Q., Weisel, R. D., Merante, F., & Mickle, D. A. G. (1999). Smooth Muscle Cell Transplantation into Myocardial Scar Tissue Improves Heart Function. *Journal of Molecular and Cellular Cardiology*, *31*(3), 513–522. https://doi.org/10.1006/jmcc.1998.0882

Lin, J. Y. (2011). A User's Guide to Channelrhodopsin Variants: Features, Limitations and Future Developments. *Experimental Physiology*, *96*(1), 19–25. https://doi.org/10.1113/expphysiol.2009.051961

Lindsey, S. E., Butcher, J. T., & Yalcin, H. C. (2014). Mechanical regulation of cardiac development. *Frontiers in Physiology*, *5*, 318. https://doi.org/10.3389/fphys.2014.00318

Lionetti, V., Linke, A., Chandler, M., Young, M., Penn, M., Gupte, S., Dagostino, C., Hintze, T., Stanley, W., & Recchia, F. (2005). Carnitine palmitoyl transferase-I inhibition prevents ventricular remodeling and delays decompensation in pacing-induced heart failure. *Cardiovascular Research*, *66*(3), 454–461. https://doi.org/10.1016/j.cardiores.2005.02.004

Lippi, G., & Sanchis-Gomar, F. (2020). Global epidemiology and future trends of heart failure. *AME Medical Journal*, *5*(15). https://doi.org/doi: 10.21037/amj.2020.03.03

Liu, C., Xin, Q., Qin, C., Jiang, M., Lo, G. V., Dou, Y., & Yuan, S. (2023). The Mechanism of Channel Opening of Anion Channelrhodopsin GtACR1: A Molecular Dynamics Simulation. *Processes*, *11*(2), Article 2. https://doi.org/10.3390/pr11020510

Livak, K. J., & Schmittgen, T. D. (2001). Analysis of relative gene expression data using real-time quantitative PCR and the 2(-Delta Delta C(T)) Method. *Methods (San Diego, Calif.)*, *25*(4), 402–408. https://doi.org/10.1006/meth.2001.1262

Loch, D., Hoey, A., & Brown, L. (2006). Attenuation of Cardiovascular Remodeling in DOCA-Salt Rats by the Vasopeptidase Inhibitor, Omapatrilat. *Clinical and Experimental Hypertension*, *28*(5), 475–488. https://doi.org/10.1080/10641960600798754

Lu, F., Langenbacher, A. D., & Chen, J.-N. (2016). Transcriptional Regulation of Heart Development in Zebrafish. *Journal of Cardiovascular Development and Disease*, *3*(2), Article 2. https://doi.org/10.3390/jcdd3020014

Maerz, L. D., Burkhalter, M. D., Schilpp, C., Wittekindt, O. H., Frick, M., & Philipp, M. (2019). Pharmacological cholesterol depletion disturbs ciliogenesis and ciliary function in developing zebrafish. *Communications Biology*, *2*(1), Article 1. https://doi.org/10.1038/s42003-018-0272-7

Magid, N. M., Opio, G., Wallerson, D. C., Young, M. S., & Borer, J. S. (1994). Heart failure due to chronic experimental aortic regurgitation. *The American Journal of Physiology*, *267*(2 Pt 2), H556-562. https://doi.org/10.1152/ajpheart.1994.267.2.H556

Manthorpe, R., & Svensson, O. (1996). Cardiomyopathy following intravenous cyclophosphamide therapy in a patient with Wegener's granulomatosis. *Clinical and Experimental Rheumatology*, *14*(6), 702–703.

Marín-García, J., Goldenthal, M. J., & Moe, G. W. (2002). Selective endothelin receptor blockade reverses mitochondrial dysfunction in canine heart failure. *Journal of Cardiac Failure*, *8*(5), 326–332. https://doi.org/10.1054/jcaf.2002.127770

Maron, B. J., Towbin, J. A., Thiene, G., Antzelevitch, C., Corrado, D., Arnett, D., Moss, A. J., Seidman, C. E., & Young, J. B. (2006). Contemporary Definitions and Classification of the Cardiomyopathies. *Circulation*, *113*(14), 1807–1816. https://doi.org/10.1161/CIRCULATIONAHA.106.174287

Martin, K. E., & Waxman, J. S. (2021). Atrial and Sinoatrial Node Development in the Zebrafish Heart. *Journal of Cardiovascular Development and Disease*, *8*(2), 15. https://doi.org/10.3390/jcdd8020015

Martin, R. T., & Bartman, T. (2009). Analysis of heart valve development in larval zebrafish. *Developmental Dynamics*, *238*(7), 1796–1802. https://doi.org/10.1002/dvdy.21976

Matsumori, A., & Kawai, C. (1984). Animal Models of Congestive Heart Failure and Congestive (Dilated) Cardiomyopathy Due to Viral Myocarditis in Mice. In H.-D. Bolte (Ed.), *Viral Heart Disease* (pp. 35–56). Springer. https://doi.org/10.1007/978-3-642-95448-1_6

Mazumder, P. K., O'Neill, B. T., Roberts, M. W., Buchanan, J., Yun, U. J., Cooksey, R. C., Boudina, S., & Abel, E. D. (2004). Impaired Cardiac Efficiency and Increased Fatty Acid Oxidation in Insulin-Resistant *ob/ob* Mouse Hearts. *Diabetes*, *53*(9), 2366–2374. https://doi.org/10.2337/diabetes.53.9.2366

Mi, P., Li, N., Ai, K., Li, L., & Yuan, D. (2023). AhR-mediated lipid peroxidation contributes to TCDD-induced cardiac defects in zebrafish. *Chemosphere*, *317*, 137942. https://doi.org/10.1016/j.chemosphere.2023.137942

Michael, L. H., Ballantyne, C. M., Zachariah, J. P., Gould, K. E., Pocius, J. S., Taffet, G. E., Hartley, C. J., Pham, T. T., Daniel, S. L., Funk, E., & Entman, M. L. (1999). Myocardial infarction and remodeling in mice: Effect of reperfusion. *American Journal of Physiology-Heart and Circulatory Physiology*, *277*(2), H660–H668. https://doi.org/10.1152/ajpheart.1999.277.2.H660

Mihl, C., Dassen, W. R. M., & Kuipers, H. (2008). Cardiac remodelling: Concentric versus eccentric hypertrophy in strength and endurance athletes. *Netherlands Heart Journal*, *16*(4), 129–133.

Milan, D. J., Peterson, T. A., Ruskin, J. N., Peterson, R. T., & MacRae, C. A. (2003). Drugs That Induce Repolarization Abnormalities Cause Bradycardia in Zebrafish. *Circulation*, *107*(10), 1355–1358. https://doi.org/10.1161/01.CIR.0000061912.88753.87

Milani-Nejad, N., & Janssen, P. M. L. (2014). Small and Large Animal Models in Cardiac Contraction Research: Advantages and Disadvantages. *Pharmacology & Therapeutics*, *141*(3), 235–249. https://doi.org/10.1016/j.pharmthera.2013.10.007

Miyawaki, A., Llopis, J., Heim, R., McCaffery, J. M., Adams, J. A., Ikura, M., & Tsien, R. Y. (1997). Fluorescent indicators for Ca2+based on green fluorescent proteins and calmodulin. *Nature*, *388*(6645), Article 6645. https://doi.org/10.1038/42264

Moainie, S. L., Gorman, J. H., Guy, T. S., Bowen, F. W., Jackson, B. M., Plappert, T., Narula, N., St John-Sutton, M. G., Narula, J., Edmunds, L. H., & Gorman, R. C. (2002). An ovine model of postinfarction dilated cardiomyopathy. *The Annals of Thoracic Surgery*, *74*(3), 753–760. https://doi.org/10.1016/s0003-4975(02)03827-4

Moe, G. W., Angus, C., Howard, R. J., De Bold, A. J., & Armstrong, P. W. (1990). Pathophysiological role of changing atrial size and pressure in modulation of atrial natriuretic factor during evolving experimental heart failure. *Cardiovascular Research*, *24*(7), 570–577. https://doi.org/10.1093/cvr/24.7.570

Moe, G. W., Grima, E. A., Angus, C., Wong, N. L., Hu, D. C., Howard, R. J., & Armstrong, P. W. (1991). Response of atrial natriuretic factor to acute and chronic increases of atrial pressures in experimental heart failure in dogs. Role of changes in heart rate, atrial dimension, and cardiac tissue concentration. *Circulation*, *83*(5), 1780–1787. https://doi.org/10.1161/01.cir.83.5.1780

Moe, G. W., Stopps, T. P., Howard, R. J., & Armstrong, P. W. (1988). Early recovery from heart failure: Insights into the pathogenesis of experimental chronic pacing-induced heart failure. *The Journal of Laboratory and Clinical Medicine*, *112*(4), 426–432.

Moens, A. L., Leyton-Mange, J. S., Niu, X., Yang, R., Cingolani, O., Arkenbout, E. K., Champion, H. C., Bedja, D., Gabrielson, K. L., Chen, J., Xia, Y., Hale, A. B., Channon, K. M., Halushka, M. K., Barker, N., Wuyts, F. L., Kaminski, P. M.,

Wolin, M. S., Kass, D. A., & Barouch, L. A. (2009). Adverse ventricular remodeling and exacerbated NOS uncoupling from pressure-overload in mice lacking the β3-adrenoreceptor. *Journal of Molecular and Cellular Cardiology*, *47*(5), 576–585. https://doi.org/10.1016/j.yjmcc.2009.06.005

Mohammed, S. F., Storlie, J. R., Oehler, E. A., Bowen, L. A., Korinek, J., Lam, C. S. P., Simari, R. D., Burnett, J. C., & Redfield, M. M. (2012). Variable phenotype in murine transverse aortic constriction. *Cardiovascular Pathology*, *21*(3), 188–198. https://doi.org/10.1016/j.carpath.2011.05.002

Muders, F., & Elsner, D. (2000). Animal models of chronic heart failure. *Pharmacological Research*, *41*(6), 605–612. https://doi.org/10.1006/phrs.1999.0652

Muders, F., Friedrich, E., Luchner, A., Pfeifer, M., Ickenstein, G., Hamelbeck, B., Riegger, G. A. J., & Elsner, D. (1999). Hemodynamic changes and neurohumoral regulation during development of congestive heart failure in a model of epinephrine-induced cardiomyopathy in conscious rabbits. *Journal of Cardiac Failure*, *5*(2), 109–116. https://doi.org/10.1016/S1071-9164(99)90033-7

Murray, D. R., Prabhu, S. D., & Chandrasekar, B. (2000). Chronic β-Adrenergic Stimulation Induces Myocardial Proinflammatory Cytokine Expression. *Circulation*, *101*(20), 2338–2341. https://doi.org/10.1161/01.CIR.101.20.2338

Nadrowski, P., Chudek, J., Grodzicki, T., Mossakowska, M., Skrzypek, M., Wiecek, A., Zdrojewski, T., & Kozakiewicz, K. (2013). Plasma level of N-terminal pro brain natriuretic peptide (NT-proBNP) in elderly population in Poland—The PolSenior Study. *Experimental Gerontology*, *48*(9), 852–857. https://doi.org/10.1016/j.exger.2013.05.060

Nagel, G., Szellas, T., Huhn, W., Kateriya, S., Adeishvili, N., Berthold, P., Ollig, D., Hegemann, P., & Bamberg, E. (2003). Channelrhodopsin-2, a directly light-gated cation-selective membrane channel. *Proceedings of the National Academy of Sciences of the United States of America*, *100*(24), 13940–13945. https://doi.org/10.1073/pnas.1936192100

Narumanchi, S., Wang, H., Perttunen, S., Tikkanen, I., Lakkisto, P., & Paavola, J. (2021). Zebrafish Heart Failure Models. *Frontiers in Cell and Developmental Biology*, *9*. https://www.frontiersin.org/articles/10.3389/fcell.2021.662583

Nemtsas, P., Wettwer, E., Christ, T., Weidinger, G., & Ravens, U. (2010). Adult zebrafish heart as a model for human heart? An electrophysiological study.

Journal of Molecular and Cellular Cardiology, *48*(1), 161–171. https://doi.org/10.1016/j.yjmcc.2009.08.034

Nishikimi, T., Maeda, N., & Matsuoka, H. (2006). The role of natriuretic peptides in cardioprotection. *Cardiovascular Research*, *69*(2), 318–328. https://doi.org/10.1016/j.cardiores.2005.10.001

North, B., & Sinclair, D. (2012). The Intersection Between Aging and Cardiovascular Disease | Circulation Research. *Circulation Research*, *110*, 1097–1108.

Nossuli, T. O., Lakshminarayanan, V., Baumgarten, G., Taffet, G. E., Ballantyne, C. M., Michael, L. H., & Entman, M. L. (2000). A chronic mouse model of myocardial ischemia-reperfusion: Essential in cytokine studies. *American Journal of Physiology. Heart and Circulatory Physiology*, *278*(4), H1049-1055. https://doi.org/10.1152/ajpheart.2000.278.4.H1049

O'Brien, P. J., Ianuzzo, C. D., Moe, G. W., Stopps, T. P., & Armstrong, P. W. (1990). Rapid ventricular pacing of dogs to heart failure: Biochemical and physiological studies. *Canadian Journal of Physiology and Pharmacology*, *68*(1), 34–39. https://doi.org/10.1139/y90-004

Ogawa, K., Yoshida, K., Uehara, Y., Ebine, M., Kimata, A., Nishina, H., Takeyasu, N., Noguchi, Y., Ieda, M., Aonuma, K., & Nogami, A. (2018). Mechanistic implication of decreased plasma atrial natriuretic peptide level for transient rise in the atrial capture threshold early after ICD or CRT-D implantation. *Journal of Interventional Cardiac Electrophysiology*, *53*(1), 131–140. https://doi.org/10.1007/s10840-018-0409-0

Olson, E. N., & Schneider, M. D. (2003). Sizing up the heart: Development redux in disease. *Genes & Development*, *17*(16), 1937–1956. https://doi.org/10.1101/gad.1110103

Paavola, J., Schliffke, S., Rossetti, S., Kuo, I. Y.-T., Yuan, S., Sun, Z., Harris, P. C., Torres, V. E., & Ehrlich, B. E. (2013). Polycystin-2 mutations lead to impaired calcium cycling in the heart and predispose to dilated cardiomyopathy. *Journal of Molecular and Cellular Cardiology*, *58*, 199–208. https://doi.org/10.1016/j.yjmcc.2013.01.015

Park, S. A., Lee, S.-R., Tung, L., & Yue, D. T. (2014). Optical mapping of optogenetically shaped cardiac action potentials. *Scientific Reports*, *4*(1), Article 1. https://doi.org/10.1038/srep06125

Parlakian, A., Charvet, C., Escoubet, B., Mericskay, M., Molkentin, J. D., Gary-Bobo, G., De Windt, L. J., Ludosky, M.-A., Paulin, D., Daegelen, D., Tuil, D., & Li, Z. (2005). Temporally Controlled Onset of Dilated Cardiomyopathy Through Disruption of the SRF Gene in Adult Heart. *Circulation*, *112*(19), 2930–2939. https://doi.org/10.1161/CIRCULATIONAHA.105.533778

Pashmforoush, M., Lu, J. T., Chen, H., Amand, T. S., Kondo, R., Pradervand, S., Evans, S. M., Clark, B., Feramisco, J. R., Giles, W., Ho, S. Y., Benson, D. W., Silberbach, M., Shou, W., & Chien, K. R. (2004). Nkx2-5 Pathways and Congenital Heart Disease: Loss of Ventricular Myocyte Lineage Specification Leads to Progressive Cardiomyopathy and Complete Heart Block. *Cell*, *117*(3), 373–386. https://doi.org/10.1016/S0092-8674(04)00405-2

Patton, E. E., Zon, L. I., & Langenau, D. M. (2021). Zebrafish disease models in drug discovery: From preclinical modelling to clinical trials. *Nature Reviews Drug Discovery*, *20*(8), Article 8. https://doi.org/10.1038/s41573-021-00210-8

Paul, T., Bertram, H., Bökenkamp, R., & Hausdorf, G. (2000). Supraventricular Tachycardia in Infants, Children and Adolescents. *Paediatric Drugs*, *2*(3), 171–181. https://doi.org/10.2165/00128072-200002030-00002

Perkins, J. R., Dawes, J. M., McMahon, S. B., Bennett, D. L., Orengo, C., & Kohl, M. (2012). ReadqPCR and NormqPCR: R packages for the reading, quality checking and normalisation of RT-qPCR quantification cycle (Cq) data. *BMC Genomics*, *13*(1), 296. https://doi.org/10.1186/1471-2164-13-296

Perreault, C. L., Shannon, R. P., Komamura, K., Vatner, S. F., & Morgan, J. P. (1992). Abnormalities in intracellular calcium regulation and contractile function in myocardium from dogs with pacing-induced heart failure. *The Journal of Clinical Investigation*, *89*(3), 932–938. https://doi.org/10.1172/JCI115674

Pfaffl, M. W., Tichopad, A., Prgomet, C., & Neuvians, T. P. (2004). Determination of stable housekeeping genes, differentially regulated target genes and sample integrity: BestKeeper – Excel-based tool using pair-wise correlations. *Biotechnology Letters*, *26*(6), 509–515. https://doi.org/10.1023/B:BILE.0000019559.84305.47

Pfeffer, M. A., Pfeffer, J. M., Steinberg, C., & Finn, P. (1985). Survival after an experimental myocardial infarction: Beneficial effects of long-term therapy with captopril. *Circulation*, *72*(2), 406–412. https://doi.org/10.1161/01.cir.72.2.406

Pitoulis, F. G., & Terracciano, C. M. (2020). Heart Plasticity in Response to Pressure- and Volume-Overload: A Review of Findings in Compensated and Decompensated Phenotypes. *Frontiers in Physiology*, *11*. https://www.frontiersin.org/articles/10.3389/fphys.2020.00092

Poon, K. L., & Brand, T. (2013). The zebrafish model system in cardiovascular research: A tiny fish with mighty prospects. *Glob. Cardiol. Sci. Pract.*, *2013*(1), 9–28. Scopus.

Powers, J. C., & Recchia, F. (2018). Canine Model of Pacing-Induced Heart Failure. In K. Ishikawa (Ed.), *Experimental Models of Cardiovascular Diseases: Methods and Protocols* (pp. 309–325). Springer. https://doi.org/10.1007/978-1-4939-8597-5_24

Quill, J. L., Eggen, M. D., & Richardson, E. S. (2010). Use of Large Animal Models for Cardiac Electrophysiology Studies. In D. C. Sigg, P. A. Iaizzo, Y.-F. Xiao, & B. He (Eds.), *Cardiac Electrophysiology Methods and Models* (pp. 281–304). Springer US. https://doi.org/10.1007/978-1-4419-6658-2_14

Rafferty, S. A., & Quinn, T. A. (2018). A beginner's guide to understanding and implementing the genetic modification of zebrafish. *Progress in Biophysics and Molecular Biology*, *138*, 3–19. https://doi.org/10.1016/j.pbiomolbio.2018.07.005

Rai, N., Veeroju, S., Schymura, Y., Janssen, W., Wietelmann, A., Kojonazarov, B., Weissmann, N., Stasch, J.-P., Ghofrani, H. A., Seeger, W., Schermuly, R. T., & Novoyatleva, T. (2018). Effect of Riociguat and Sildenafil on Right Heart Remodeling and Function in Pressure Overload Induced Model of Pulmonary Arterial Banding. *BioMed Research International*, *2018*, 3293584. https://doi.org/10.1155/2018/3293584

Rau, C. D., Wang, J., Avetisyan, R., Romay, M. C., Martin, L., Ren, S., Wang, Y., & Lusis, A. J. (2015). Mapping Genetic Contributions to Cardiac Pathology Induced by Beta-Adrenergic Stimulation in Mice. *Circulation: Cardiovascular Genetics*, *8*(1), 40–49. https://doi.org/10.1161/CIRCGENETICS.113.000732

Ravens, U. (2018). Ionic basis of cardiac electrophysiology in zebrafish compared to human hearts. *Progress in Biophysics and Molecular Biology*, *138*, 38–44. https://doi.org/10.1016/j.pbiomolbio.2018.06.008

Raymond-Paquin, A., Nattel, S., Wakili, R., & Tadros, R. (2018). Mechanisms and Clinical Significance of Arrhythmia-Induced Cardiomyopathy. *Canadian Journal of Cardiology*, *34*(11), 1449–1460. https://doi.org/10.1016/j.cjca.2018.07.475

Razaghi, B., Steele, S. L., Prykhozhij, S. V., Stoyek, M. R., Hill, J. A., Cooper, M. D., McDonald, L., Lin, W., Daugaard, M., Crapoulet, N., Chacko, S., Lewis, S. M., Scott, I. C., Sorensen, P. H. B., & Berman, J. N. (2018). Hace1 Influences zebrafish cardiac development via ROS-dependent mechanisms. *Developmental Dynamics: An Official Publication of the American Association of Anatomists*, *247*(2), 289–303. https://doi.org/10.1002/dvdy.24600

Redfield, M. M., Aarhus, L. L., Wright, R. S., & Burnett, J. C. (1993). Cardiorenal and neurohumoral function in a canine model of early left ventricular dysfunction. *Circulation*, *87*(6), 2016–2022. https://doi.org/10.1161/01.CIR.87.6.2016

Riegger, A., & Liebau, G. (1982). The Renin-Angiotensin-Aldosterone System, Antidiuretic Hormone and Sympathetic Nerve Activity in an Experimental Model of Congestive Heart Failure in the Dog | Clinical Science | Portland Press. *Clinical Science*, *62*(5), 465–469.

Riehle, C., & Bauersachs, J. (2019). Small animal models of heart failure. *Cardiovascular Research*, *115*(13), 1838–1849. https://doi.org/10.1093/cvr/cvz161

Rodrigues, S. F., & Granger, D. N. (2012). Cerebral microvascular inflammation in DOCA salt-induced hypertension: Role of angiotensin II and mitochondrial superoxide. *Journal of Cerebral Blood Flow & Metabolism*, *32*(2), 368–375. https://doi.org/10.1038/jcbfm.2011.139

Rona, G., Chappel, C. I., Balazs, T., & Gaudry, R. (1959). An infarct-like myocardial lesion and other toxic manifestations produced by isoproterenol in the rat. *A.M.A Archives of Pathology*, *67*(4), 443–455.

RStudio Team. (2021). *RStudio: Integrated development for R.* (1.4.1103-4). RStudio Inc.

Rungatscher, A., Linardi, D., Milani, E., Ucci, G., Nicolato, E., Merigo, F., Salvetti, B., Mazzucco, A., Luciani, G. B., & Faggian, G. (2014). Chronic overcirculation-induced pulmonary arterial hypertension in aorto-caval shunt. *Microvascular Research*, *94*, 73–79. https://doi.org/10.1016/j.mvr.2014.05.005

Sarmah, S., & Marrs, J. A. (2017). Embryonic Ethanol Exposure Affects Early- and Late-Added Cardiac Precursors and Produces Long-Lasting Heart Chamber Defects in Zebrafish. *Toxics*, *5*(4), Article 4. https://doi.org/10.3390/toxics5040035

Sassen, W. A., & Köster, R. W. (2015). A molecular toolbox for genetic manipulation of zebrafish. *Advances in Genomics and Genetics*, *5*, 151–163. https://doi.org/10.2147/AGG.S57585

Savarese, G., Kishi, T., Vardeny, O., Adamsson, E. S., Bodeg, ård J., Lund, L. H., Thuresson, M., & Bozkurt, B. (2023). Heart Failure Drug Treatment—Inertia, Titration, and Discontinuation. *JACC: Heart Failure*, *11*(1), 1–14. https://doi.org/10.1016/j.jchf.2022.08.009

Scherz, P. J., Huisken, J., Sahai-Hernandez, P., & Stainier, D. Y. R. (2008). High-speed imaging of developing heart valves reveals interplay of morphogenesis and function. *Development*, *135*(6), 1179–1187. https://doi.org/10.1242/dev.010694

Scheuermann-Freestone, M., Freestone, N. S., Langenickel, T., Höhnel, K., Dietz, R., & Willenbrock, R. (2001). A new model of congestive heart failure in the mouse due to chronic volume overload. *European Journal of Heart Failure*, *3*(5), 535–543. https://doi.org/10.1016/S1388-9842(01)00160-X

Schmitto, J. D., Doerge, H., Post, H., Coulibaly, M., Sellin, C., Popov, A. F., Sossalla, S., & Schoendube, F. A. (2009). Progressive right ventricular failure is not explained by myocardial ischemia in a pig model of right ventricular pressure overload. *European Journal of Cardio-Thoracic Surgery*, *35*(2), 229–234. https://doi.org/10.1016/j.ejcts.2008.09.010

Schnabel, K., Wu, C.-C., Kurth, T., & Weidinger, G. (2011). Regeneration of Cryoinjury Induced Necrotic Heart Lesions in Zebrafish Is Associated with Epicardial Activation and Cardiomyocyte Proliferation. *PLOS ONE*, *6*(4), e18503. https://doi.org/10.1371/journal.pone.0018503

Schroder, E. A., Tobita, K., Tinney, J. P., Foldes, J. K., & Keller, B. B. (2002). Microtubule Involvement in the Adaptation to Altered Mechanical Load in Developing Chick Myocardium. *Circulation Research*, *91*(4), 353–359. https://doi.org/10.1161/01.RES.0000030179.78135.FA

Schwarzl, M., Hamdani, N., Seiler, S., Alogna, A., Manninger, M., Reilly, S., Zirngast, B., Kirsch, A., Steendijk, P., Verderber, J., Zweiker, D., Eller, P., Höfler, G., Schauer, S., Eller, K., Maechler, H., Pieske, B. M., Linke, W. A., Casadei, B., & Post, H. (2015). A porcine model of hypertensive cardiomyopathy: Implications for heart failure with preserved ejection fraction. *American Journal of Physiology-Heart and Circulatory Physiology*, *309*(9), H1407–H1418. https://doi.org/10.1152/ajpheart.00542.2015

Sedmera, D., Reckova, M., deAlmeida, A., Sedmerova, M., Biermann, M., Volejnik, J., Sarre, A., Raddatz, E., McCarthy, R. A., Gourdie, R. G., & Thompson, R. P. (2003). Functional and morphological evidence for a ventricular conduction system in zebrafish and Xenopus hearts. *American Journal of Physiology-Heart and Circulatory Physiology*, *284*(4), H1152–H1160. https://doi.org/10.1152/ajpheart.00870.2002

Shannon, R., Komamura, K., Stambler, S., Bigaud, M., Manders, W., & Vatner, S. (1991). Alterations in myocardial contractility in conscious dogs with dilated cardiomyopathy | American Journal of Physiology-Heart and Circulatory Physiology. *American Journal of Physiology-Heart and Circulatory Physiology*, *260*(6), H1903–H1911.

Shi, X., Verma, S., Yun, J., Brand-Arzamendi, K., Singh, K. K., Liu, X., Garg, A., Quan, A., & Wen, X.-Y. (2017). Effect of empagliflozin on cardiac biomarkers in a zebrafish model of heart failure: Clues to the EMPA-REG OUTCOME trial? *Molecular and Cellular Biochemistry*, *433*(1), 97–102. https://doi.org/10.1007/s11010-017-3018-9

Shi, X., Zhang, Y., Chen, R., Gong, Y., Zhang, M., Guan, R., Rotstein, O. D., Liu, X., & Wen, X.-Y. (2020). Ndufa7 plays a critical role in cardiac hypertrophy. *Journal of Cellular and Molecular Medicine*, *24*(22), 13151–13162. https://doi.org/10.1111/jcmm.15921

Shimano, M., Tsuji, Y., Inden, Y., Kitamura, K., Uchikawa, T., Harata, S., Nattel, S., & Murohara, T. (2008). Pioglitazone, a peroxisome proliferator-activated receptor-gamma activator, attenuates atrial fibrosis and atrial fibrillation promotion in rabbits with congestive heart failure. *Heart Rhythm*, *5*(3), 451–459. https://doi.org/10.1016/j.hrthm.2007.12.010

Shimizu, H., Langenbacher, A. D., Huang, J., Wang, K., Otto, G., Geisler, R., Wang, Y., & Chen, J.-N. (2017). The Calcineurin-FoxO-MuRF1 signaling pathway regulates myofibril integrity in cardiomyocytes. *ELife*, *6*, e27955. https://doi.org/10.7554/eLife.27955

Shin, H. S., Shin, H. H., & Shudo, Y. (2021). Current Status and Limitations of Myocardial Infarction Large Animal Models in Cardiovascular Translational Research. *Frontiers in Bioengineering and Biotechnology*, *9*. https://www.frontiersin.org/articles/10.3389/fbioe.2021.673683

Shizukuda, Y., Buttrick, P. M., Geenen, D. L., Borczuk, A. C., Kitsis, R. N., & Sonnenblick, E. H. (1998). β-Adrenergic stimulation causes cardiocyte apoptosis:

Influence of tachycardia and hypertrophy. *American Journal of Physiology-Heart and Circulatory Physiology*, *275*(3), H961–H968. https://doi.org/10.1152/ajpheart.1998.275.3.H961

Silver, N., Best, S., Jiang, J., & Thein, S. L. (2006). Selection of housekeeping genes for gene expression studies in human reticulocytes using real-time PCR. *BMC Molecular Biology*, *7*(1), 33. https://doi.org/10.1186/1471-2199-7-33

Singleman, C., & Holtzman, N. G. (2012). Analysis of postembryonic heart development and maturation in the zebrafish, Danio rerio. *Developmental Dynamics*, *241*(12), 1993–2004. https://doi.org/10.1002/dvdy.23882

Smiley, D., Smith, M. A., Carreira, V., Jiang, M., Koch, S. E., Kelley, M., Rubinstein, J., Jones, W. K., & Tranter, M. (2014). Increased fibrosis and progression to heart failure in MRL mice following ischemia/reperfusion injury. *Cardiovascular Pathology: The Official Journal of the Society for Cardiovascular Pathology*, *23*(6), 327–334. https://doi.org/10.1016/j.carpath.2014.06.001

Smiseth, O. A., & Mjøs, O. D. (1982). A reproducible and stable model of acute ischaemic left ventricular failure in dogs. *Clinical Physiology*, *2*(3), 225–239. https://doi.org/10.1111/j.1475-097X.1982.tb00027.x

Song, W., Wang, H., & Wu, Q. (2015). Atrial Natriuretic Peptide in Cardiovascular Biology and Disease (NPPA). *Gene*, *569*(1), 1–6. https://doi.org/10.1016/j.gene.2015.06.029

Spinale, Coker, M., Thomas, C., Walker, J., Mukherjee, R., & Hebbar, L. (1998). Time-Dependent Changes in Matrix Metalloproteinase Activity and Expression During the Progression of Congestive Heart Failure | Circulation Research. *Circulation Research*, *82*, 482–495.

Spinale, F. G., Grine, R. C., Tempel, G. E., Crawford, F. A., & Zile, M. R. (1992). Alterations in the myocardial capillary vasculature accompany tachycardia-induced cardiomyopathy. *Basic Research in Cardiology*, *87*(1), 65–79. https://doi.org/10.1007/BF00795391

Spinale, F. G., Tanaka, R., Crawford, F. A., & Zile, M. R. (1992). Changes in myocardial blood flow during development of and recovery from tachycardia-induced cardiomyopathy. *Circulation*, *85*(2), 717–729. https://doi.org/10.1161/01.CIR.85.2.717

Spinale, F. G., Tempel, G. E., Mukherjee, R., Eble, D. M., Brown, R., Vacchiano, C. A., & Zile, M. R. (1994). Cellular and molecular alterations in the beta adrenergic

system with cardiomyopathy induced by tachycardia. *Cardiovascular Research*, *28*(8), 1243–1250. https://doi.org/10.1093/cvr/28.8.1243

Spinale, F. G., Zellner, J. L., Tomita, M., Crawford, F. A., & Zile, M. R. (1991). Relation between ventricular and myocyte remodeling with the development and regression of supraventricular tachycardia-induced cardiomyopathy. *Circulation Research*, *69*(4), 1058–1067. https://doi.org/10.1161/01.RES.69.4.1058

Spinale, F., Hendrick, D., Crawford, F., Smith, A., Hamada, Y., & Carabello, B. (1990). Chronic supraventricular tachycardia causes ventricular dysfunction and subendocardial injury in swine. *American Journal of Physiology*, *259*(1), H218–H229.

Srikanth, G., Prakash, P., Tripathy, N., Dikshit, M., & Nityanand, S. (2009). Establishment of a rat model of myocardial infarction with a high survival rate: A suitable model for evaluation of efficacy of stem cell therapy. *Journal of Stem Cells & Regenerative Medicine*, *5*(1), 30–36.

Stainier, D. Y. R. (2001). Zebrafish genetics and vertebrate heart formation. *Nature Reviews Genetics*, *2*(1), Article 1. https://doi.org/10.1038/35047564

Stern, A. B., & Klemmer, P. J. (2011). High-output heart failure secondary to arteriovenous fistula. *Hemodialysis International. International Symposium on Home Hemodialysis*, *15*(1), 104–107. https://doi.org/10.1111/j.1542-4758.2010.00518.x

Strafford, M. A. (2006). Chapter 3—Cardiovascular Physiology in Infants and Children. In E. K. Motoyama & P. J. Davis (Eds.), *Smith's Anesthesia for Infants and Children (Seventh Edition)* (pp. 70–108). Mosby. https://doi.org/10.1016/B978-032302647-5.50008-4

Sun, Y., Wang, Q., Fang, Y., Wu, C., Lu, G., & Chen, Z. (2017). Activation of the Nkx2.5–Calr–p53 signaling pathway by hyperglycemia induces cardiac remodeling and dysfunction in adult zebrafish. *Disease Models & Mechanisms*, *10*(10), 1217–1227. https://doi.org/10.1242/dmm.026781

Sutton, M. St. J., Pfeffer, M. A., Moye, L., Plappert, T., Rouleau, J. L., Lamas, G., Rouleau, J., Parker, J. O., Arnold, M. O., Sussex, B., & Braunwald, E. (1997). Cardiovascular Death and Left Ventricular Remodeling Two Years After Myocardial Infarction. *Circulation*, *96*(10), 3294–3299. https://doi.org/10.1161/01.CIR.96.10.3294

Tanaka, R., Fulbright, B. M., Mukherjee, R., Burchell, S. A., Crawford, F. A., Zile, M. R., & Spinale, F. G. (1993). The cellular basis for the blunted response to beta-adrenergic stimulation in supraventricular tachycardia-induced cardiomyopathy. *Journal of Molecular and Cellular Cardiology*, *25*(10), 1215–1233. https://doi.org/10.1006/jmcc.1993.1134

Tanaka, R., Spinale, F. G., Crawford, F. A., & Zile, M. R. (1992). Effect of chronic supraventricular tachycardia on left ventricular function and structure in newborn pigs. *Journal of the American College of Cardiology*, *20*(7), 1650–1660. https://doi.org/10.1016/0735-1097(92)90462-v

Tantama, M., Hung, Y. P., & Yellen, G. (2012). Optogenetic Reporters: Fluorescent Protein-Based Genetically-Encoded Indicators of Signaling and Metabolism in the Brain. *Progress in Brain Research*, *196*, 235–263. https://doi.org/10.1016/B978-0-444-59426-6.00012-4

Tessier, D., Lajos, P., Braunberger, E., Pouchelon, J.-L., Carpentier, A., Chachques, J. C., & Chetboul, V. (2003). Induction of chronic cardiac insufficiency by arteriovenous fistula and doxorubicin administration. *Journal of Cardiac Surgery*, *18*(4), 307–311. https://doi.org/10.1046/j.1540-8191.2003.02044.x

Thygesen, K., Alpert, J. S., Jaffe, A. S., Simoons, M. L., Chaitman, B. R., White, H. D., Writing Group on the Joint ESC/ACCF/AHA/WHF Task Force for the Universal Definition of Myocardial Infarction, Thygesen, K., Alpert, J. S., White, H. D., Jaffe, A. S., Katus, H. A., Apple, F. S., Lindahl, B., Morrow, D. A., Chaitman, B. A., Clemmensen, P. M., Johanson, P., Hod, H., … ESC Committee for Practice Guidelines (CPG). (2012). Third universal definition of myocardial infarction. *European Heart Journal*, *33*(20), 2551–2567. https://doi.org/10.1093/eurheartj/ehs184

Tomita, M., Spinale, F. G., Crawford, F. A., & Zile, M. R. (1991). Changes in left ventricular volume, mass, and function during the development and regression of supraventricular tachycardia-induced cardiomyopathy. Disparity between recovery of systolic versus diastolic function. *Circulation*, *83*(2), 635–644. https://doi.org/10.1161/01.cir.83.2.635

Tran, D. T., Ohinmaa, A., Thanh, N. X., Howlett, J. G., Ezekowitz, J. A., McAlister, F. A., & Kaul, P. (2016). The current and future financial burden of hospital admissions for heart failure in Canada: A cost analysis. *CMAJ Open*, *4*(3), E365–E370. https://doi.org/10.9778/cmajo.20150130

Trochu, J.-N., Mital, S., Zhang, X., Xu, X., Ochoa, M., Liao, J. K., Recchia, F. A., & Hintze, T. H. (2003). Preservation of NO production by statins in the treatment of heart failure. *Cardiovascular Research*, *60*(2), 250–258. https://doi.org/10.1016/j.cardiores.2003.08.003

Tsoupri, E., & Capetanaki, Y. (2013). Myospryn: A multifunctional desmin-associated protein. *Histochemistry and Cell Biology*, *140*(1), 55–63. https://doi.org/10.1007/s00418-013-1103-z

Tu, S., & Chi, N. C. (2012). Zebrafish models in cardiac development and congenital heart birth defects. *Differentiation; Research in Biological Diversity*, *84*(1), 4–16. https://doi.org/10.1016/j.diff.2012.05.005

van den Berg, M. P., van Gelder, I. C., & van Veldhuisen, D. J. (2004). Depletion of atrial natriuretic peptide during longstanding atrial fibrillation. *EP Europace*, *6*(5), 433–437. https://doi.org/10.1016/j.eupc.2004.04.006

van Opbergen, C. J. M., van der Voorn, S. M., Vos, M. A., de Boer, T. P., & van Veen, T. A. B. (2018). Cardiac Ca2+ signalling in zebrafish: Translation of findings to man. *Progress in Biophysics and Molecular Biology*, *138*, 45–58. https://doi.org/10.1016/j.pbiomolbio.2018.05.002

Vandesompele, J., De Preter, K., Pattyn, F., Poppe, B., Van Roy, N., De Paepe, A., & Speleman, F. (2002). Accurate normalization of real-time quantitative RT-PCR data by geometric averaging of multiple internal control genes. *Genome Biology*, *3*(7), research0034.1. https://doi.org/10.1186/gb-2002-3-7-research0034

Vanoli, E., Bacchini, S., Panigada, S., Pentimalli, F., & Adamson, P. B. (2004). Experimental models of heart failure. *European Heart Journal Supplements*, *6*(suppl_F), F7–F15. https://doi.org/10.1016/j.ehjsup.2004.09.004

Velasco, C. E., Turner, M., Cobb, M. A., Virmani, R., & Forman, M. B. (1991). Myocardial reperfusion injury in the canine model after 40 minutes of ischemia: Effect of intracoronary adenosine. *American Heart Journal*, *122*(6), 1561–1570. https://doi.org/10.1016/0002-8703(91)90272-j

Virani, S. A., Bains, M., Code, J., Ducharme, A., Harkness, K., Howlett, J. G., Ross, H., Sussex, B., & Zieroth, S. (2017). The Need for Heart Failure Advocacy in Canada. *Canadian Journal of Cardiology*, *33*(11), 1450–1454. https://doi.org/10.1016/j.cjca.2017.08.024

Volkova, M., & Russell, R. (2011). Anthracycline Cardiotoxicity: Prevalence, Pathogenesis and Treatment. *Current Cardiology Reviews*, *7*(4), 214–220. https://doi.org/10.2174/157340311799960645

Vornanen, M., & Hassinen, M. (2015). Zebrafish heart as a model for human cardiac electrophysiology. *Channels*, *10*(2), 101–110. https://doi.org/10.1080/19336950.2015.1121335

Wang, J., Bo, H., Meng, X., Wu, Y., Bao, Y., & Li, Y. (2006). A Simple and Fast Experimental Model of Myocardial Infarction in the Mouse. *Texas Heart Institute Journal*, *33*(3), 290–293.

Wang, J., Panáková, D., Kikuchi, K., Holdway, J. E., Gemberling, M., Burris, J. S., Singh, S. P., Dickson, A. L., Lin, Y.-F., Sabeh, M. K., Werdich, A. A., Yelon, D., MacRae, C. A., & Poss, K. D. (2011). The regenerative capacity of zebrafish reverses cardiac failure caused by genetic cardiomyocyte depletion. *Development*, *138*(16), 3421–3430. https://doi.org/10.1242/dev.068601

Watanabe, S., Bikou, O., Hajjar, R. J., & Ishikawa, K. (2018). Swine Model of Mitral Regurgitation Induced Heart Failure. *Methods in Molecular Biology (Clifton, N.J.)*, *1816*, 327–335. https://doi.org/10.1007/978-1-4939-8597-5_25

Weber, K. T., Janicki, J. S., Pick, R., Abrahams, C., Shroff, S. G., Bashey, R. I., & Chen, R. M. (1987). Collagen in the hypertrophied, pressure-overloaded myocardium. *Circulation*, *75*(1 Pt 2), I40-7.

Weber, M., & Hamm, C. (2006). Role of B-type natriuretic peptide (BNP) and NT-proBNP in clinical routine. *Heart*, *92*(6), 843–849. https://doi.org/10.1136/hrt.2005.071233

West, J., & Gill, W. W. (2016). Genome Editing in Large Animals. *Journal of Equine Veterinary Science*, *41*, 1–6. https://doi.org/10.1016/j.jevs.2016.03.008

Whipple, G., Sheffield, L., & Woodman, E. (1962). *Reversible congestive heart failure due to chronic rapid stimulation of the normal heart*. *20*, 39–40.

Wijffels, M. C. E. F., Kirchhof, C. J. H. J., Dorland, R., & Allessie, M. A. (1995). Atrial Fibrillation Begets Atrial Fibrillation. *Circulation*, *92*(7), 1954–1968. https://doi.org/10.1161/01.CIR.92.7.1954

Wilson, J. R., Douglas, P., Hickey, W. F., Lanoce, V., Ferraro, N., Muhammad, A., & Reichek, N. (1987). Experimental congestive heart failure produced by rapid

ventricular pacing in the dog: Cardiac effects. *Circulation*, *75*(4), 857–867. https://doi.org/10.1161/01.CIR.75.4.857

Xie, F., Xiao, P., Chen, D., Xu, L., & Zhang, B. (2012). miRDeepFinder: A miRNA analysis tool for deep sequencing of plant small RNAs. *Plant Molecular Biology*, *80*(1), 75–84. https://doi.org/10.1007/s11103-012-9885-2

Xu, X., Meiler, S. E., Zhong, T. P., Mohideen, M., Crossley, D. A., Burggren, W. W., & Fishman, M. C. (2002). Cardiomyopathy in zebrafish due to mutation in an alternatively spliced exon of titin. *Nature Genetics*, *30*(2), Article 2. https://doi.org/10.1038/ng816

Yamamoto, E., Lai, Z.-F., Yamashita, T., Tanaka, T., Kataoka, K., Tokutomi, Y., Ito, T., Ogawa, H., & Kim-Mitsuyama, S. (2006). Enhancement of cardiac oxidative stress by tachycardia and its critical role in cardiac hypertrophy and fibrosis. *Journal of Hypertension*, *24*(10), 2057. https://doi.org/10.1097/01.hjh.0000244956.47114.c1

Yang, W., Ma, L., Li, S., Cui, K., Lei, L., & Ye, Z. (2017). Evaluation of the Cardiotoxicity of Evodiamine In Vitro and In Vivo. *Molecules*, *22*, 943. https://doi.org/10.3390/molecules22060943

Yutzey, K. E., & Robbins, J. (2007). Principles of Genetic Murine Models for Cardiac Disease. *Circulation*, *115*(6), 792–799. https://doi.org/10.1161/CIRCULATIONAHA.106.682534

Zellner, J. L., Spinale, F. G., Eble, D. M., Hewett, K. W., & Crawford, F. A. (1991). Alterations in myocyte shape and basement membrane attachment with tachycardia-induced heart failure. *Circulation Research*, *69*(3), 590–600. https://doi.org/10.1161/01.RES.69.3.590

Zhang, X., Shao, C., Cheng, S., Zhu, Y., Liang, B., & Gu, N. (2021). Effect of Guanxin V in animal model of acute myocardial infarction. *BMC Complementary Medicine and Therapies*, *21*(1), 72. https://doi.org/10.1186/s12906-021-03211-7

Zicha, J., Kunes, J., Lebl, M., Pohlova, I., Slaninova, J., & Jelinek, J. (1989). Antidiuretic and pressor actions of vasopressin in age-dependent DOCA-salt hypertension. *American Journal of Physiology-Regulatory, Integrative and Comparative Physiology*. https://doi.org/10.1152/ajpregu.1989.256.1.R138